RECRUITMENT OF PROGENITOR CELL POPULATIONS BY CHEMOATTRACTANT DEGRADATION PRODUCTS OF EXTRACELLULAR MATRIX SCAFFOLDS

by

Ellen P. Brennan

Bachelor of Science in Chemical Engineering, Northeastern University, 2003

Submitted to the Graduate Faculty of

Swanson School of Engineering in partial fulfillment

of the requirements for the degree of

Doctor of Philosophy in Bioengineering

University of Pittsburgh

2009

UNIVERSITY OF PITTSBURGH

SWANSON SCHOOL OF ENGINEERING

This dissertation was presented

by

Ellen P. Brennan

It was defended on

August 17, 2009

and approved by

Eric Lagasse, PharmD, PhD, Associate Professor, Department of Pathology

Kacey Marra, PhD, Assistant Professor, Department of Bioengineering

Partha Roy, PhD, Assistant Professor, Department of Bioengineering

Dissertation Director: Stephen F. Badylak, DVM, MD, PhD, Professor, Department of Surgery

RECRUITMENT OF PROGENITOR CELL POPULATIONS BY CHEMOATTRACTANT DEGRADATION PRODUCTS OF EXTRACELLULAR MATRIX SCAFFOLDS

Ellen P. Brennan, PhD

University of Pittsburgh, 2009

Biologic scaffolds composed of extracellular matrix (ECM) have been successfully used as templates for the constructive remodeling of numerous tissues in preclinical studies and human clinical applications. The mechanisms by which ECM induces remodeling are largely unknown, but the degradation products of ECM may play key roles in constructive remodeling. This dissertation investigated the hypothesis that ECM degradation products possess chemoattractant properties for progenitor cell (PC) populations that participate in constructive remodeling.

We investigated different methods of *in vitro* degradation of ECM and determined physiologically relevant methods of degradation yielded degradation products with chemoattractant activity. Both pepsin and collagenase digestion of ECM resulted in chemoattraction of two distinct PC populations.

We then investigated if ECM degradation products from a given tissue have more potent chemoattractant properties for PCs derived from the same tissue type than for PCs derived from other tissues. Although ECM derived from skin, liver, small intestine, and urinary bladder were all chemoattractive for at least one PC population, a tissue-specific chemotactic effect was not observed in studies using skin, liver, and intestinal PCs. However, results showed that the age

and species from which ECM is harvested has an effect on the chemoattractant potential of the ECM for some PC populations.

We investigated if prevention or retardation of ECM degradation *in vivo* would reduce bone marrow-derived PC involvement in constructive remodeling, yielding a different histomorphologic outcome than normal ECM degradation. Bone marrow-derived cells (BMCs) participated in the early remodeling of wounded mouse skin treated with rapidly degrading ECM scaffolds. By 28 days post-surgery, the number of BMCs returned to normal levels, suggesting that these cells do not participate in long-term constructive remodeling of mouse skin. Slowly degrading chemically crosslinked ECM scaffolds did not recruit more BMCs than are found in normal uninjured mouse skin at any time investigated. Wounds treated with rapidly degrading ECM appeared to remodel more rapidly than other treatment groups. These results suggest that scaffold type affects the temporal remodeling of injured mouse skin and that while BMCs participate in remodeling of skin wounds in mice, local tissue cells may also play an important role.

TABLE OF CONTENTS

LIST OF TABLES

LIST OF FIGURES

PREFACE

So many people have shaped my graduate school experience. I would like to begin by thanking my dissertation advisor, Dr. Stephen Badylak, for taking me into his lab and making my research possible. Thanks to his mentorship for the past five years, I have learned so much about research in general and regenerative medicine in particular. I would also like to thank my excellent dissertation committee members, Dr. Eric Lagasse, Dr. Kacey Marra and Dr. Partha Roy, for sharing their great ideas and feedback with me.

I would like to thank everyone that has been a part of the Badylak Lab over the past five years for being such a great group of people to work with. In particular, I thank Scott Johnson for all of his help with the mice and Hongbin Jiang for performing the mouse surgeries. My third specific aim could not have been completed without their help. Thanks to Janet Reing and Li Zhang for their pioneering work with the Boyden chamber in our lab, and to Allison Beattie for inducting me into the "Boyden Chamber Club" and having the great idea to stain the filters with DAPI and count the migrated cells with ImageJ. Thank you to Rena Kasick for her immunofluorescence work. I thank Ann Stewart-Akers, Denver Faulk and Tiffany Sellaro for their decellularization help. Thanks to Danny Freytes for developing the pepsin digestion protocol and giving me rides home from the lab when we were both working too late. Thanks to Bryan Brown for his work as Production Manager for the lab. I thank Neill Turner and Vineet Agrawal for their IHC tips and general random knowledge. Thanks also go out to Steve Tottey for both making me think and making me laugh, Kerry Daly for sharing her excellent music and

company, Julie Myers-Irvin for making me take lunch breaks, Jolene Valentin for being my #1 lab notebook witness, John Freund for being a great lab manager, John Wainwright for his general helpfulness and advice and Tom Gilbert for giving the grad students in the lab hope that one day we would graduate too. Thank you to Jocelyn Runyon and Dawn Robertson for their efforts toward keeping Dr. Badylak's schedule going. Many thanks to Jennifer DeBarr for her excellent histological processing and social planning.

I would also like to acknowledge our collaborators on the work included in this dissertation. Thank you to Dr. Lorraine Gudas and Dr. Xiao-Han Tang at Weill Cornell Medical College for their help in characterizing the human epidermal keratinocytes. Thanks to Rohan Manohar and Helene Fohrer from Dr. Lagasse's lab for culturing and characterizing the human fetal liver cells. Thank you to Dr. Mervin Yoder at Indiana University for providing us with the GFP bone marrow chimera mice. Thank you to the Center for Biologic Imaging at the University of Pittsburgh for providing outstanding microscopy facilities and staff to the university.

Thank you to the Department of Bioengineering, especially Dr. Harvey Borovetz, Lynette Spataro, Joan Williamson, and Judy Repp.

Finally, I need to thank my amazing family and friends for all of their support. I am so grateful for my fiancé, Jeff Pierce, who has been a bottomless source of happiness, love and support. And most importantly, I would not be where I am today without my parents, John and Rose Brennan. I am very grateful for their life-long love, support and unwavering confidence in me.

1.0 INTRODUCTION AND SPECIFIC AIMS

Biologic scaffolds composed of extracellular matrix (ECM) have been successfully used as templates for the constructive remodeling of numerous tissues in preclinical studies and human clinical applications [1-15]. ECM scaffolds are rapidly degraded *in vivo* [16, 17] and have been shown to recruit bone marrow derived cells to the site of remodeling [18, 19]. These marrow derived cells remain in the remodeling site beyond the stages of inflammation, integrate into the remodeled tissue, and may differentiate into site-appropriate mature cell types [19]. The mechanisms by which ECM induces remodeling are largely unknown, but it appears that the degradation products of ECM scaffolds may play key roles in the cell recruitment and constructive remodeling effect. Furthermore, because ECM produced by the resident cells of each tissue is optimized for that particular tissue, the composition of ECM harvested from different tissues will vary. It is logical or at least plausible therefore, that ECM derived from a particular tissue may generate degradation products that preferentially recruit cells that are lineage directed for that same tissue.

This dissertation is based upon the findings of preliminary studies which show: 1) ECM scaffolds used in preclinical studies recruit bone marrow-derived cells which remain at the site of remodeling long beyond the stages of inflammation, and these cells appear to differentiate into site-appropriate cell types [18, 19]; 2) ECM scaffolds derived from several tissues including porcine small intestine, liver, and urinary bladder can be chemically degraded *in vitro*, generating

degradation products with chemotactic and antibacterial activities [20-22]; 3) prevention or retardation of ECM scaffold degradation by chemical cross-linking results in less constructive remodeling than an ECM scaffold that is allowed to degrade normally [23].

The central hypothesis of this dissertation is that degradation products of ECM scaffolds possess chemoattractant properties for tissue-specific, lineage-directed progenitor cells and bone marrow-derived progenitor cells that participate in constructive remodeling. The long-range objective of this work is to develop methods to induce migration of progenitor cells to tissue sites in need of repair, thereby stimulating a regenerative tissue response rather than scar tissue formation.

1.1 EXTRACELLULAR MATRIX IN REGENERATIVE MEDICINE

The ECM of each tissue or organ is secreted by resident cells of that tissue, thus providing tissue specific ECM the appropriate composition and structure to maintain normal structure and function of that tissue. ECM is composed of structural proteins, functional proteins, glycosaminoglycans, proteoglycans, cytokines, and growth factors [24].

Biologic scaffolds composed of ECM have been successfully used as inductive templates for tissue regeneration in various preclinical and clinical applications, including orthopedic, esophageal, lower urinary tract, dermal, cardiovascular, central nervous system, and other surgical applications [1-14, 23, 25-36]. Regardless of the tissue or organ from which the ECM scaffold is prepared (for example, porcine small intestine or urinary bladder), implantation of the scaffold results in site-specific constructive remodeling of the injured tissue with the remodeled tissue appearing grossly and histologically similar to healthy native tissue [2, 6, 15, 23, 24, 26].

These results suggest that a common mechanism for remodeling is induced by the ECM, regardless of its tissue of origin, that simultaneously allows for cell recruitment and/or cell proliferation and the cell differentiation and spatial organization processes that define each anatomic location.

Various off-the-shelf biologic scaffold devices composed of ECM have become commercially available in recent years. Table 1 lists many of the commercially available ECM devices. These ECM scaffolds are derived from several different tissue sources, including porcine small intestinal submucosa (SIS-ECM), porcine skin, fetal bovine skin, human skin, human fascia lata, porcine pericardium, bovine pericardium, and horse pericardium. Approved applications of commercially available ECM devices include treatment of partial and full thickness wounds, superficial and second degree burns, venous leg ulcers, soft tissue repair and reinforcement, spinal and cranial repair, pelvic reconstruction, treatment of urinary incontinence, and reconstruction of blood vessels in the neck, leg and arms.

Table 1. List of commercially available medical devices composed of ECM

Product	Company	Material
AlloDerm	Lifecell	Human skin
AlloPatch®	Musculoskeletal Transplant Foundation	Human fascia lata
Axis™ dermis	Mentor	Human dermis
Bard® Dermal Allograft	Bard	Cadaveric human dermis
Bio-Blanket®	Kensey Nash	Bovine dermis
CollaMend	Bard	Porcine dermis
CuffPatch™	Arthrotek	Porcine small intestinal submucosa (SIS)
DurADAPT™	Pegasus Biologicals	Horse pericardium
Dura-Guard®	Synovis Surgical	Bovine pericardium
Durasis®	Cook SIS	Porcine small intestinal submucosa (SIS)
Durepair®	TEI Biosciences	Fetal bovine skin
FasLata®	Bard	Cadaveric fascia lata
Graft Jacket®	Wright Medical Tech	Human skin
Oasis®	Healthpoint	Porcine small intestinal submucosa (SIS)
OrthADAPT™	Pegasus Biologicals	Horse pericardium
Pelvicol®	Bard	Porcine dermis
Peri-Guard®	Synovis Surgical	Bovine pericardium
Permacol™	Tissue Science Laboratories	Porcine skin
PriMatrix™	TEI Biosciences	Fetal bovine skin
Restore™	DePuy	Porcine small intestinal submucosa (SIS)
Shelhigh No-React® Patch	Shelhigh	Bovine or porcine pericardium
Stratasis®	Cook SIS	Porcine small intestinal submucosa (SIS)
SurgiMend™	TEI Biosciences	Fetal bovine skin
Surgisis®	Cook SIS	Porcine small intestinal submucosa (SIS)
Suspend™	Mentor	Human fascia lata
TissueMend®	TEI Biosciences	Fetal bovine skin
Vascu-Guard®	Synovis Surgical	Bovine pericardium
Veritas®	Synovis Surgical	Bovine pericardium

Table 1 (continued)

Xelma™	Molnlycke	ECM protein, PGA, water
Xenform™	TEI Biosciences	Fetal bovine skin
Zimmer Collagen Patch ®	Tissue Science Laboratories	Porcine dermis

Processing methods used to prepare these ECM devices vary, and can greatly affect the biologic response of the patient treated with the device. The use of harsh decellularization methods to produce an ECM scaffold from tissue can disrupt structural and functional components of the ECM, which can affect host cell interaction with the ECM scaffold (for example, cell migration and adhesion) as well as reducing the bioactivity of the scaffold. Chemical crosslinking of an ECM scaffold, a processing step commonly used to produce many of the commercially available ECM scaffold devices, slows or prevents the degradation of the scaffold, which can affect the remodeling response. Chemical crosslinking is commonly used when producing ECM scaffolds because the molecular crosslinks are thought to prevent antigenic recognition and increase mechanical strength. It is our hypothesis that degradation of ECM scaffolds plays a key role in the constructive remodeling process and that preventing or slowing degradation by chemical crosslinking reduces the constructive modeling benefits of ECM scaffolds. This hypothesis is the focus of the third specific aim of this dissertation.

1.2 ECM DEGRADATION

Degradation of the ECM scaffold appears to play a key role in a constructive remodeling process. Scaffolds used for tissue engineering and regenerative medicine applications are degraded *in vivo* by several different mechanisms. Cell-mediated and enzymatic reactions are

important mechanisms of scaffold degradation, and are closely related to each other. Immediately following implantation of a scaffold material, the host's innate immune system responds to the presence of the scaffold. Inflammatory cells, including neutrophils, monocytes, and lymphocytes, infiltrate the implantation site. Neutrophils and macrophages can phagocytose or degrade the scaffold, depending on the scaffold composition [37]. Phagocytes are capable of producing oxidants, such as the superoxide anion and several others generated by the Haber-Weiss cycle, which can participate in the degradation of scaffolds [38]. Activated neutrophils and macrophages release a variety of enzymes that can contribute to scaffold degradation, including collagenases, elastases, gelatinases, cathepsin G, proteinase 3, plasminogen activator, and phospholipase [39]. Other enzymes secreted by various cell types and present in various tissues, particularly members of the matrix metalloproteinase (MMP) family of enzymes, are likely also involved in scaffold degradation [40].

Biologic scaffolds composed of porcine ECM degrade rapidly and are completely resorbed within 90 days [14, 16, 41]. Scaffolds composed of bovine type I collagen cross-linked with hexamethylene diisocyanate used in a murine myocardium model have been shown to be degraded by high levels of MMP-8 secreted by neutrophils [42]. Collagen-based scaffolds are normally degraded by collagenases, which attack the triple helix at a specific location. The collagen molecule fragments resulting from this reaction denature to gelatin at physiological temperatures and are then cleaved to oligopeptides by nonspecific proteases [43].

Chemical crosslinking of biologic scaffold materials decreases or halts the rate of degradation by these naturally occurring mechanisms [43]. The slow degradation rate can be beneficial in applications that require extended mechanical support from the scaffold, but crosslinking can also lead to a prolonged and more intense inflammatory response to the scaffold

than would occur if the chemical crosslinking was not present [23]. It has recently been shown that peripheral blood monocytes are necessary for the early and rapid degradation of SIS-ECM scaffolds in a rat abdominal wall reconstruction model, and that chemically crosslinked SIS-ECM was resistant to macrophage-mediated degradation [44]. These findings underscore the importance of host cell interactions in the complex process of ECM degradation and remodeling *in vivo*, as well as the effects of chemical crosslinking on this process.

1.2.1 Matricryptic Molecules and Sites

During ECM degradation, in addition to the release of constituent growth factors, many large insoluble molecules present within the matrix are broken down into low molecular weight fragments which possess biological activities that are not possessed by the parent molecules. These matrix-derived bioactive fragment molecules are known as matricryptic molecules, matricryptins, or matrikines [45]. In addition to proteolysis-generated bioactive fragments, functional sites of the parent molecules that are hidden and inactive within the ECM can also become active due to structural or conformational changes [45, 46]. Such sites are known as matricryptic sites [45]. Some of the ECM molecules that have been shown to possess these properties are collagen (types I, II, IV, VIII, XIV, XV, and XVIII) [47-51], fibronectin [52], elastin [45, 53, 54], laminin [46, 55], hyaluronan [56-58], perlecan [59], and osteopontin [60]. This phenomenon also applies to other non-matrix proteins such as plasminogen, calreticulin, α1-antitrypsin, and latent TNF-α [61, 62].

The major enzymes involved in cleavage of ECM molecules are the matrix metalloproteinases and the bone morphogenetic protein 1 and tolloid family of metalloproteinases. Serine proteinases, members of the cysteine proteinase family, and the

aspartic proteinase family are also involved in ECM degradation. Conformational changes can be caused by cell-generated tension or by cells binding to other ECM molecules or cell-surface receptors [46]. Therefore, a number of mechanisms of ECM degradation can result in bioactive fragment molecules. Table 2 summarizes some of the matrix components and the bioactive fragment molecules produced by degradation.

Table 2. Summary of ECM components with bioactive fragment molecules

Parent Molecule	Fragment Molecule	Biologic Activity
Collagen I	Trimer carboxyl propeptide fragments	Chemotactic for endothelial cells, dermal fibroblasts, peripheral monocytes [47]
Collagen II	Chondrocalcin Other fragments	Cartilage calcification Inhibit collagen synthesis and MMP secretion by chondrocytes [47]
Collagen IV	Arresten, canstatin, tumstatin, a6 chain of NC1 domain Site exposed by degradation from human umbilical vein endothelial cells	Anti-angiogenic [48] Required for angiogenesis and tumor growth *in vivo* [49]
Collagen VIII	Vastatin	Inhibits proliferation and induces apoptosis of bovine aortic endothelial cells [50]
Collagen XIV	Fragment from N-terminal	Chemotactic for neutrophils [47]
Collagen XV	Restin	Anti-angiogenic (inhibits endothelial cell migration) [51]
Collagen XVIII	Endostatin Fragment from NC1 domain	Anti-angiogenic (inhibits endothelial cell migration and proliferation [51], inhibits branching morphongenesis [47]) Induce migration of neural and non-neural cells in C. elegans [47]
Elastin	VGVAPG sites	Chemotactic for monocytes[45, 63] and fibroblasts [54, 63]
Fibronectin	Anastellin	Block growth of cultured human dermal microvascular endothelial cells [52]
Laminin-1	More than 20. Most potent: A13, C16 B1 chain	Angiogenic (bind to endothelial cell integrins, promote adhesion and tube formation) [55] Anti-angiogenic [55]
Laminin-5	DIII	Induces migration of mammary epithelial cells [46]
Hyaluronan	3-10 disaccharide unit degradation products	Angiogenic (stimulates endothelial cell proliferation and migration) [56-58]

Table 2 (continued)

Perlecan (proteoglycan in basement membrane)	Endorepellin	Anti-angiogenic (inhibits endothelial cell migration, collagen-induced endothelial tube morphongenesis, blood vessel growth in chorioallantoic membrane and Matrigel plug assays) [59]
Osteopontin (secreted glycoprotein in ECM)	GRGDS-containing fragment produced by thrombin cleavage	Haptotaxis [60]

Numerous bioactive fragment molecules are produced by the degradation of various ECM components, suggesting that degradation of ECM scaffolds would generate degradation products possessing a variety of bioactivities. The first specific aim of this dissertation investigates molecules with chemoattractant capability that are released by *in vitro* degradation of ECM scaffolds.

1.2.2 Bioactive Degradation Products of ECM Scaffolds

ECM scaffolds implanted *in vivo* in preclinical studies have been shown to result in constructive remodeling, promote angiogenesis, and be resistant to bacterial infection [7, 11, 19, 23, 64-67]. *In vitro* studies have further shown that degradation of ECM derived from several tissues generates low molecular weight peptides with biological properties such as chemotactic, mitogenic, angiogenic, and antimicrobial activity [20-22, 68]. In contrast, intact ECM has been shown not to possess such activity [69], suggesting that these biological activities are associated with the products of ECM degradation, rather than molecules present in intact ECM. Low molecular weight peptides isolated from acid-hydrolyzed SIS-ECM have been shown to possess

chemotactic activity for primary murine adult liver, heart, and kidney endothelial cells and to promote vascularization *in vivo* in Matrigel plug assays [21]. Studies also suggest that subcutaneous implantation of porcine SIS-ECM induces migration of bone marrow-derived cells to the site of constructive remodeling [18], and that this phenomenon is associated with complete ECM degradation. Bone marrow-derived cells were also shown to be recruited to the site of SIS-ECM-induced remodeling in a mouse tendon, and appeared to integrate into the remodeled tissue and differentiate into site-appropriate mature cell types [19]. It has also recently been shown that ECM subjected to *in vivo* degradation and remodeling possesses chemoattractant activity for multipotential progenitor cells *in vitro* [70]. The second specific aim of this dissertation investigates the effect of ECM source (tissue, species, and age) on chemoattractant activity of ECM degradation products for lineage-directed progenitor cells.

In summary, non-chemically crosslinked porcine-derived ECM scaffolds have been shown to induce constructive remodeling of injured tissue, and the results of several studies suggest that the degradation products of these scaffolds recruit cells that participate in the constructive remodeling. Bioactive fragment molecules are produced by the degradation of various ECM components, and ECM scaffolds have been shown to generate degradation products with bioactivities that are not present within intact ECM scaffolds. This dissertation investigates the hypothesis that degradation products of ECM scaffolds possess chemoattractant properties for tissue-specific, lineage-directed progenitor cells and bone marrow-derived progenitor cells that participate in constructive remodeling.

1.3 MECHANISMS OF CHEMOTAXIS

Chemotaxis is the migration of cells in response to an external concentration gradient of a particular substance. The first step of chemotaxis is the binding of the chemoattractant molecule to its specific receptor on the cell. This binding step triggers chemotactic signals within the cell and activates several downstream effectors of migration such as cell polarity. In order for cells to migrate directionally, as in a chemoattractant gradient, cytoskeleton rearrangements that promote F-actin polymerization at the front of the cell and actomyosin assembly at the back of the cell must occur. These cytoskeleton rearrangements result in leading-edge formation at the cell front, oriented in the direction of chemotaxis, and retraction at the trailing edge. The forces that drive cell movement are produced by protrusions from the leading edge driven by the outward extension of actin filaments and by actomyosin-based contraction, which breaks adhesions to the substrate. During chemotaxis, many cell types secrete chemokines that relay the chemoattractant signal to neighboring cells, thereby amplifying the chemotactic response [71, 72]. This dissertation investigates the *in vitro* chemotaxis of progenitor cells in response to degradation products of ECM scaffolds, as well as the *in vivo* recruitment of bone marrow-derived progenitor cells by ECM scaffolds.

1.4 SPECIFIC AIMS

Specific Aim #1: To determine if bioactive degradation products of ECM scaffolds can be produced *in vitro* by methods that mimic physiologic conditions.

Hypothesis$_1$: ECM scaffolds can be degraded *in vitro* by methods that mimic *in vivo* events, and the resultant degradation products possess chemotactic activity.

Rationale: Results from *in vivo* studies suggest that degradation of ECM scaffolds is necessary for constructive remodeling to occur. In addition, ECM scaffolds have been degraded *in vitro* by chemical and physical methods, generating bioactive degradation products. If these bioactive degradation products are also produced *in vivo*, then physiologic degradation processes must be active. We will mimic the *in vivo* processes in an *in vitro* environment and determine if chemoattractant molecules are released.

Specific Aim #2: To determine if degradation products of ECM have tissue-specific preferential chemoattractant properties for progenitor cells derived from their respective tissue.

Hypothesis$_2$: ECM degradation products from a given tissue have more potent chemoattractant properties for progenitor cells derived from that same tissue or lineage directed to become cells of that tissue, compared to progenitor cells derived from other tissues.

Rationale: Since ECM degradation products recruit bone marrow-derived cells to the site of remodeling where these cells appear to differentiate with a site-appropriate phenotype, it is plausible that tissue-specific, lineage-directed progenitor cells may also be recruited by ECM degradation products. It would be logical for local, lineage-committed progenitor cells to be preferentially recruited to the site of remodeling and participate in the constructive remodeling process.

Specific Aim #3: To determine if prevention of ECM scaffold degradation affects the involvement of progenitor cells in the remodeling response *in vivo*.

Hypothesis$_3$*:* Prevention or retardation of ECM degradation *in vivo* by chemical crosslinking of the scaffold reduces progenitor cell involvement in remodeling, yielding a different outcome with histologic characteristics that are less constructive and desirable than would have resulted if the progenitor cells had been allowed to participate in the remodeling process.

Rationale: If degradation of the ECM scaffold causes the recruitment of progenitor cells which participate in the constructive remodeling of the tissue, then prevention or retardation of scaffold degradation should reduce the participation of progenitor cells in remodeling and yield a histologically different result than an ECM scaffold subjected to normal degradation and remodeling.

2.0 SPECIFIC AIM 1: ECM DEGRADATION *IN VITRO*

2.1 BACKGROUND

Previous work has shown that non chemically crosslinked ECM scaffolds are rapidly degraded *in vivo* [16, 17] and that these inductive acellular scaffolds are repopulated by host cells, resulting in site-specific constructive remodeling of injured tissue, rather than being subjected to the default adult mammalian wound healing process of scar tissue formation [2, 7, 15-17, 23, 73]. ECM scaffolds have been shown to recruit bone marrow-derived cells that participate in the long-term constructive remodeling of tissue *in vivo* [18, 19] and it has recently been shown that ECM subjected to *in vivo* degradation and remodeling possesses chemoattractant activity for multipotential progenitor cells *in vitro* [70].

In vitro studies have demonstrated that degradation products of ECM possess bioactive properties that likely play a role in ECM-induced constructive remodeling. A low molecular weight fraction of small intestinal submucosa (SIS-ECM) digested using acid and heat has been shown to possess chemoattractant activity for primary endothelial cells *in vitro* and to promote vascularization *in vivo* [21]. In addition, certain fractions of acid and heat degraded SIS-ECM, urinary bladder submucosa, urinary bladder matrix (UBM-ECM) and liver ECM have all been shown to possess antibacterial activity *in vitro* [20, 22].

While instructive, these *in vitro* studies investigated bioactive degradation products within ECM that was digested using acid and extreme heat, which may not be physiologically

relevant. The objective of the present study was to determine if bioactive degradation products of ECM scaffolds can be produced *in vitro* by methods that mimic physiologic conditions more closely than in previous studies. In particular, this chapter focused on *in vitro* chemoattractant activity of ECM degradation products for progenitor cells.

2.2 MATERIALS AND METHODS

2.2.1. Preparation of UBM-ECM degradation products

UBM-ECM was prepared from the urinary bladders of market weight pigs (~110 – 130 kg) as previously described [74]. In brief, urothelial cells were removed by soaking the urinary bladders in 1.0 N saline. Connective and adipose tissue were removed from the serosal surface of the urinary bladder, and the tunica serosa, tunica muscularis externa, tunica submucosa, and most of the tunica muscularis mucosa were mechanically removed, leaving a biomaterial composed of only the basement membrane and the subjacent tunica propria of the tunica mucosa. Decellularization was completed by treatment with 0.1% peracetic acid/4% ethanol for two hours followed by rinsing with phosphate buffered saline (PBS) and deionized water. Complete decellularization was confirmed by both 4'-6-Diamidino-2-phenylindole (DAPI) nuclear staining and hematoxylin and eosin staining. The UBM-ECM was then lyophilized in sheet form, frozen, and comminuted into a particulate form using a Wiley Mill with a #60 mesh screen [75].

UBM-ECM was digested *in vitro* using pepsin. Pepsin, a digestive protease found in the stomach, hydrolyzes only peptide bonds and does not hydrolyze non-peptide amide or ester bonds. Pepsin preferentially cleaves at the carboxyl side of phenylalanine and leucine and at the carboxyl side of glutamic acid residues. Pepsin does not cleave at valine, alanine, or glycine

linkages [76]. Particulate lyophilized UBM-ECM was added to 1 mg/ml pepsin (Sigma) in 0.01 N HCl for a final concentration of 10 mg UBM-ECM/ml suspension. The suspension was mixed on a stir plate at room temperature for 48 h, at which time no visible pieces of UBM-ECM remained. Pepsin control samples were prepared by mixing the pepsin digestion solution (1 mg/ml pepsin in 0.01 N HCl) at room temperature for 48 h.

UBM-ECM was also digested *in vitro* using crude collagenase. Crude collagenase produced by *Clostridium histolyticum* consists of two forms of the collagenase enzyme as well as other enzymes such as an elastase and nonspecific proteases [77]. Collagenases attack the triple helix of the collagen molecule at a specific location, resulting in the N-terminal fragment (about two-thirds of the molecule) and the C-terminal fragment. At physiologic temperatures, these fragments are spontaneously denatured to gelatin and the gelatinized fragments are then cleaved to oligopeptides by nonspecific proteases [43]. Particulate lyophilized UBM-ECM was added to 50 μg/ml collagenase (Sigma) in 250 μM $CaCl_2$ in PBS for a final concentration of 10 mg UBM-ECM/ml suspension. The suspension was then placed on a rocker at 37ºC for 24 h, at which time no visible pieces of UBM-ECM remained. The collagenase activity was then quenched by addition of ethylenediaminetetraacetic acid (EDTA) to a final concentration of 50 mM EDTA. Collagenase control samples were prepared by mixing 50 μg/ml collagenase in 250 μM $CaCl_2$ in PBS, placing the solution on a rocker at 37ºC for 24 h, and quenching the collagenase activity by adding EDTA to a final concentration of 50 mM EDTA.

Attempts at *in vitro* degradation of UBM-ECM by culture of primary human white blood cells or a CD14-expressing subpopulation of primary human white blood cells on UBM-ECM sheets were not successful. However, control groups used in these *in vitro* white blood cell mediated-degradation experiments demonstrated that soaking UBM-ECM sheets in cell culture

medium resulted in the release of molecules with chemoattractant activity for multipotential cells. To further examine this effect, UBM-ECM sheets were soaked in PBS or Dulbecco's Modified Eagle's Medium (DMEM) in six-well plates in 95% air/5% CO_2 at 37ºC for 18 hours. Controls of PBS and DMEM alone were also incubated in six-well plates in 95% air/5% CO_2 at 37ºC for 18 hours. Supernatants were then collected from the wells.

2.2.2 SDS-PAGE analysis of UBM-ECM digests

An SDS-PAGE analysis was conducted for each of the UBM-ECM digests and supernatants. For the UBM-ECM pepsin digest, SDS-PAGE analysis was performed using a 7.5% polyacrylamide gel with a prestained protein standard [78]. For the UBM-ECM collagenase digest, a bicinchoninic acid (BCA) assay (Pierce Biotechnology, Rockford, IL) was performed to estimate protein concentration of the UBM-ECM collagenase digest. Based on BCA assay results, approximately 10 μg protein was loaded into each lane of a 12.5% polyacrylamide gel, with a prestained protein standard (Bio-Rad, Hercules, CA) in the range 10–250 kD. The gel was run at a voltage of 80 V until the dye front entered the separating gel, then at a constant voltage of 100 V until the dye front reached the bottom of the gel. The gel was stained with Imperial Protein Stain (Pierce Biotechnology). For the UBM-ECM releasates in PBS or DMEM, the supernatants and control samples were loaded into each lane of a 12.5% polyacrylamide gel, with a prestained protein standard (Bio-Rad, Hercules, CA) in the range 10–250 kDa. The gel was run and stained as described for the UBM-ECM collagenase digest.

2.2.3 Chemotaxis assay with MRL blastema-like cells

MRL blastema-like cells (MRL-B cells) were isolated from the ears of MRL/MpJ mice, a strain of mice that has been shown to have a unique regenerative capacity [79-82], as previously described [68]. Briefly, a 2.0 mm hole was punched through the ear of each mouse. Unlike other mouse strains, in MRL mice the site of the hole punch exhibits a blastema-like structure and closes with typical site appropriate tissue architecture and no scarring within 4 weeks after the time of punching [79]. Eleven days after creating the hole punch, cells were isolated from the healing edge of the hole. These isolated MRL-B cells were then cultured in DMEM supplemented with 10% fetal calf serum (FCS), 2 mM glutamine, 100 U/ml penicillin, and 100 μg/ml streptomycin in 95% air/5% CO_2 at 37ºC. MRL-B cells were shown to express molecules associated with progenitor cell populations and tissue regeneration, including Tenascin-C, Thy1, Dlk/Pref-1, Msx1, Thrombospondin, and Tbx5 [68]. Cells used in these studies were passage 13-17.

In vitro chemotaxis of MRL-B cells toward pepsin and collagenase digests of UBM-ECM was evaluated using a 48-well micro-chemotaxis chamber (Neuro Probe, Gaithersburg, MD). When the MRL-B cells reached 70-90% confluency, they were starved overnight in DMEM containing 0.5% heat inactivated FCS before use in chemotaxis assays the following morning. Then the MRL-B cells were trypsinized, neutralized, centrifuged, resuspended in serum-free DMEM and incubated in suspension for 1 h at 37ºC.

UBM-ECM pepsin digest samples were diluted in serum-free DMEM to concentrations ranging from 10 to 200 μg UBM-ECM digest/ml. UBM-ECM collagenase digest samples were diluted in serum-free DMEM to concentrations ranging from 10 to 1000 μg UBM-ECM

digest/ml. A negative control for each sample was prepared by diluting the pepsin or collagenase control sample in serum-free DMEM at the same ratios as the UBM-ECM digest samples. Undiluted UBM-ECM releasates in PBS and DMEM and negative controls of PBS and DMEM alone were also evaluated. A positive control of 10% heat inactivated FCS in DMEM was also included in each assay. Samples were loaded to the lower chamber of each well of the chemotaxis chamber. A 12 μm pore size polycarbonate filter coated with 0.05 mg/ml collagen I (BD Biosciences, San Jose, CA) divided the lower and upper chamber of each well. Approximately 30,000 cells were added to the upper chamber of each well. The chemotaxis chamber was incubated at 37ºC for 3 h. Cells that had not migrated through the pores of the filter were removed and migrated cells were fixed and stained with Diff-Quick staining kit for manual cell counting or permeabilized and stained with DAPI for ImageJ software-assisted cell counting.

Three random fields from each well, located in the upper left, upper right and lower central regions of each well, were photographed at 200X magnification and migrated cells were counted from these fields, by manual counting or ImageJ software. Samples were tested in quadruplicate for each chemotaxis assay performed. The percentage change in migrated cells in response to UBM-ECM digest/releasate samples compared to negative control samples was calculated for each assay performed. To compare results between different assays, the percentage change was normalized by the percentage change induced by the positive control for each assay. Reported results are expressed as mean and standard error of the mean (SEM) of percentage change in migration normalized by positive control from one to three assays (n = 1-3 independent assays, with samples run in quadruplicate in each assay, for n = 4-12 samples tested). The statistical significance between samples was determined by Student's t-test with α = 0.05.

2.2.4 Chemotaxis assay with neonatal human epidermal keratinocytes

Neonatal human epidermal keratinocytes (HEKn) were obtained from Cascade Biologics and cultured in EpiLife medium (Cascade Biologics, Portland, OR) supplemented with human keratinocyte growth supplement (HKGS; Cascade Biologics), yielding final supplemented medium concentrations of 0.2% v/v bovine pituitary extract, 5 μg/ml bovine insulin, 0.18 μg/ml hydrocortisone, 5 μg/ml bovine transferrin and 0.2 ng/ml human epidermal growth factor. HEKn were cultured according to the manufacturer's instructions under a humidified atmosphere in 95% air/5% CO_2 at 37ºC. This cell population has been shown to express Rex-1, a putative stem cell marker, and other stem cell markers such as Oct 4 and cMyc [83]. Cells used in these studies were passage 4–7.

In vitro chemotaxis of HEKn toward pepsin and collagenase digests of UBM-ECM was evaluated using a 48-well micro-chemotaxis chamber (Neuro Probe). When the HEKn reached 70–80% confluency, they were starved overnight in unsupplemented EpiLife medium before use in chemotaxis assays the following morning. Then the HEKn were trypsinized, neutralized and centrifuged according to HEKn product instructions, resuspended in unsupplemented EpiLife medium and incubated in suspension for 1 h at 37ºC.

UBM-ECM pepsin and collagenase digest samples were diluted in unsupplemented EpiLife medium to concentrations ranging from 50 to 500 μg UBM-ECM digest/ml. A negative control for each sample was prepared by diluting the pepsin or collagenase control sample in unsupplemented EpiLife medium at the same ratios as the UBM-ECM digest samples. A positive control of 10% HKGS in unsupplemented EpiLife medium was also included in each assay. Samples were loaded to the lower chamber of each well of the chemotaxis chamber. An 8 μm pore size polycarbonate filter coated with 0.05 mg/ml collagen I (BD Biosciences, San Jose, CA)

divided the lower and upper chamber of each well. Approximately 30,000 cells were added to the upper chamber of each well. The chemotaxis chamber was incubated at 37ºC for 3 h. Cells that had not migrated through the pores of the filter were removed and migrated cells were fixed, permeabilized and stained with DAPI.

Three random fields from each well, located in the upper left, upper right and lower central regions of each well, were photographed at 200X magnification and migrated cells were counted from these fields using ImageJ software. Samples were tested in quadruplicate for each chemotaxis assay performed. The percentage change in migrated cells in response to UBM-ECM digest samples compared to negative control samples was calculated for each assay performed. To compare results between different assays, the percentage change was normalized by the percentage change induced by the positive control for each assay. Reported results are expressed as mean and SEM of percentage change in migration normalized by positive control from three to five assays (n = 3-5 independent assays, with samples run in quadruplicate in each assay, for n = 12-20 samples tested). The statistical significance between samples was determined by Student's t-test with $\alpha = 0.05$.

2.3 RESULTS

SDS-PAGE analysis of UBM-ECM releasates in PBS and DMEM showed that both releasate samples contained peptides ranging from 10-250 kD while the PBS and DMEM control samples did not (Figure 1A). The two releasates showed similar protein profiles, although the PBS-UBM-ECM releasate showed slightly stronger staining than the DMEM-UBM-ECM releasate. SDS-PAGE analysis of UBM-ECM pepsin digest and UBM-ECM collagenase digest showed that

both digests contained peptides over a wide range of molecular weights (Figure 1B and C). The two digests showed differences in their protein profiles. The pepsin digest of UBM-ECM showed strongest staining in bands located at 100-184 kD, while the collagenase digest of UBM-ECM showed strongest staining in bands located at less than 20 kD. These differences in protein profiles suggest that degradation of the UBM-ECM using the two different enzymes yields different degradation products.

More MRL-B cells migrated in response to UBM-ECM releasates in PBS and DMEM than in response to the PBS and DMEM control samples ($p<0.05$, Figure 2). There was no significant difference between the chemoattractant activity of PBS-UBM-ECM and DMEM-UBM-ECM releasates for MRL-B cells (Figure 3).

Pepsin digested UBM-ECM showed chemoattractant activity for MRL-B cells at concentrations of 100 and 200 μg/ml ($p<0.05$, Figure 4), but not at lower concentrations. Collagenase digested UBM-ECM showed chemoattractant activity for MRL-B cells at 1000 μg/ml ($p<0.05$, Figure 5), but not at lower concentrations. Pepsin digestion of UBM-ECM appeared to result in stronger chemoattractant activity for MRL-B cells than collagenase digestion or incubation in PBS or DMEM (Figures 3-5).

At 50 and 100 μg/ml, both pepsin and collagenase digested UBM-ECM showed chemoattractant activity for HEKn ($p<0.05$, Figure 6). At 100 μg/ml, collagenase digested UBM-ECM showed significantly stronger chemoattractant activity for HEKn than did pepsin digested UBM-ECM. Pepsin digested UBM-ECM also showed significant chemoattractant activity for HEKn at 200 and 500 μg/ml, while at these concentrations the collagenase and EDTA within the

collagenase digested UBM-ECM and its control solution completely inhibited HEKn migration, overshadowing any chemoattractant activity that these UBM-ECM degradation products may have possessed.

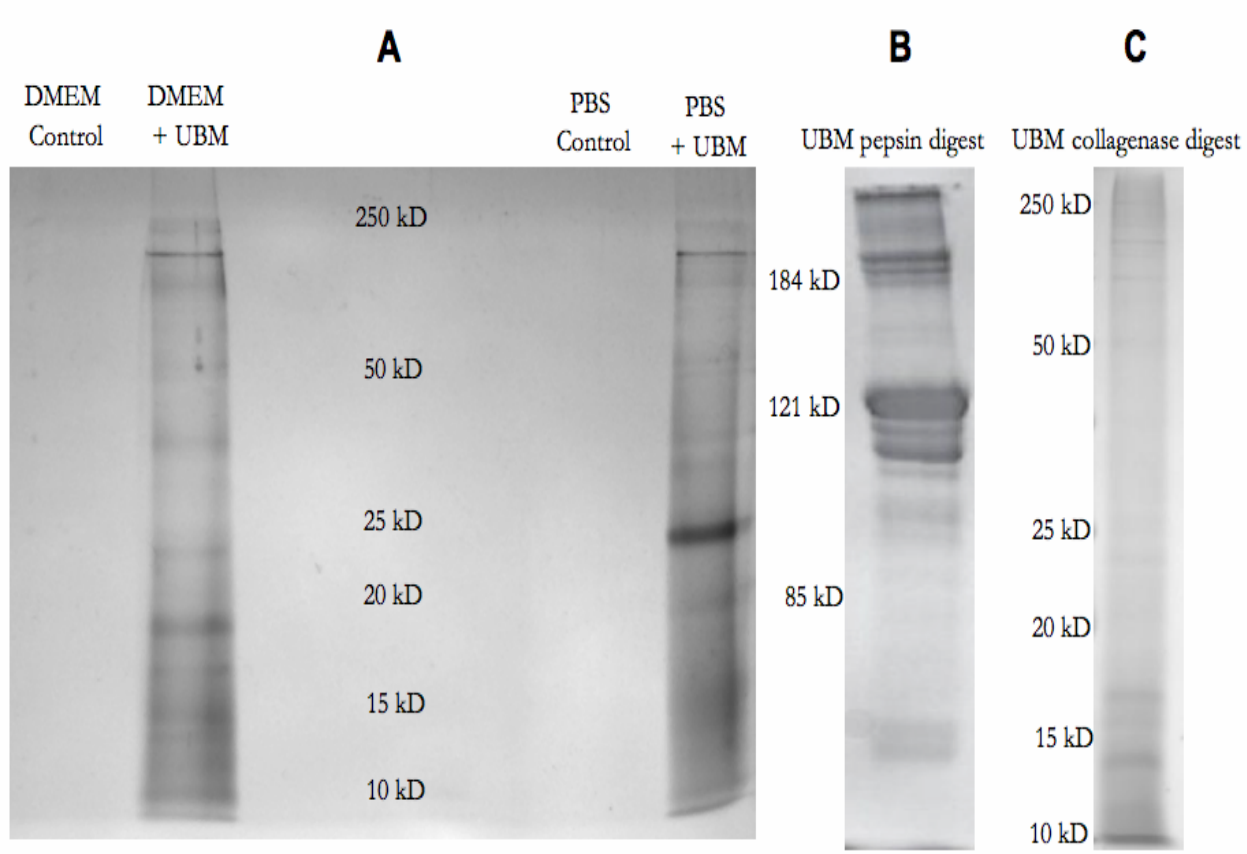

Figure 1. SDS-PAGE analysis of: (A) UBM-ECM releasates and controls; (B) UBM-ECM pepsin digest [78]; and (C) UBM-ECM collagenase digest.

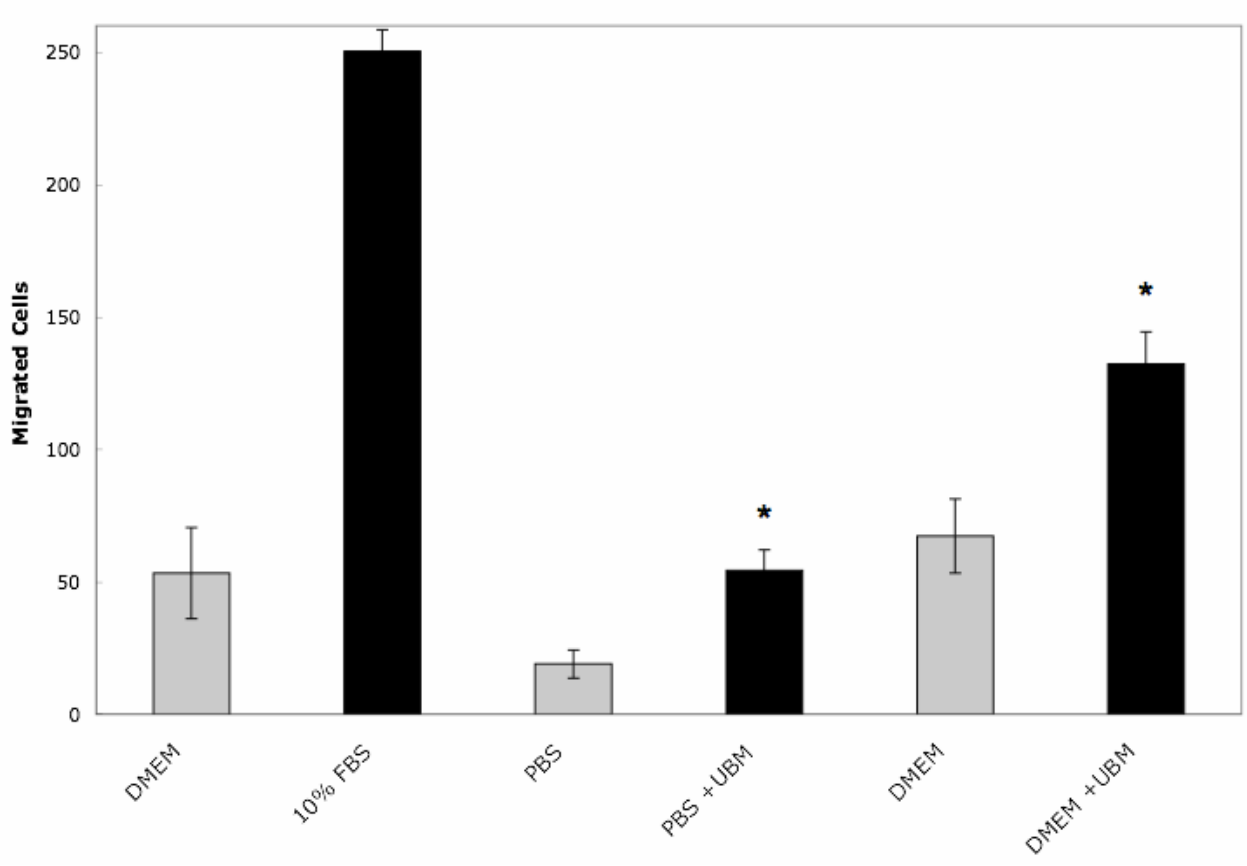

Figure 2. Migration of MRL-B cells in response to UBM-ECM releasates and controls. Mean ± standard deviation (n = 4); * = p< 0.05 compared to PBS and DMEM control samples. Equivalent trends were observed on one further occasion.

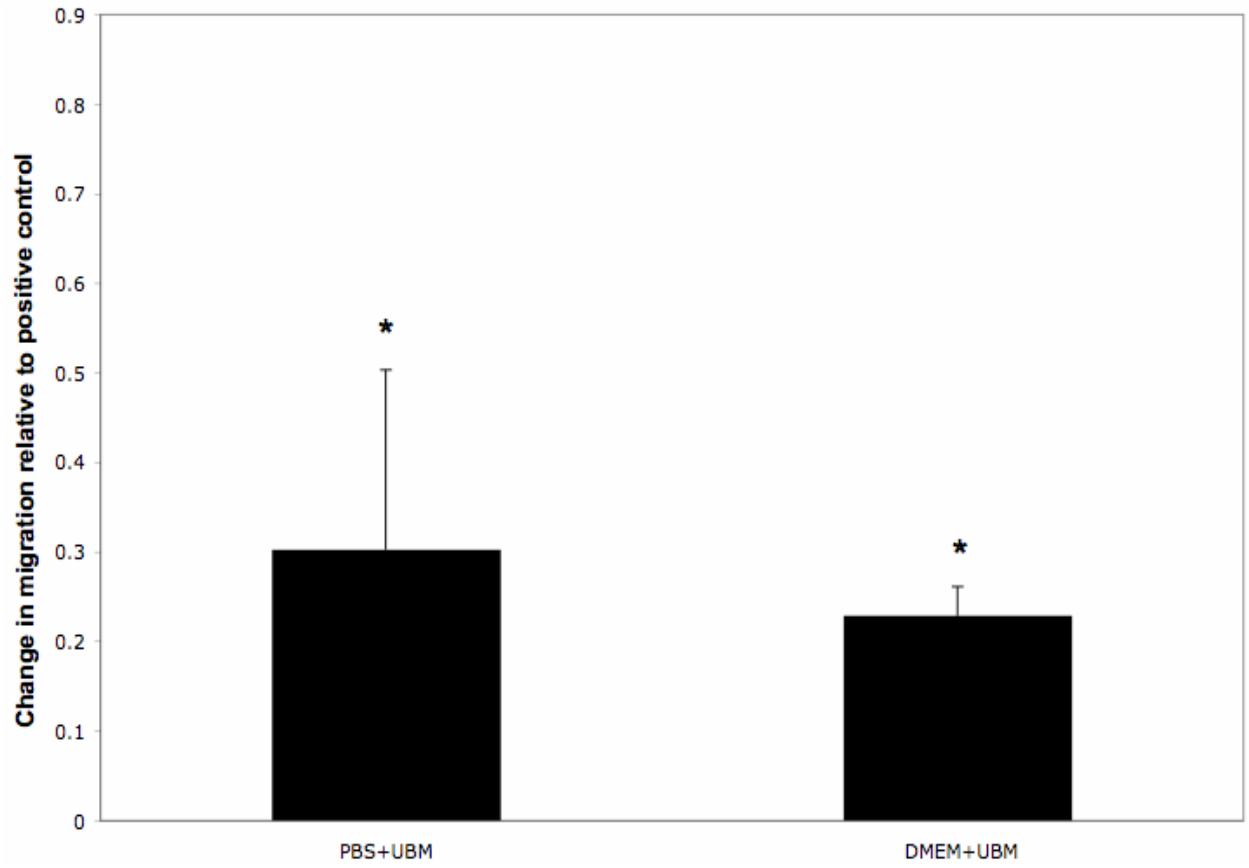

Figure 3. Chemoattractant activity of UBM-ECM releasates for MRL-B cells. Mean± SEM (n=2 independent assays with samples tested in quadruplicate in each assay); * = p< 0.05 compared to PBS and DMEM control samples

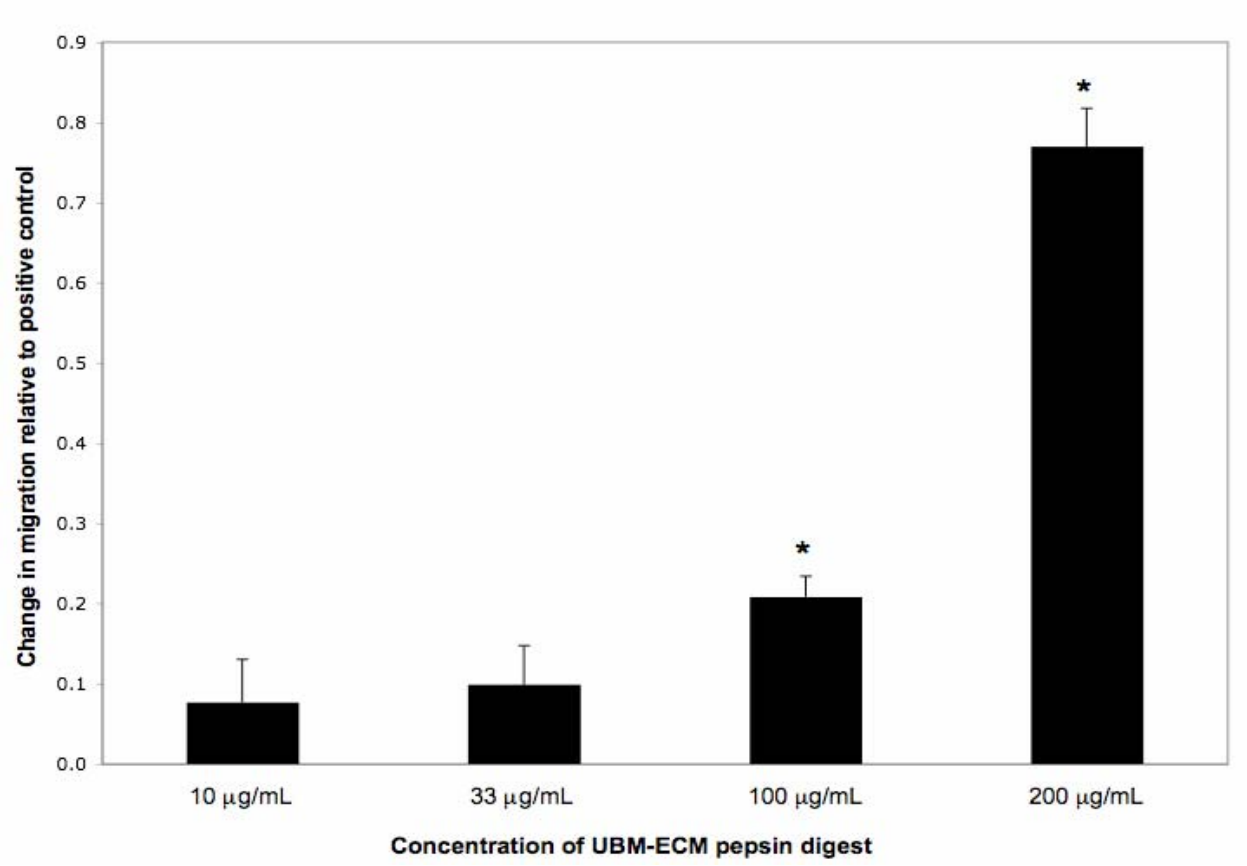

Figure 4. Chemoattractant activity of pepsin digest of UBM-ECM for MRL-B cells. Mean ± SEM (n = 2- 3 independent assays with samples tested in quadruplicate in each assay); * = p< 0.05 compared to pepsin control samples

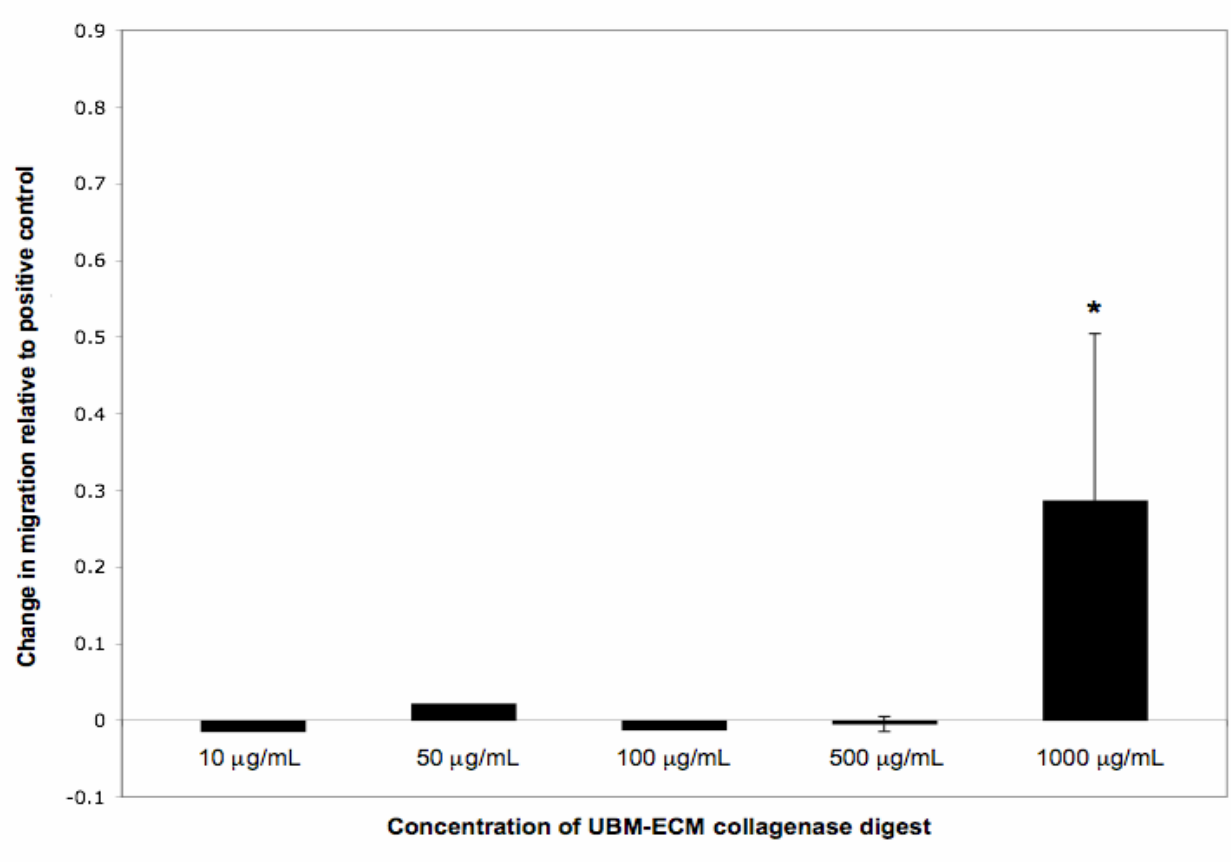

Figure 5. Chemoattractant activity of collagenase digest of UBM-ECM for MRL-B cells. Mean ± SEM (n = 1-2 independent assays with samples tested in quadruplicate in each assay); * = p< 0.05 compared to collagenase control sample

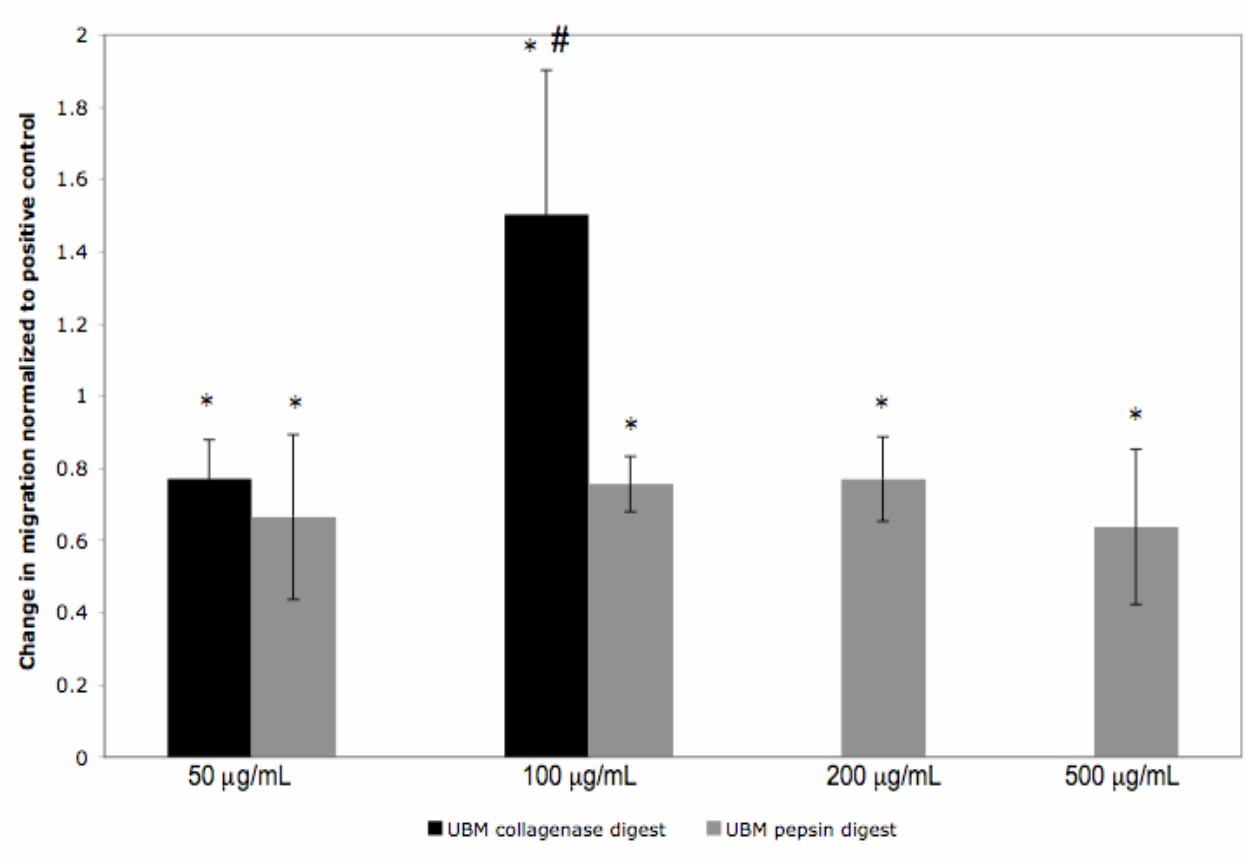

Figure 6. Chemoattractant activity of pepsin and collagenase digests of UBM-ECM for HEKn. Mean ± SEM (n = 3-5 independent assays with samples tested in quadruplicate in each assay); * = p< 0.05 compared to collagenase or pepsin control sample, # = p< 0.05 compared to UBM-ECM pepsin digest at 100 µg/mL

2.4 DISCUSSION

The present study demonstrates that molecules produced by degradation of UBM-ECM with either pepsin or collagenase have chemoattractant activity for two progenitor cell populations, a multipotential population of cells harvested from the healing ear of the MRL mouse and a population of human epidermal keratinocyte stem/progenitor cells. In addition, incubation of UBM-ECM in PBS or DMEM also resulted in the release of molecules that have chemoattractant

activity for multipotential cells harvested from the healing ear of the MRL mouse. These findings are an interesting corollary to an *in vivo* study that investigated the regenerative process that occurs in the MRL mouse ear, in which it was shown that basement membrane degradation occurred more rapidly in healing ears of MRL mice than in C57BL/6 mice and that MMP-2 and MMP-9 were upregulated in MRL mice compared to expression in C57BL/6 mice [80]. These results suggest that ECM degradation may be an important factor in this unique mammalian regenerative process, as well as in ECM scaffold induced constructive remodeling.

The pepsin digest of UBM-ECM showed chemoattractant activity for the MRL-B cells at a lower concentration than did the collagenase digest of UBM-ECM. In contrast, the collagenase digest of UBM-ECM showed stronger chemoattractant activity for the HEKn at one concentration than did the pepsin digest of UBM-ECM. These differences in chemoattractant activity hint at the complexities of the effects of the different molecules produced by different digestion methods on a given cell type, and also suggest that different progenitor cell populations respond differently to the same molecules. Similarly, a recent study has shown that UBM-ECM digested using pepsin or papain resulted in molecules that had chemoattractant activity for MRL-B cells but inhibited migration of several mature endothelial cell populations [68]. Pepsin digested UBM-ECM also enhanced proliferation of MRL-B cells and inhibited proliferation of mature endothelial cells [68]. Taken together, along with the observation from this study that UBM-ECM soaked in PBS released molecules with chemoattractant activity for multipotent cells, these *in vitro* results may partially explain some of the mechanisms that take place as degrading ECM scaffolds recruit cell populations that facilitate constructive remodeling *in vivo*.

We speculate that when an ECM scaffold is implanted, degradation molecules with chemoattractant activity for progenitor cells may be released by hydrolysis, and intact growth

factors within the ECM may be released as well. As host cells, including inflammatory cells, interact with the implanted ECM, the ECM is further degraded by various proteolytic enzymes, resulting in the release of different matricryptic molecules over time. Some of these matricryptic molecules may have chemoattractant activity for different cell populations that are thereby recruited to the site of ECM remodeling. Multipotent progenitor cells are among the recruited cells, originating both from the bone marrow and local tissue stem cell niches. Several studies have shown that stem and progenitor cells are able to proliferate in hypoxic environments [84-86], suggesting that recruited progenitor cells could proliferate at the site of ECM remodeling during the early stages, before the remodeled tissue becomes well vascularized. As tissue remodeling continues, the progenitor cells may differentiate into site appropriate cell types, as suggested in an *in vivo* mouse tendon repair study [19]. Also as the remodeling tissue matures, mature endothelial cells and other cell types may be recruited by matricryptic molecules and other signaling molecules (e.g., HIF-1, SDF-1, VEGF) present in the remodeling tissue milieu. Much remains to be determined about the specific molecules, the temporal patterns, and the mechanisms involved in these processes.

In vitro digestion of ECM using enzymatic methods such as pepsin or collagenase is more similar to the processes by which ECM is degraded *in vivo* than previous studies in which ECM was degraded *in vitro* using acid and extreme heat. Other more physiologic methods of *in vitro* degradation of ECM were examined in this study, including human white blood cell-mediated degradation and purified MMP-mediated degradation of UBM-ECM, but the results of these methods of degradation did not show positive chemotactic effects in this assay system. Of the two successful *in vitro* degradation methods described in this study, collagenase digestion is likely more physiologically relevant, but pepsin digests can be evaluated for *in vitro*

chemoattractant activity for keratinocyte stem/progenitor cells and likely other cell populations over a greater range of concentrations. In addition, pepsin digestion does not require the addition of other chemicals to quench the pepsin activity, which comparatively would simplify purification of the ECM digests and analysis of fractionated digests. Furthermore, cleavage of ECM molecules by pepsin digestion occurs at more specific amino acid locations than by collagenase digestion, which may be beneficial for long-term goals of identifying chemoattractant molecules with the ECM degradation products.

2.5 LIMITATIONS AND FUTURE WORK

This study investigated *in vitro* degradation of UBM-ECM using several methods, including pepsin, collagenase, a heterogeneous population of primary human white blood cells, CD14+ primary human white blood cells, and purified matrix metalloproteinases (MMP-2 and MMP-9). The white blood cell and purified MMP-mediated degradation methods did not show positive chemotactic results. Other enzymatic methods of *in vitro* degradation of UBM-ECM that would be interesting and physiologically relevant include other MMPs, elastase, lysozyme, and cysteine proteases such as cathepsin G, cathepsin K, caspases, and calpains. It would also be of interest to continue investigating human white blood cell-mediated degradation of ECM. In particular, much recent and ongoing work in our laboratory has shown polarization of macrophages toward M1 and M2 phenotypes in response to different biomaterials [87, 88]. It would be interesting to analyze the degradation products of UBM-ECM seeded with M1-polarized macrophages (or crosslinked UBM-ECM that drives macrophages toward an M1 phenotype) compared to degradation products of UBM-ECM seeded with M2-polarized macrophages.

In addition, the two progenitor cell populations that were investigated in this study showed slightly different migratory responses to the UBM-ECM degradation products. The addition of another progenitor cell population to the study would have been interesting. Human umbilical cord blood-derived multi-lineage progenitor cells (BioE, St. Paul, MN) were investigated in pilot studies, but it was challenging to obtain sufficient numbers of these cells for chemotaxis assays. Haptotactic and chemokinetic effects of the chemotaxis assay were not directly investigated in this study, and it is important to note that the chemoattractant activity of the ECM digests evaluated in the present study represent the net bioactivity of molecules present within each of the digests. This net effect of chemoattractant activity is logical and relevant from an *in vivo* injury repair perspective.

3.0 SPECIFIC AIM 2: TISSUE-SPECIFIC CHEMOATTRACTANT DEGRADATION PRODUCTS OF ECM

3.1 BACKGROUND

Biological scaffolds composed of naturally occurring extracellular matrix (ECM) have been successfully used as templates for the constructive remodeling of numerous tissues in preclinical studies and human clinical applications [1-12, 89]. The mechanisms by which ECM induces constructive remodeling are largely unknown, but it appears that the degradation products of ECM scaffolds play a key role in the cell recruitment and constructive remodeling effect [20-22, 68, 70]. ECM scaffolds that are not chemically crosslinked (e.g. not carbodiimide-treated) are rapidly degraded *in vivo* [14, 16, 41] and have been shown to recruit bone marrow-derived cells to the site of remodeling [18, 19]. These marrow-derived cells remain in the remodeling site beyond the time period of an expected inflammatory response, integrate into the remodeled tissue, and may differentiate into site-appropriate mature cell types [19].

Most, if not all, tissues and organs within the adult human body harbor multipotential stem and progenitor cell populations that are specific for the tissue or organ within which they reside. These tissue-specific stem and progenitor cells play important roles in tissue homeostasis and repair following injury, and are found within bone marrow, muscle, adipose tissue, lungs, liver, small intestine and skin, among other tissues [90-100]. Human keratinocyte stem and progenitor cells have been well characterized and numerous markers have been identified for

these cells, including keratinocyte stem and progenitor cell marker β1 integrin [101-104], keratinocyte stem cell markers cytokeratin 15 (CK15) [104-106] and cytokeratin 19 (CK19) [101, 107], as well as Rex-1, a putative human stem cell marker [83, 108, 109]. Liver stem and progenitor cells are thought to exist within the adult and fetal liver. Fetal liver progenitor cells have been isolated and shown to have bipotential capability of differentiating into hepatocytes and bile duct cells both *in vitro* and *in vivo* [110-113]. While consensus has not yet been reached on immunophenotypic markers of liver progenitor cells, many recent reports agree on epithelial cell adhesion molecule (EpCAM), CD44, and CK19 [114]. The small intestine has long been accepted to harbor a population of multipotent stem cells within the base of the intestinal crypts [115, 116]. The IEC-6 rat small intestinal epithelial cell line has been shown to have morphologic and immunochemical characteristics consistent with undifferentiated cells derived from the crypts of the small intestine [117], and several reports have used this cell line as a model small intestinal progenitor cell population [118-120].

Because ECM produced by the resident cells of each tissue is uniquely suited with regard to composition and structure for that particular tissue, the composition of ECM harvested from different tissues will vary [74, 121, 122]. It is logical and possible that ECM derived from a particular tissue may generate degradation products that recruit progenitor cells that are lineage-directed for that same tissue. Furthermore, it is known that fetal tissue has a greater regenerative capacity, particularly in skin wounds, than adult tissue [123]. Differences between fetal and adult wound healing are likely due to differences in both the cell population and the ECM [123].

The objective of the present study was to determine if degradation products of ECM scaffolds possess preferential chemoattractant activity for tissue-specific, lineage-directed progenitor cells derived from the same tissue type as that from which the ECM is prepared. The

effects of age and species of the tissue from which ECM is harvested on the chemoattractant activity of degradation products of ECM were also investigated. Skin and liver-derived ECM and progenitor cells were the main focus of this study, and the chemotactic response of small intestinal progenitor cells to digests of porcine small intestine, urinary bladder, and liver-derived ECM was also investigated. A diagrammatic overview of the types of cells and ECMs investigated in the chemotaxis studies is shown in Figure 7.

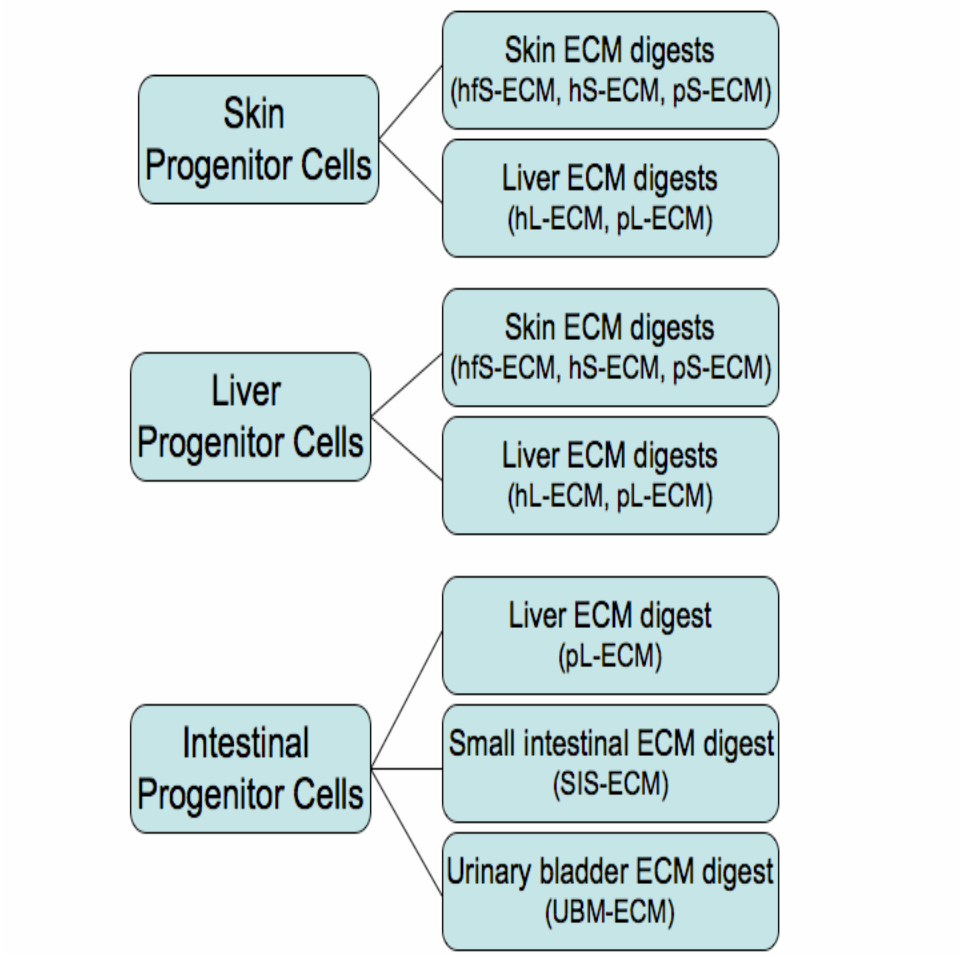

Figure 7. Overview of the types of cells and ECMs investigated in chemotaxis studies

3.2 MATERIALS AND METHODS

3.2.1 Response of skin and liver-derived progenitor cells to degradation products of skin and liver-derived ECM

3.2.1.1 Preparation of ECM from fetal and adult tissues Human fetal skin ECM (hfS-ECM) was prepared from fetal skin samples obtained from elective pregnancy termination at 18–23 weeks gestation, in a protocol approved by the University of Pittsburgh Institutional Review Board (IRB# 0504158). Fetal skin was immersed in water at 4ºC for 4–18h to facilitate the removal of excess connective tissue. The tissue was then placed in 0.02% trypsin (Sigma, St. Louis, MO)/0.05% ethylenediaminetetraacetic acid (EDTA; Sigma) at 37ºC for 1 h, then placed on a rocker in 3% v/v Triton-X (Sigma) at 4ºC for 48 h, and finally in 4% w/v deoxycholic acid (Sigma) at 4ºC for 24 h.

Human adult skin ECM (hS-ECM) was prepared from an adult skin sample obtained from elective surgery, in a protocol approved by the University of Pittsburgh IRB (IRB# 0511186). The skin was immersed in water at 4ºC for 4–18 h to facilitate the removal of excess connective tissue. The epithelium was removed from the skin sample and the remaining tissue was then placed in 0.02% trypsin/0.05% EDTA at 37ºC for 3 h, then placed on a rocker in 3% v/v Triton-X at 4ºC for 48 h, and finally in 4% w/v deoxycholic acid at 4ºC for 24 h. To remove adherent adipose tissue, the sample was incubated in 1-propanol (Sigma) for three 2 h washes on an orbital shaker at room temperature. The sample was then washed extensively in water to remove all traces of alcohol.

Porcine adult skin ECM (pS-ECM) was prepared from skin obtained from a local abattoir immediately after the death of pigs weighing approximately 100–120 kg. Connective tissue and the epithelium were removed from the skin samples and the remaining tissue was placed in

deionized water at 4ºC for 24 h. The tissue was then placed in 0.02% trypsin/0.05% EDTA at 37 ºC for 5 h, then placed on a rocker in 3% v/v Triton-X at 4◦C for 48 h, and finally in 4% w/v deoxycholic acid at 4ºC for 48 h.

Human liver was harvested from the cadaver of a 43-year-old male that died from cardiac arrest, in a protocol approved by the University of Pittsburgh IRB. Porcine livers were obtained from a local abattoir immediately after the death of pigs weighing approximately 100-120 kg. Porcine liver ECM (pL-ECM) and human liver ECM (hL-ECM) were prepared as previously described [74, 121]. Briefly, hL-ECM and pL-ECM were prepared by slicing lobes of liver to 3 mm thick sheets, then rinsing the sheets in deionized water with agitation on an orbital shaker for a total of three 20-minute rinses. Slices were then placed on a polypropylene mesh and subjected to uniform manual pressure to burst the hepatocytes. The tissue was returned to a flask and submerged in 0.02% trypsin/0.05% EDTA for 1 h at 37˚C, agitated at room temperature in 3% (v/v) Triton X-100 for 1 h, then in 4% (w/v) deoxycholic acid for 1 h. The tissue was rinsed with deionized water and massaged between each treatment step.

Following these processing steps, all ECMs were treated with 0.1% peracetic acid/4% ethanol for 2 h and rinsed with deionized water and phosphate-buffered saline (PBS). Complete decellularization was confirmed by both 4 -6-diamidino-2-phenylindole (DAPI) nuclear staining and hematoxylin and eosin (H&E) staining of 5 μm thick sections of the ECMs. The ECM sheets were then frozen and lyophilized. Lyophilized hS-ECM, pS-ECM, hL-ECM, and pL-ECM sheets were frozen and comminuted into a particulate form using a Waring commercial blender and Wiley Mill [75]. Due to quantitative limitations for hfS-ECM material and loss of material associated with use of the Wiley Mill, hfS-ECM was manually cut into small pieces.

3.2.1.2 Preparation of ECM degradation products Each type of ECM (hfS-ECM, hS-ECM, pS-ECM, hL-ECM, pL-ECM) was digested using pepsin. Particulate lyophilized ECM was added to 1 mg/ml pepsin (Sigma) in 0.01 N HCl for a final concentration of 10 mg ECM/ml suspension. The suspension was mixed on a stir plate at room temperature for 48 h, at which time no visible pieces of ECM remained. Pepsin control samples were prepared by mixing the pepsin digestion solution (1 mg/ml pepsin in 0.01 N HCl) at room temperature for 48 h.

3.2.1.3 SDS–PAGE analysis of ECM digests A bicinchoninic acid (BCA) assay (Pierce Biotechnology, Rockford, IL) was performed to estimate protein concentration of each type of ECM pepsin digest. Based on BCA assay results, uniform quantities of protein were loaded into each lane of a 12.5% polyacrylamide gel, with a prestained protein standard (Bio-Rad, Hercules, CA) in the range 15–250 kDa. The gel was subjected to a voltage of 80 V until the dye front entered the separating gel, then at a constant voltage of 100 V until the dye front reached the bottom of the gel. The gel was stained with Imperial Protein Stain (Pierce Biotechnology).

3.2.1.4 Culture and Characterization of HEKn Neonatal human epidermal keratinocytes (HEKn) were obtained from Cascade Biologics and cultured in EpiLife medium (Cascade Biologics, Portland, OR) supplemented with human keratinocyte growth supplement (HKGS; Cascade Biologics), yielding final supplemented medium concentrations of 0.2% v/v bovine pituitary extract, 5 μg/ml bovine insulin, 0.18 μg/ml hydrocortisone, 5 μg/ml bovine transferrin and 0.2 ng/ml human epidermal growth factor. HEKn were cultured according to the manufacturer's instructions under a humidified atmosphere in 95% air/5% CO_2 at 37ºC. Cells used in these studies were passage 4–7.

HEKn were plated into CultureSlides (BD Falcon, Franklin Lakes, NJ) and cultured as described above. The cells were fixed in 4% paraformaldehyde in PBS for 15 min and permeabilized in 0.1% Triton X-100 in PBS for 5 min (except the cells for β1 integrin staining), then blocked in 1% bovine serum albumin and 0.1% Tween 20 in PBS for 30 min at room temperature. The cells were then incubated with primary antibodies for 1 h at room temperature and subsequently incubated with Alexa Fluor 594- and/or Alexa Fluor 488-conjugated secondary antibodies (Molecular Probes, now a part of Invitrogen) for 1 h at room temperature. The cells were washed in PBS and mounted using Vectashield mounting medium containing DAPI to counterstain the nuclei (Vector Laboratories, Burlingame, CA), and examined using a Nikon Eclipse TE-2000-E fluorescence microscope and Nikon Elements Advanced Research quantitation software. For each primary antibody, the cells of 9–12 fields were photographed and counted. The primary antibodies used in this study were: rabbit anti-human Rex-1 antibody, raised in the Laboratory of Dr. Lorraine Gudas at Weill Medical College of Cornell University (1 : 10 dilution); mouse monoclonal anti-human CK15 and CK19 antibodies (1 : 200 dilution), purchased from Novocastra (Newcastle on Tyne, UK); and mouse monoclonal anti-human β1 integrin antibody (1 : 200 dilution) purchased from Chemicon (now a subsidiary of Millipore). Reported results are expressed as the mean and standard error of mean (SEM) of the percentage of cells staining positive for each antibody.

3.2.1.5 Chemotaxis assay with HEKn *In vitro* chemotaxis of HEKn toward ECM pepsin digests was evaluated using a 48-well micro-chemotaxis chamber (Neuro Probe, Gaithersburg, MD). When the HEKn reached 70–80% confluency, they were starved overnight in unsupplemented EpiLife medium before use in chemotaxis assays the following morning. Then the HEKn were

trypsinized, neutralized and centrifuged according to HEKn product instructions, resuspended in unsupplemented EpiLife medium and incubated in suspension for 1 h at 37ºC.

HEKn were first tested in this assay for chemotaxis in response to growth factors, including recombinant human epidermal growth factor (EGF) at 10, 50, and 100 ng/mL in unsupplemented EpiLife medium and transforming growth factor alpha (TGF-α) at 10 and 50 ng/mL in unsupplemented EpiLife medium. 10% HKGS was evaluated as a potential positive control sample in these assays. HEKn were then tested for chemotaxis in response to ECM degradation products. Pepsin digests of hfS-ECM, hS-ECM, pS-ECM, hL-ECM, and pL-ECM were diluted in unsupplemented EpiLife medium to concentrations of 100, 200, 500 and 1000 µg ECM digest/ml. A negative control for each sample was prepared by diluting the pepsin control sample in unsupplemented EpiLife medium at the same ratios as the ECM pepsin digest samples. A positive control of 10% HKGS in unsupplemented EpiLife medium was also included in each assay. Samples were loaded to the lower chamber of each well of the chemotaxis chamber. An 8 µm pore size polycarbonate filter coated with 0.05 mg/ml collagen I (BD Biosciences, San Jose, CA, USA) divided the lower and upper chamber of each well. Approximately 30,000 cells were added to the upper chamber of each well. The chemotaxis chamber was incubated at 37ºC for 3 h. Cells that had not migrated through the pores of the filter were removed and migrated cells on the bottom side of the filter were fixed, permeabilized and stained with DAPI.

Three random fields from each well, located in the upper left, upper right and lower central regions of the filter from each well were photographed at 200X magnification and migrated cells were counted from these fields, using ImageJ software. Samples were tested in quadruplicate for each chemotaxis assay performed. The percentage change in migrated cells in response to ECM pepsin digest samples compared to negative control samples was calculated for

each assay performed. To compare results between different independent assays, the percentage change was normalized by the percentage change induced by the positive control for each assay. Reported results are expressed as mean and standard error of the mean (SEM) of percentage change in migration normalized by positive control from four assays (n = 4 independent assays, with samples run in quadruplicate, for n = 16 samples tested). The statistical significance of the difference between human fetal skin ECM pepsin digest and all adult ECM pepsin digest sample values was determined by one-way ANOVA with $\alpha = 0.05$ followed by post-hoc Tukey's test with $\alpha = 0.05$. The statistical significance of the difference between adult skin and liver ECM pepsin digest sample values and the statistical significance of the difference between adult porcine and human ECM pepsin digest sample values were determined by Student's t-test with $\alpha = 0.05$.

3.2.1.6 Culture and characterization of human fetal liver cells Primary cells were isolated from human fetal livers at 16-18 weeks gestation by 1 mg/ml collagenase II + 1 mg/ml of hyaluronidase treatment followed by 0.05% trypsin/EDTA, and cultured on a rat epithelial feeder layer. The mammary tumor cell line, LA7 (ATCC® number CRL-2283™), was used as a feeder layer. Only epithelial cells from primary tissue expand on these feeder cells [124]. The LA7 cell line was grown in DMEM/F-12 supplemented with 5% heat inactivated fetal calf serum (HI-FCS), 1% penicillin/streptomycin, 50 nM hydroxycortisone, and 5 μg/ml insulin in a humidified atmosphere in 95% air/5% CO2 at 37ºC. Upon confluence, the cells were trypsinized with 0.05% trypsin/EDTA and γ-irradiated at 17,000 rads to render the cells mitotically inactive. Cell culture flasks were then seeded at an approximate density of 70,000 cells/mm2 to generate a monolayer of feeder cells. Primary human fetal liver cells were grown on these feeder layers with DMEM/F-12 supplemented with 0.5% HI-FCS, 25 μg/ml gentamicin and 1% insulin-transferrin

supplement (ITS). After roughly 2 passages, the cells were stained with CD26-PE (DPPIV) and CD227-FITC (MUC1). CD26+CD277+ cells were sorted with a BD FACSVantageSE Cell Sorter. CD26 is considered to a hepatocyte marker, while CD227, is considered a biliary marker. CD26+CD227+ cells were expanded on the LA7 feeder cell layer as described previously. Flow cytometric analyses at later passages have shown that these cells have a stable CD26+CD227+ phenotype. These cells were also shown to express the candidate liver stem cell marker EpCAM and the mesenchymal stem cell marker CD73. The cells are negative for expression of candidate liver stem cell marker CD49f [125]. Cells used in these studies were passages 5-7 after the CD26/CD227 sort.

3.2.1.7 Chemotaxis assay with human fetal liver cells *In vitro* chemotaxis of human fetal liver cells toward ECM pepsin digests was evaluated using a 48-well micro chemotaxis chamber. When human fetal liver cells reached 80-90% confluency, they were starved overnight in serum-free DMEM before use in chemotaxis assays the following morning. The human fetal liver cells were then trypsinized, neutralized, resuspended in serum-free DMEM, and incubated in suspension for one hour at 37ºC.

Pepsin digests of hfS-ECM, hS-ECM, pS-ECM, hL-ECM, and pL-ECM were diluted in serum-free DMEM to concentrations of 100, 500 and 1000 μg ECM digest/ml. A negative control for each sample was prepared by diluting the pepsin control sample in serum-free DMEM at the same ratios as the ECM pepsin digest samples. A positive control of 10% heat inactivated FCS in serum-free DMEM was also included in each assay. Samples were loaded to the lower chamber of each well of the chemotaxis chamber. A 12 μm pore size polycarbonate filter coated with 0.01 mg/ml fibronectin (Sigma) divided the lower and upper chamber of each well. Approximately 60,000 cells were added to the upper chamber of each well. The chemotaxis

chamber was incubated at 37ºC for 6 h. Cells that had not migrated through the pores of the filter were removed and migrated cells on the bottom side of the filter were fixed, permeabilized and stained with DAPI.

Three random fields from each well, located in the upper left, upper right and lower central regions of the filter from each well were photographed at 200X magnification and migrated cells were counted from these fields, using ImageJ software. Samples were tested in quadruplicate for each chemotaxis assay performed. The percentage change in migrated cells in response to ECM pepsin digest samples compared to negative control samples was calculated for each assay performed. To compare results between different independent assays, the percentage change was normalized by the percentage change induced by the positive control for each assay. Reported results are expressed as mean and SEM of percentage change in migration normalized by positive control. Results are from two to five assays (n = 2-5 independent assays, with samples run in quadruplicate, for n = 8-20 samples tested), with the exceptions of hS-ECM and pS-ECM at 1000 μg/mL, which were tested in one assay (n = 1 independent assay with samples run in quadruplicate, for n = 4 samples tested). The statistical significance of the difference in values between samples was determined by one-way ANOVA with $\alpha = 0.05$.

3.2.2 Response of intestinal progenitor cells to degradation products of porcine adult ECM

3.2.2.1 Preparation of ECM from small intestine, urinary bladder and liver Porcine adult urinary bladder matrix (UBM-ECM) was prepared as previously described [74]. In brief, urothelial cells were removed by soaking the urinary bladders in 1.0 N saline. Connective and adipose tissue were removed from the serosal surface of the urinary bladder, and the tunica serosa, tunica muscularis externa, tunica submucosa, and most of the tunica muscularis mucosa

were mechanically removed, leaving a biomaterial composed of only the basement membrane and the subjacent tunica propria of the tunica mucosa. Porcine adult small intestinal submucosa (SIS-ECM) was prepared as previously described [1, 126]. In brief, the mesenteric tissues were removed from the small intestine and after rinsing, the tunica serosa, tunica muscularis externa, and the luminal portion of the tunica mucosa including most of the lamina propria were mechanically removed. The remaining layers of the tunica submucosa and basilar portion of the tunica mucosa, including the muscularis mucosa and the stratum compactum of the lamina propria, represented SIS. Porcine adult liver ECM (pL-ECM) was prepared as described in section 3.2.1.1.

Decellularization of all ECMs was completed by treatment with 0.1% peracetic acid/4% ethanol for two hours followed by rinsing with PBS and deionized water. Complete decellularization was confirmed by both DAPI nuclear staining and H&E staining. The UBM-ECM, SIS-ECM, and pL-ECM were then lyophilized in sheet form, frozen, and comminuted into a particulate form using a Wiley Mill with a #60 mesh screen [75].

3.2.2.2 Preparation of ECM degradation products Each type of ECM (UBM-ECM, SIS-ECM, pL-ECM) was digested using pepsin. Particulate lyophilized ECM was added to 1 mg/ml pepsin (Sigma) in 0.01 N HCl for a final concentration of 10 mg ECM/ml suspension. The suspension was mixed on a stir plate at room temperature for 48 h, at which time no visible pieces of ECM remained. Pepsin control samples were prepared by mixing the pepsin digestion solution (1 mg/ml pepsin in 0.01 N HCl) at room temperature for 48 h.

3.2.2.3 Culture of rat small intestinal epithelial cells The IEC-6 rat small intestinal epithelial cell line was obtained from the American Type Culture Collection (ATCC, Manassas, VA). IEC-6 cells were cultured in DMEM supplemented with 5% fetal calf serum, 1X

penicillin/streptomycin, 2.5 μg/ml gentamicin, and 0.1 U/ml bovine insulin (DMEM-IEC6) under a humidified atmosphere in 95% air/5% CO_2 at 37ºC. Cells used in these studies were passage 26 and 27.

3.2.2.4 Chemotaxis assay with rat small intestinal epithelial cells *In vitro* chemotaxis of IEC-6 cells toward ECM pepsin digests was evaluated using a 48-well micro chemotaxis chamber. When IEC-6 cells reached 70-80% confluency, they were starved overnight in serum-free unsupplemented DMEM (DMEM-SF) before use in chemotaxis assays the following morning. Then, IEC-6 cells were trypsinized, neutralized, centrifuged, resuspended in DMEM-SF, and incubated in suspension for one hour at 37ºC.

Pepsin digests of UBM-ECM, SIS-ECM, and pL-ECM were diluted in DMEM-SF to a concentration of 500 μg ECM digest/mL. A negative control sample was prepared by diluting the pepsin digestion solution in DMEM-SF at the same ratio as the ECM pepsin digest samples. A positive control of DMEM-IEC6 was also included in each assay. Samples were loaded to the lower chamber of each well of the chemotaxis chamber. An 8 μm pore size polycarbonate filter coated with 0.05 mg/ml collagen I divided the lower and upper chamber of each well. Approximately 30,000 cells were added to the upper chamber of each well. The chemotaxis chamber was incubated at 37ºC for 3 hours. Cells that had not migrated through the pores of the filter were removed and migrated cells on the bottom side of the filter were fixed, permeabilized, and stained with DAPI.

Three random fields from each well, located in the upper left, upper right and lower central regions of the filter from each well were photographed at 200X magnification and migrated cells were counted from these fields, using ImageJ software. Samples were tested in quadruplicate for each chemotaxis assay performed. Reported results are expressed as the mean

and standard deviation of migrated cells from one representative assay (n=4 samples tested) of two assays performed. Statistical significance of the difference in values between samples was determined by one-way ANOVA with $\alpha = 0.05$ followed by post-hoc Tukey's test with $\alpha = 0.05$.

3.3 RESULTS

SDS–PAGE analysis of hfS-ECM, hS-ECM, pS-ECM, hL-ECM, and pL-ECM digests (Figure 8) showed that all five ECM digests contained numerous peptides in the size range 15–250 kDa. Certain peptides appeared to be present in all five ECM digests, while others were only present in one type of ECM digest, suggesting that there were variations in molecules released by pepsin digestion of the different ECMs. Bands that were present in all five ECM digests showed different intensities, suggesting quantitative differences between the amounts of the respective molecules.

HEKn in culture were found to express human Rex-1 [83, 108, 109], CK15 [104-106] and CK19 [101, 107] mRNA (Figure 9), markers known to be present in keratinocyte stem cell populations. Fluorescent immunolabeling demonstrated that Rex-1 signal was present in both the cytoplasm and the nucleus of HEKn, and the Rex-1 signal in the nucleus was greater than that in the cytoplasm (Figure 10A). CK15 and CK19 signals were detected in the cytoplasm of HEKn (Figure 10B, C). β1 integrin, a cell surface marker found on both skin stem cells and progenitor cells [101, 102, 104, 127], was present in the cytoplasmic membrane of HEKn (Figure 10D). Quantification of the fluorescently immunolabeled cell populations showed that 100% of HEKn stained positively for β1 integrin (Figure 11). Approximately 26% of HEKn stained positively for Rex-1 and CK15 and approximately 12% of HEKn stained positively for CK19 (Figure 11).

CK15 and CK19 were often co-localized with Rex-1. These results indicate that the HEKn population used in chemotaxis assays consisted of approximately 26% keratinocyte stem cells, and that the remainder were more differentiated skin progenitor cells.

In vitro chemotaxis assays using HEKn showed that a significantly higher number of cells migrated in response to EGF at 10, 50, and 100 ng/mL and TGF-α at 10 and 50 ng/mL than in response to the negative control of unsupplemented EpiLife medium (Figure 12). 10% HKGS also significantly increased HEKn migration compared to the negative control.

Pepsin-digested hfS-ECM showed strong, dose dependent chemoattractant activity for HEKn. A >500% increase in HEKn migration was observed at 1000 μg/ml hfS-ECM pepsin digest compared to the negative control (Table 3).

Pepsin digests of porcine skin and porcine liver ECM showed significant chemoattractant activity for HEKn at 200, 500, and 1000 μg/ml, however there were no differences between the chemoattractant activity of the porcine skin and porcine liver ECM digests (Figure 13). Pepsin digests of human skin and human liver ECM did not show chemoattractant activity for HEKn, however at 1000 μg/ml the human skin ECM digest showed significantly less inhibition of HEKn migration than human liver ECM digest ($p<0.05$, Figure 13). Pepsin-digested hfS-ECM showed significantly stronger chemoattractant activity for HEKn than hS-ECM pepsin digest at 200 μg/ml, significantly stronger chemoattractant activity than all other ECM digests at 500 μg/ml, and significantly stronger chemoattractant activity than hS-ECM, pS-ECM, and hL-ECM pepsin digests at 1000 μg/mL ($p<0.05$, Figure 13). pS-ECM pepsin digest showed significantly stronger chemoattractant activity than hS-ECM pepsin digest at 200, 500 and 1000 μg/ml ($p<0.05$, Figure 13). pL-ECM pepsin digest showed significantly stronger chemoattractant activity than hL-ECM at 500 and 1000 μg/ml ($p<0.05$, Figure 13).

Migrated and fixed HEKn on chemotaxis chamber filters were fluorescently immunolabeled for Rex-1, CK15 and CK19. Nearly all HEKn that had migrated in response to hfS-ECM pepsin digest stained positive for Rex-1, CK15 and CK19, suggesting that hfS-ECM was particularly chemoattractant for keratinocyte stem cells compared to keratinocyte progenitor cells (Figure 14).

All skin and liver ECM digests tested showed chemoattractant activity for human fetal liver cells (Figure 15). There appeared to be a trend of hfS-ECM pepsin digest showing stronger chemoattractant activity than the other ECM digests at 100 and 500 μg/mL, but ANOVA results showed that there were no significant differences between the chemoattractant activity of the different skin and liver ECM digests for the human fetal liver cells at any of the concentrations tested.

The 500 μg/mL pepsin digests of UBM-ECM and SIS-ECM showed significant chemoattractant activity for IEC-6 cells ($p<0.05$, Figure 16), while the 500 μg/mL pepsin digest of pL-ECM did not significantly increase IEC-6 cell migration compared to negative control (Figure 16). The number of IEC-6 cells that migrated in response to the SIS-ECM digest was not significantly different from the number of cells that migrated in response to the UBM-ECM digest.

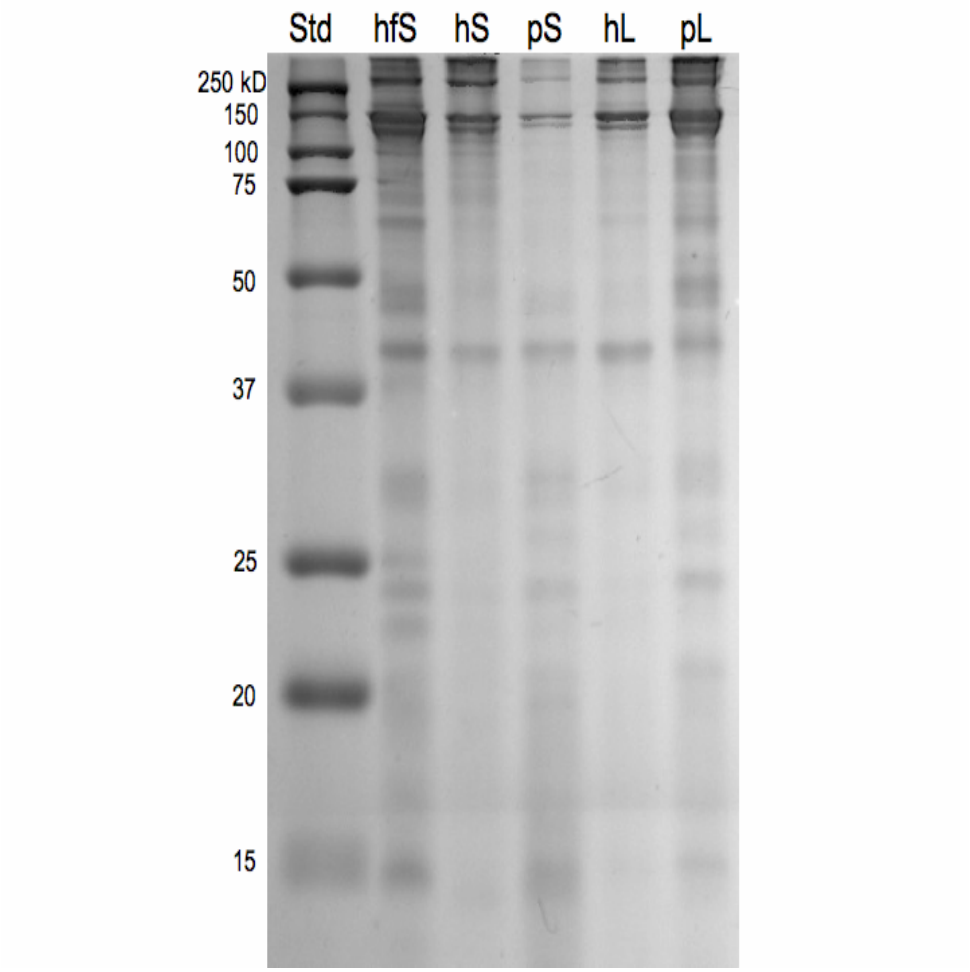

Figure 8. Pepsin digests of human fetal skin ECM (hfS), human adult skin ECM (hS), porcine adult skin ECM (pS), human adult liver ECM (hL), and porcine adult liver ECM (pL) were separated on 12.5% SDS-PAGE. Protein bands were visualized by Imperial protein stain and photographed.

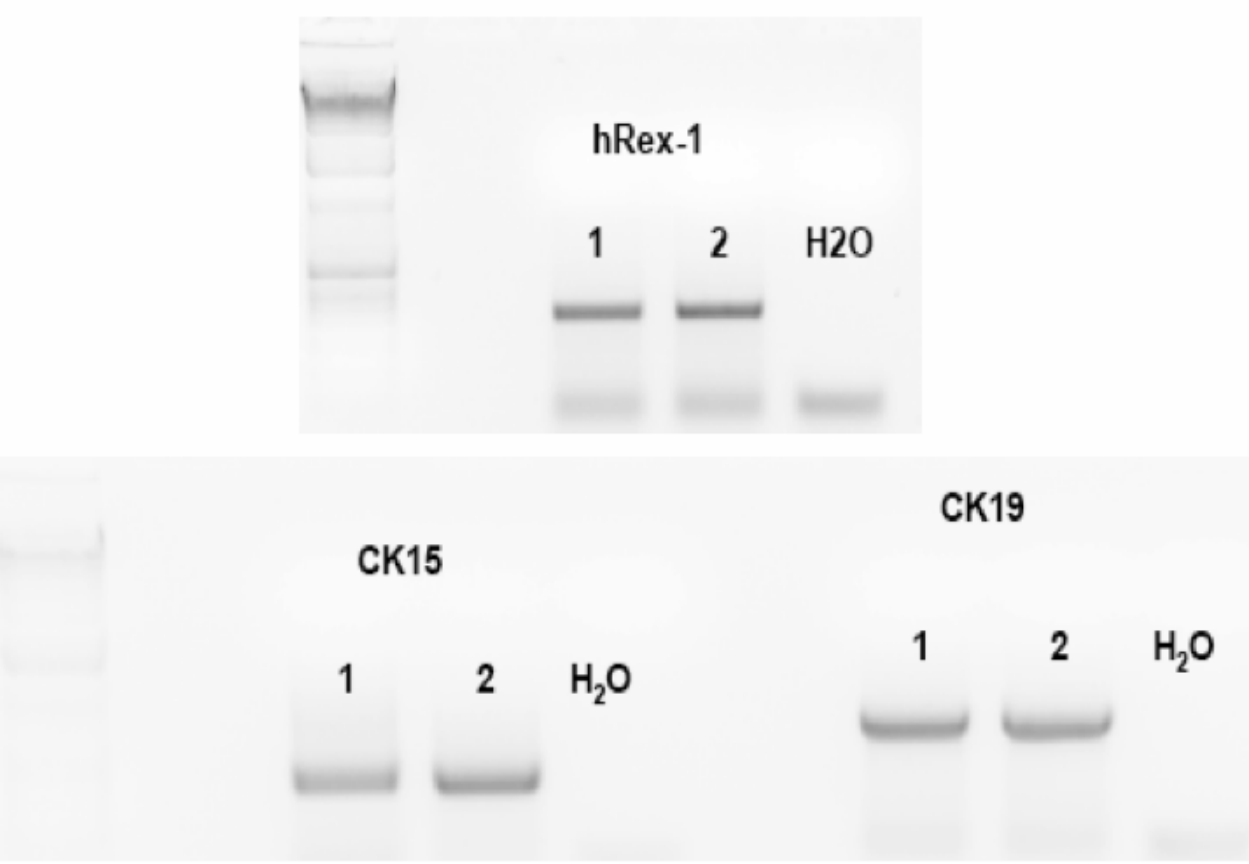

Figure 9. mRNA expression of human Rex-1, cytokeratin 15 (CK15), and cytokeratin 19 (CK19) in cultured HEKn by RT-PCR analysis

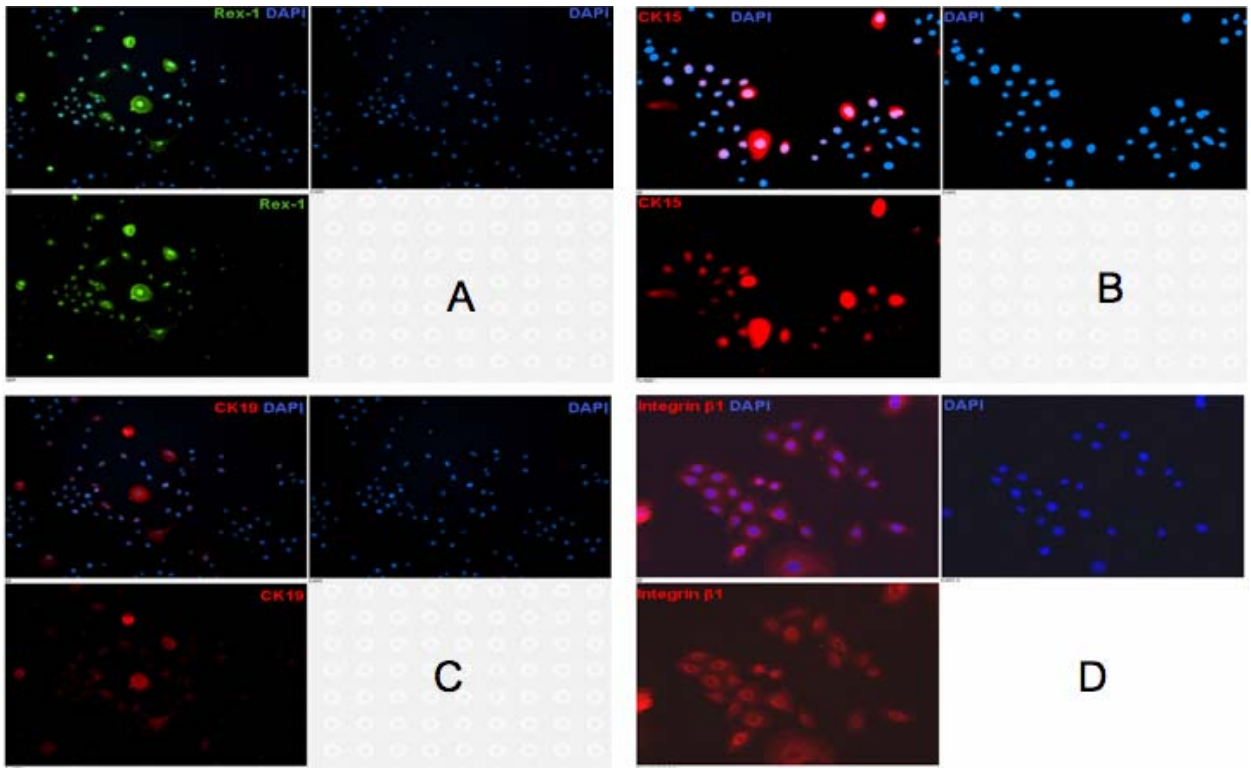

Figure 10. Fluorescent immunolabeling of cultured HEKn for: (A) Rex-1; (B) cytokeratin 15 (CK15); (C) cytokeratin 19 (CK19); (D) β1 integrin

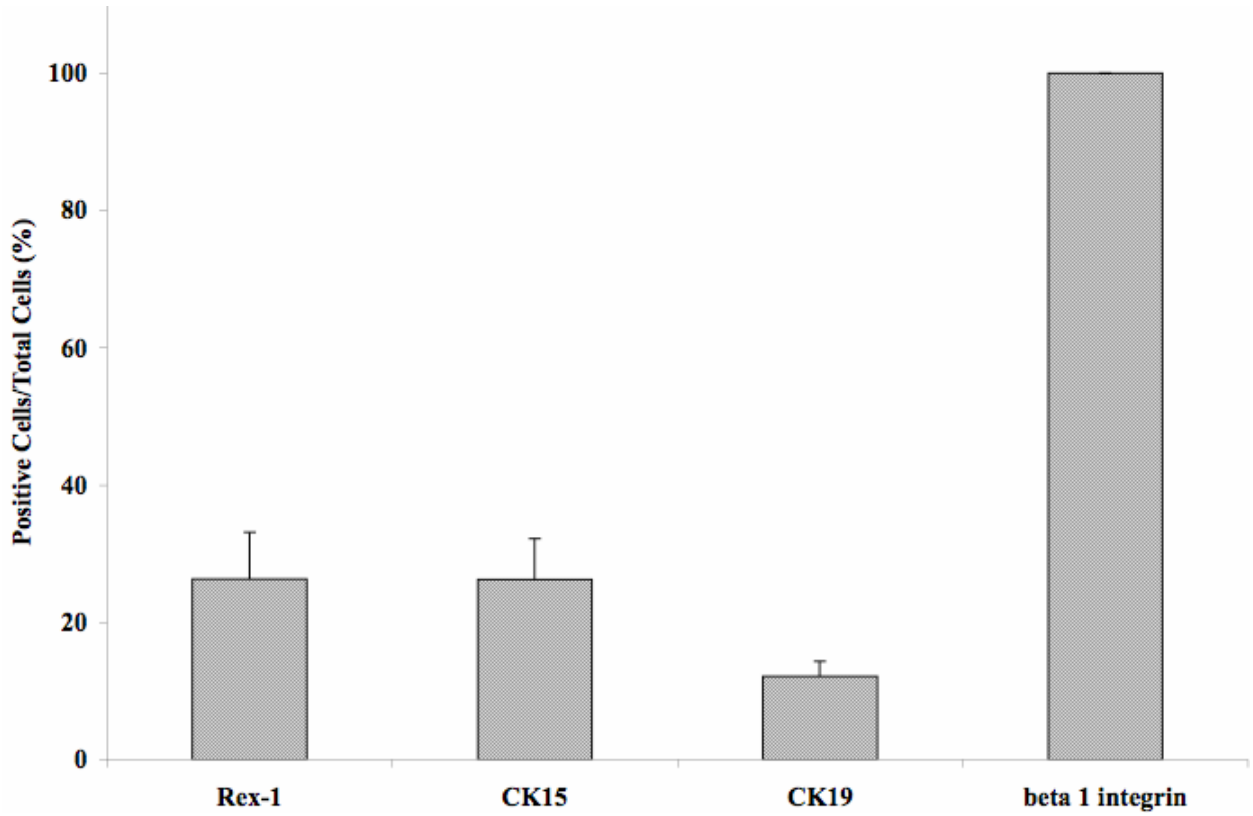

Figure 11. Quantification of HEKn staining positive for Rex-1, CK15, CK19 and β1 integrin. Mean ± SEM (n = 9-12). No error bars are shown for β1 integrin because 100% of HEKn stained positive in all photographed fields.

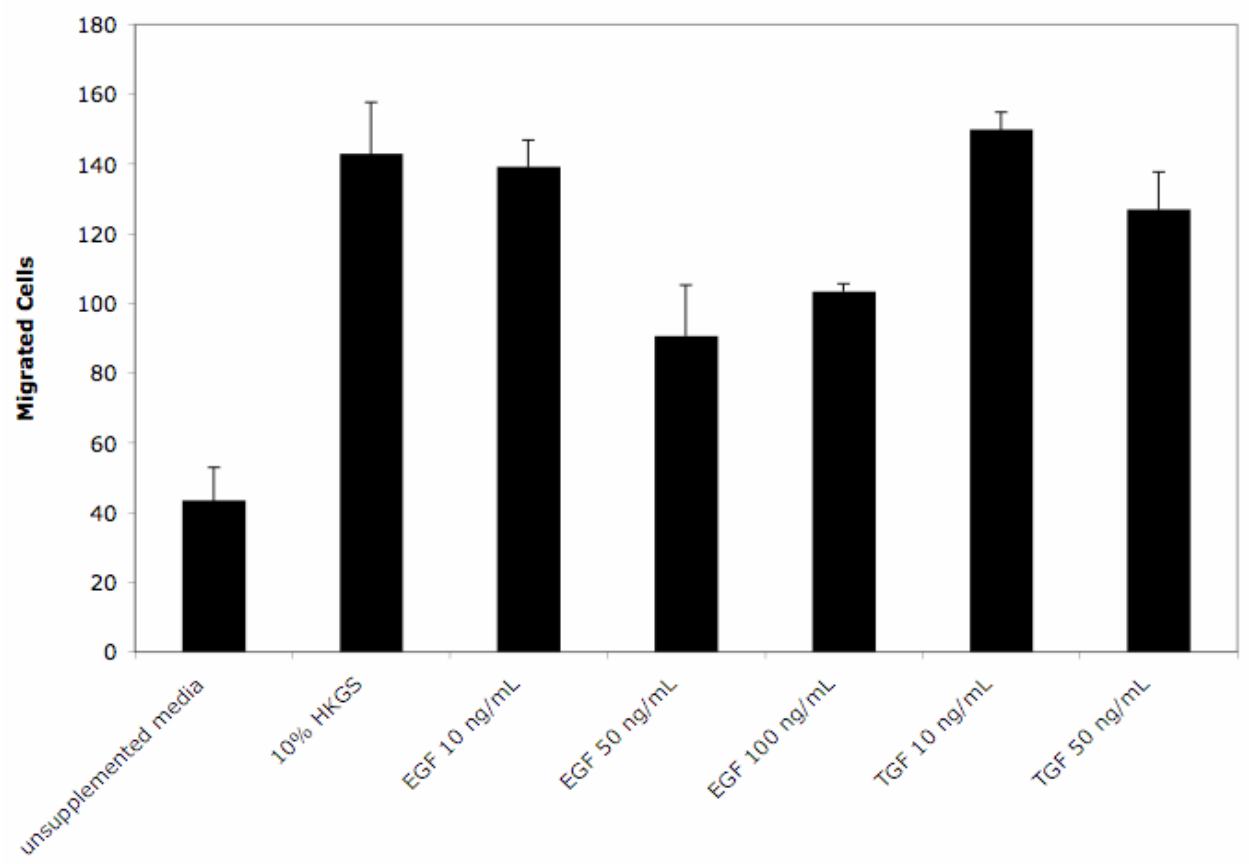

Figure 12. Migration of HEKn in response to unsupplemented EpiLife medium (negative control) and EpiLife medium containing human keratinocyte growth supplement, EGF, or TGF-α . Mean ± standard deviation (n = 4). Equivalent trends were observed on three further occasions.

Table 3. Summary of data from one representative HEKn chemotaxis assay, including number of migrated cells for each sample tested in quadruplicate, mean of migrated cells, standard error of the mean (SEM), p value from a t-test comparing each sample to its negative control, and calculated percentage change in migrated cells for each sample compared to its negative control

Sample	Migrated Cells				Mean	Standard Error	p-value	% Change from Negative Control
10% HKGS	133	146	112	100	123	10.3	0.000	485
EpiLife medium	29	19	22	14	21	3.1	--	--
100 μg/mL hfS-ECM digest	19	18	27	30	24	3.0	0.019	68
Pepsin control for 100 μg/mL hfS-ECM digest	8	15	16	17	14	2.0	--	--
200 μg/mL hfS-ECM digest	33	39	22	18	28	4.8	0.016	96
Pepsin control for 200 μg/mL hfS-ECM digest	14	14	17	12	14	1.0	--	--
500 μg/mL hfS-ECM digest	26	49	28	30	33	5.3	0.001	393
Pepsin control for 500 μg/mL hfS-ECM digest	6	6	8	7	7	0.5	--	--
1000 μg/mL hfS-ECM digest	35	39	19	35	32	4.4	0.000	540
Pepsin control for 1000 μg/mL hfS-ECM digest	6	4	6	4	5	0.6	--	--

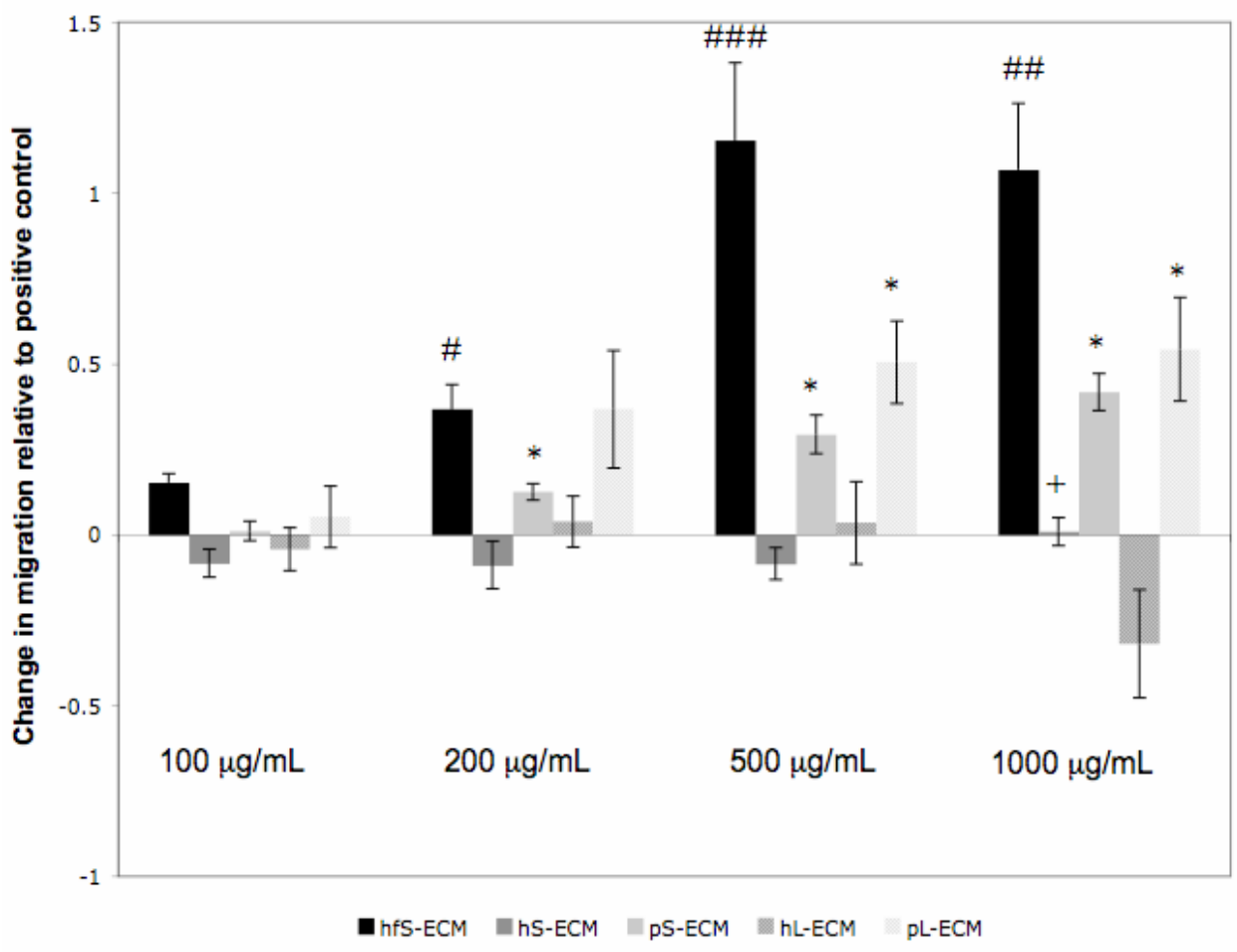

Figure 13. Chemoattractant activity of pepsin digests of hfS-ECM, hS-ECM, pS-ECM, hL-ECM and pL-ECM for HEKn. Mean ± SEM (n=4 independent assays with samples tested in quadruplicate in each assay); # = p< 0.05 versus hS-ECM, ## = p<0.05 versus hS-ECM, pS-ECM, hL-ECM, ### = p<0.05 versus all other ECMs, * = p<0.05 versus same tissue from other species, + = p<0.05 versus different tissue from same species

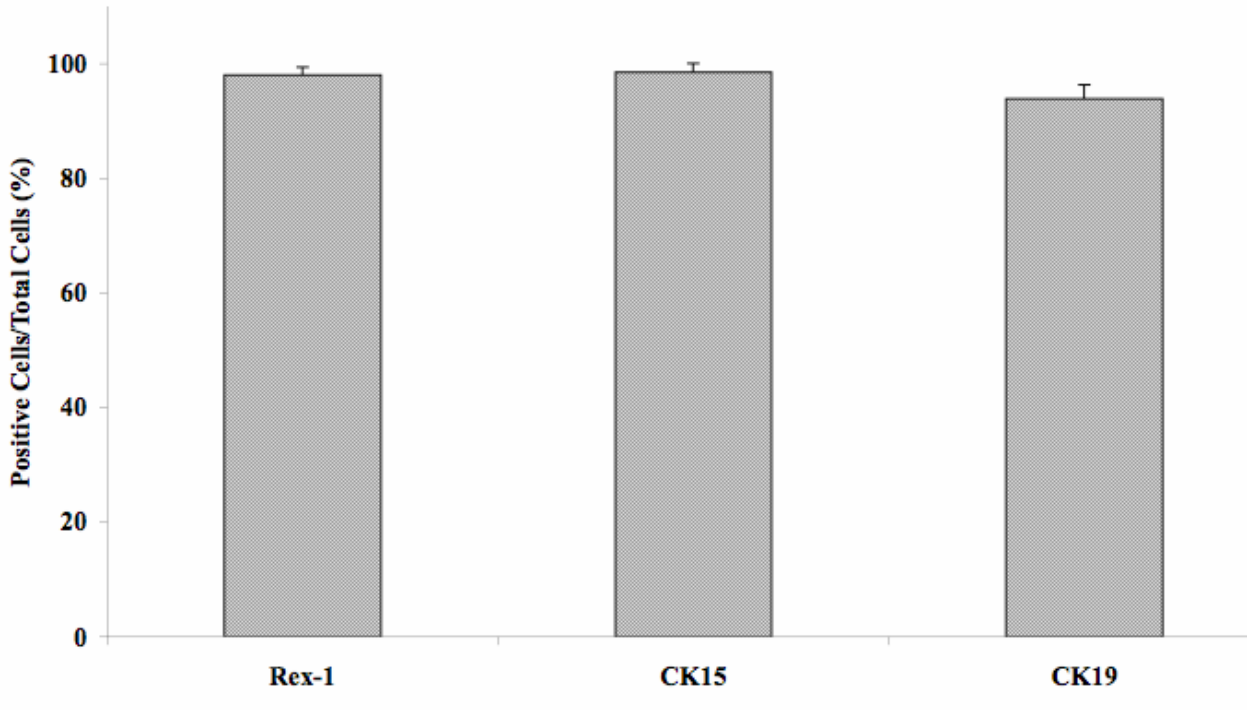

Figure 14. Quantification of positive staining for keratinocyte stem cell markers on HEKn that had migrated in response to hfS-ECM pepsin digest. Mean ± SEM (n=5-6)

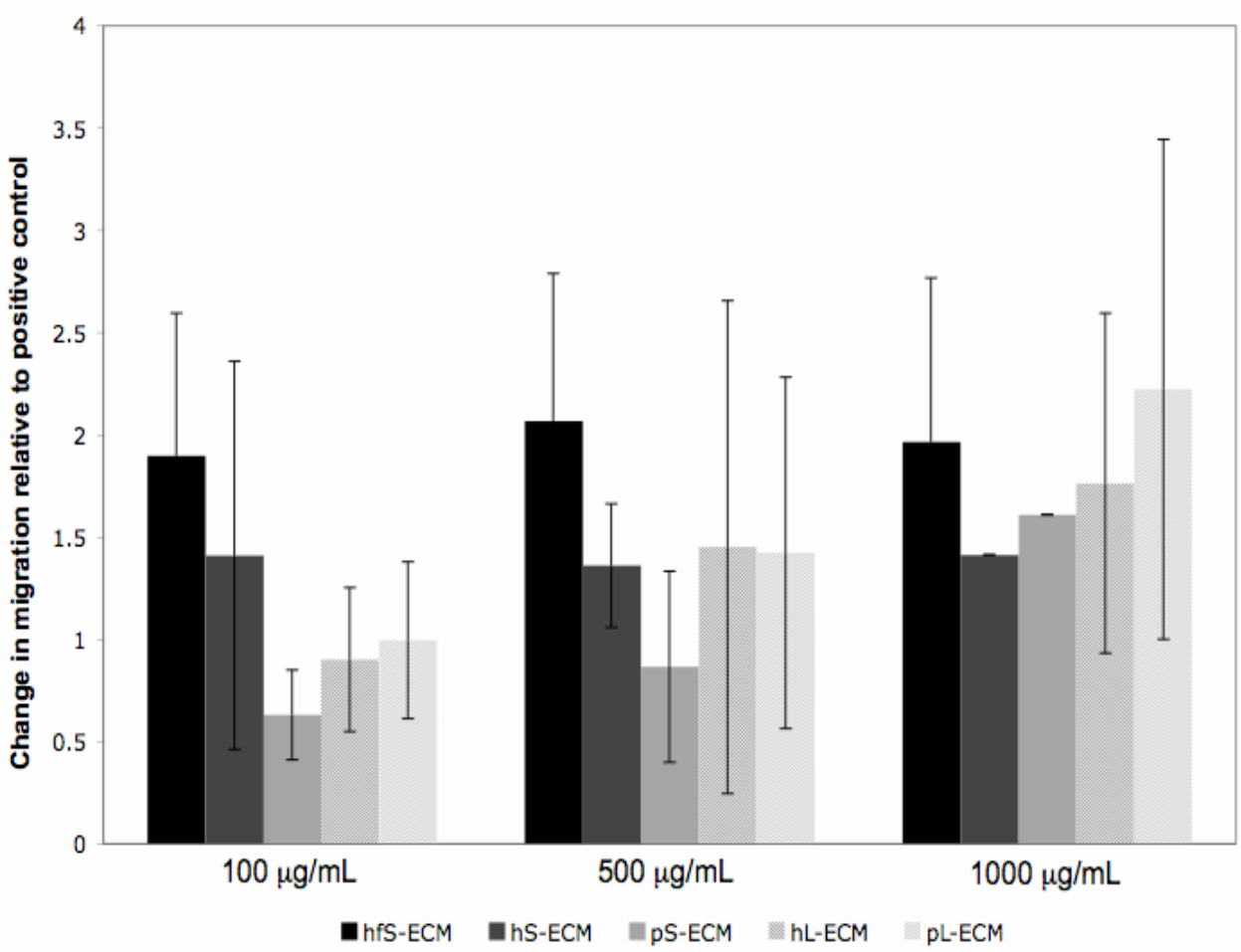

Figure 15. Chemoattractant activity of pepsin digests of hfS-ECM, hS-ECM, pS-ECM, hL-ECM and pL-ECM for human fetal liver cells. Mean ± SEM (n=1-5 independent assays with samples tested in quadruplicate in each assay); there were no statistical differences between the different ECMs.

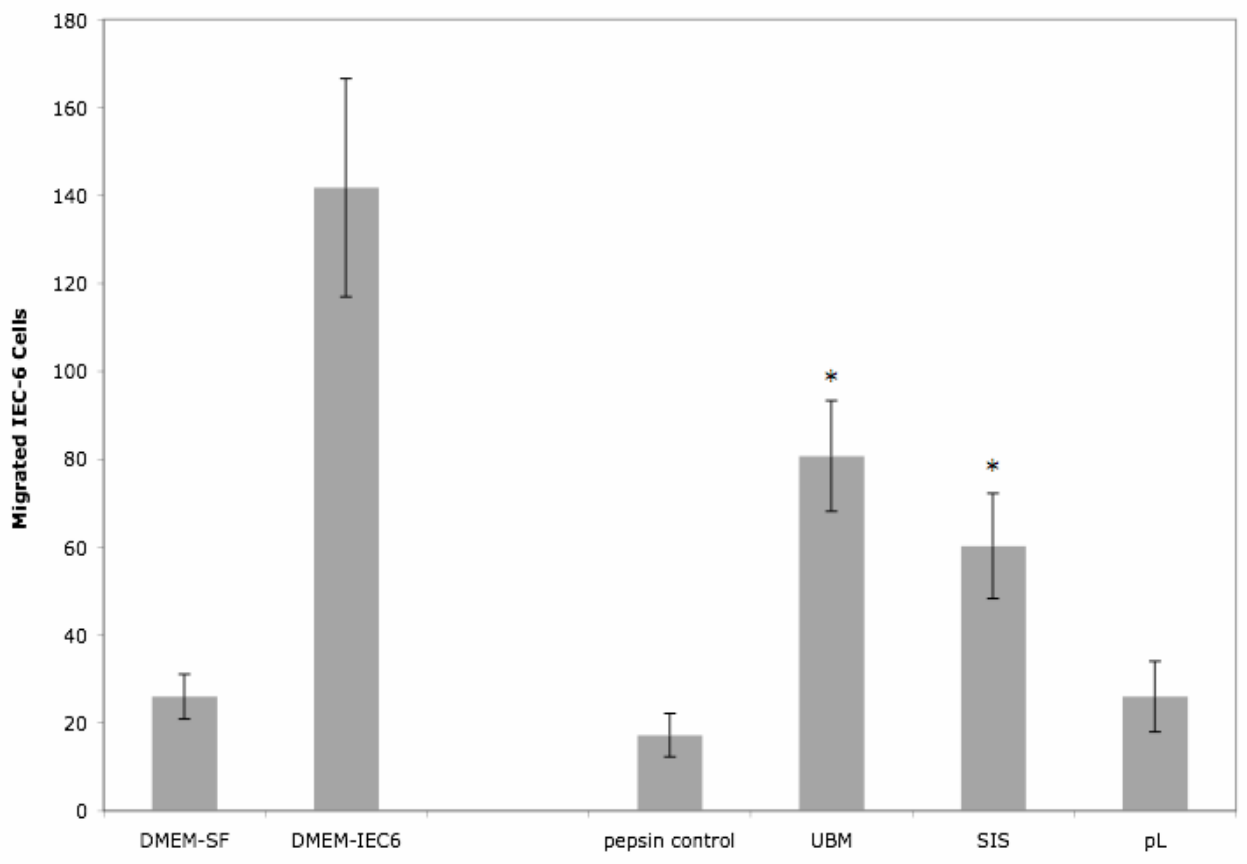

Figure 16. Chemoattractant activity of pepsin digests of UBM-ECM, SIS-ECM, and pL-ECM at 500 μg/mL for IEC-6 cells. Number of migrated cells ± standard deviation (n=4); * = $p<0.05$ versus pepsin control. Equivalent trends were observed on one further occasion.

3.4 DISCUSSION

The present study demonstrates that the degradation products of human fetal skin-derived ECM possess stronger chemoattractant activity for skin-specific lineage-directed stem and progenitor cells than do the degradation products of porcine adult skin, porcine adult liver, human adult skin, and human adult liver-derived ECM. Interestingly, the cells that migrated in response to the

degradation products of human fetal skin-derived ECM were enriched for keratinocyte stem cells, suggesting that these molecules were particularly chemoattractant for keratinocyte stem cells compared to keratinocyte progenitor cells. In addition, the degradation products of porcine adult skin and liver-derived ECM showed stronger chemoattractant activity for skin-specific lineage-directed stem and progenitor cells than did the degradation products of human adult skin and liver-derived ECM. There were no significant differences in chemoattractant activity between degradation products of porcine adult skin and porcine adult liver-derived ECM for skin-specific stem and progenitor cells. These results suggest that ECM degradation products from younger tissue sources may have more potent chemoattractant activity for local tissue stem or progenitor cells than older tissue sources, and that the species of the tissue source also has an effect on chemoattractant activity.

All of these degradation products of skin and liver-derived ECM showed chemoattractant activity for a candidate liver progenitor cell population, but there were no significant differences in the chemoattractant activity between the different tissue sources for the ECMs for this cell population. Degradation products of ECM derived from the adult porcine small intestine and urinary bladder showed chemoattractant activity for small intestinal progenitor cells, but there were no significant differences in the chemoattractant activity between the different tissue sources for the ECMs for the small intestinal progenitor cell population. The present study suggests that pepsin digests of skin, liver, and small intestinal ECM do not have preferential chemoattractant properties for progenitor cells derived from their respective tissue. However, for some lineage-directed progenitor cell populations, the age and species of the tissue from which ECM is harvested appear to have a greater effect on chemoattractant activity than tissue type.

The early gestation (<24 weeks) human fetus, unlike the later-gestation fetus or adult, is able to heal incisional skin wounds without scarring [128]. This scarless wound-healing ability of fetal skin may be due to the fetal cells and/or the fetal ECM. Fetal platelets, inflammatory cells and fibroblasts all demonstrate differences from their adult counterparts that may contribute to the scarless wound-healing phenomenon. Fetal ECM contains a higher proportion of type III collagen and a greater concentration of hyaluronic acid than the ECM of adult skin. Unwounded fetal skin at gestational ages associated with scarless wound healing has also been shown to express low levels of TGFβ1, high levels of TGFβ3 and increased expression of matrix metalloproteinases, a family of proteases associated with ECM degradation and remodeling [123]. Although the present study does not address the relative contribution of cells vs. ECM to scarless fetal wound healing, it appears clear that the ECM, which represents the secreted product of local cells, contains signaling molecules that can affect stem and progenitor cell activity such as chemotaxis.

ECM scaffolds implanted *in vivo* in preclinical studies have been shown to result in constructive remodeling, promote angiogenesis and resist bacterial infection [21, 24, 64, 65, 129]. *In vitro* studies have shown that degradation of ECM derived from several tissues generates low molecular weight peptides with biological properties such as chemotactic, angiogenic and antimicrobial activity [20-22]. In contrast, intact ECM does not possess such activity [69], suggesting that these biological activities are associated with the products of ECM degradation, rather than molecules present in intact ECM. Low molecular weight peptides isolated from acid-hydrolyzed small intestinal submucosa (SIS-ECM) have been shown to possess chemotactic activity for primary murine adult liver, heart and kidney endothelial cells and to promote vascularization *in vivo* in Matrigel plug assays [21]. Previous studies have also

shown that porcine SIS-ECM used for subcutaneous implantation or tendon repair in mice induces migration of bone marrow-derived cells to the site of constructive remodeling [18, 19], and that this phenomenon is associated with complete degradation of the ECM scaffold. The present study adds a new perspective to the role of the ECM in response to injury; specifically, that local, tissue-specific lineage-directed progenitor and stem cells may be selectively recruited to the appropriate site.

In the context of regenerative medicine, the findings of the present study support the concept of progenitor cell recruitment associated with ECM scaffold remodeling and its potential upon constructive remodeling of tissues. The findings also suggest that the chemoattractant activity of ECM degradation products for progenitor and stem cells decreases as the age of the tissue from which the ECM is harvested increases. Given the known phenomenon of scarless fetal wound healing [123] and the greater capacity for wound healing in young children compared to adults [130], these results are not surprising. The apparent greater chemotactic activity of adult porcine vs. human tissue may be the result of the relative age of the two 'adult' species. Six to seven month-old pigs are considered mature but are unlikely to be as 'aged' as adult humans, who can by definition be any number of years older than 21. A more comprehensive study with different ages of animals would be necessary to fully address this issue.

The concept of functional matricryptic peptides is not new. During ECM degradation, many large insoluble molecules present within the matrix are reduced to fragments which possess biological activities that are not possessed by the parent molecules. In addition to proteolysis-generated bioactive fragments, functional sites of the parent molecules that are hidden and inactive within the ECM can also become active due to conformational changes [46].

Some of the ECM molecules that have been shown to possess this property are collagen [47-51], fibronectin [52], elastin [45, 63], laminin [46, 55], and hyaluronan [56-58], all of which are present in ECM scaffold materials [24].

It is important to note that the chemoattractant activity of the ECM digests evaluated in the present study represent the net activity of bioactive molecules present within each of the digests. This net effect of chemoattractant activity is logical and relevant from an *in vivo* injury repair perspective. It is unclear whether the concentrations of ECM digests evaluated in the present study are the same as the concentrations that occur *in vivo* during the process of ECM degradation, and whether the chemoattractant molecules released by pepsin digestion of ECM would also be released during *in vivo* degradation. However, a recent study has confirmed that *in vivo* degradation of UBM-ECM can produce bioactive matricryptic peptides that cause *in vitro* chemotaxis of multi-potential progenitor cells [70]. The specific peptides/molecules responsible for these chemoattractant effects have not yet been identified and clearly this is an important next step.

The results of this study suggest that degradation products of ECM possess chemoattractant activity for local tissue progenitor and stem cells, that this chemoattractant activity may decline as a function of the age of the tissue from which the ECM is harvested, and that ECM may vary between different species. These findings add a new perspective to the role of ECM in wound healing and the differences between fetal and adult wound healing. Although fetal ECM is not a likely candidate for tissue engineering/regenerative medicine applications because of the scarce availability of the raw material, the findings of the present study could be

applied to the development of methods to induce migration of lineage-directed progenitor cells to tissue sites in need of repair, thereby facilitating a regenerative tissue response rather than default scar tissue formation.

3.5 LIMITATIONS AND FUTURE WORK

There were a few limitations to the present study that should be noted. The human adult skin sample was obtained from a person undergoing elective surgery and the human adult liver was obtained from a cadaver and was considered unsuitable for organ transplantation. The composition of these tissues may differ from those of a healthy human donor, and any pathology that may be associated with the donor tissue may also affect the chemoattractant potential of the ECM degradation products.

Differences in the decellularization procedures of the different tissues from which ECM was prepared in this study may also affect the chemoattractant potential of the different tissues. It would be logical for ECM prepared from tissues that were exposed to more harsh chemicals or longer decellularization processes to lose some of their native bioactivity due to these processing steps, and chemoattractant activity of ECM degradation products may be similarly affected.

Since the degradation products of human fetal skin ECM showed the strongest chemoattractant activity for the skin progenitor cells, it would have been logical to also investigate chemoattractant activity of pepsin digested human fetal liver ECM for skin and liver progenitor cells. However, sufficient human fetal liver ECM to complete these studies could not be obtained in a timely manner.

The response of non-lineage-directed stem or progenitor cells to these ECM degradation products would also be of interest. Human umbilical cord blood-derived multi-lineage progenitor cells (BioE, St. Paul, MN) were investigated in pilot studies, but it was challenging to obtain sufficient numbers of these cells for chemotaxis assays.

Haptotactic and chemokinetic effects of the chemotaxis assay were not directly investigated in this study. However, we have shown that migration of HEKn in response to pepsin digested hfS-ECM is not dependent on collagen coating of the chemotaxis assay filter. Additionally, other studies within our laboratory have shown that migration of human perivascular progenitor cells in response to pepsin digested UBM-ECM is due to chemotaxis rather than chemokinesis.

Finally, identifying the specific molecules responsible for the chemoattractant activity of the ECM digests is an important next step. This work would include evaluating the effect of these ECM digests and purified chemoattractant molecules *in vivo*. A pilot study evaluating subcutaneous injection of pepsin digested human fetal skin ECM digest has been performed in mice, and others in the laboratory are working toward identification of chemoattractant molecules within ECM digests and additional *in vivo* studies.

4.0 SPECIFIC AIM 3: EFFECTS OF PREVENTION OF ECM DEGRADATION ON CELL RECRUITMENT AND CONSTRUCTIVE REMODELING *IN VIVO*

4.1 BACKGROUND

Biologic scaffolds composed of naturally occurring ECM have been used as inductive templates for the constructive remodeling of numerous tissues [1-13]. Previous studies have shown differences between the host response to chemically crosslinked and non-chemically crosslinked ECM scaffolds in abdominal wall repair *in vivo* [23, 44, 87]. In one of these studies, Restore™, a commercially available non-chemically crosslinked multilayer small intestinal submucosa (SIS-ECM) device, was compared to several chemically crosslinked commercially available ECM devices: CuffPatch™, Permacol™, and TissueMend®. Histological analyses of samples taken up to 4 months after implantation showed that a foreign body response with fibrosis and accumulation of multinucleated giant cells occurred in animals implanted with heavily cross-linked ECM devices, while the non-cross-linked SIS-ECM device completely degraded and induced constructive remodeling [23]. These findings suggest that scaffold degradation plays a key role in the constructive remodeling response induced by non-chemically crosslinked ECM scaffolds. Other recent studies, and the studies described in the previous chapters, have shown that degradation products of ECM scaffolds have chemoattractant activity for several cell populations [21, 68, 70, 131], suggesting that scaffold degradation specifically plays a role in recruiting cells that participate in ECM-induced constructive remodeling.

Bone marrow-derived cells have been shown to contribute to constructive remodeling induced by ECM scaffolds. In one study, ECM scaffolds composed of porcine SIS-ECM and urinary bladder submucosa (UBS-ECM), as well as scaffolds composed of poly(L)lactic-co-glycolic acid (PLGA), a PLGA-UBS composite material, and type I collagen were implanted in dorsal subcutaneous tissue of chimeric mice expressing glucose phosphate isomerase 1a (Gpi-1^a) in all bone marrow cells. After 56-days the SIS-ECM and UBS-ECM scaffolds had been completely resorbed and replaced by differentiated host tissues and no evidence for active inflammation was seen at these sites. Gpi-1 isoenzyme results showed that scaffolds composed of SIS-ECM, UBS-ECM, and the PLGA-UBS composite were populated with a significant number of bone marrow-derived cells 56 days after implantation. Histological evaluation showed that these bone marrow-derived cells were phenotypically consistent with endothelial cells and fibroblasts but their specific phenotype was not confirmed. These results suggest that *in vivo*, resorbable ECM scaffolds recruit bone marrow-derived cells to the implant site, and that the bone marrow-derived cells participate in the long-term constructive remodeling process [18].

In a similar study, the Achilles tendons of a chimeric mouse model in which all bone marrow cells expressed green fluorescence protein (GFP) were resected and replaced with a single-layer sheet of SIS-ECM. Compared to control mice treated with an autologous Achilles tendon graft, the SIS-ECM-treated mice showed more marrow-derived cells at 4 weeks after implantation at the implant site. These cells remained uniformly distributed throughout the SIS-ECM at 8 and 16 weeks post-implantation, a time point long after the inflammatory response had diminished and the tendon had fully remodeled. The control mice contained no GFP-positive cells at the tendon remodeling site at the 8 and 16 week time points. The results of this study confirmed that bone marrow-derived cells recruited to and populating the SIS-ECM-treated

tendons represent a population of cells that can become site-specific cells (i.e., cells that normally reside in tendon tissue), such as fibroblasts or endothelial cells [19].

Bone marrow-derived cells consist of a hematopoietic population and a mesenchymal population. Hematopoietic stem cells give rise to monocytes/macrophages, lymphocytes, neutrophils, eosinophils, erythrocytes, megakaryocytes, and mast cells [132]. Bone marrow-derived mesenchymal stem cells are able to differentiate into bone marrow stromal cells, osteocytes, chondrocytes, myotubes, tendon/ligament fibroblasts, adipocytes and other cell types found within connective tissues [133]. Bone marrow-derived cells have been shown to contribute to epithelial populations in several organs, including the skin [134, 135], and have also been shown to differentiate into endothelial progenitor cells [136-138] and fibrocytes in skin [139, 140].

Bone marrow-derived cells have been shown to populate normal uninjured mouse skin and to contribute to wound healing in mouse skin [139, 141]. Both hematopoietic and mesenchymal bone marrow-derived cells have been observed in normal uninjured skin and in remodeling skin. Bone marrow-derived cells were also found to be responsible for the production of collagen type III in normal and remodeling skin [139]. Collagen type I, a mature collagen that promotes keratinocyte attachment and migration, is the predominant collagen type in normal skin. Collagen type III, immature collagen, is the other major collagen present in normal dermis. Collagen type III provides additional tensile strength to the skin and is deposited in the initial phase of wound healing. Type III collagen is then gradually replaced with type I collagen [142]. The Herovici stain has been shown to be a useful method to differentiate between type I and type III collagen in histological sections [143, 144].

The objective of the present study was to determine if prevention of ECM scaffold degradation by chemical crosslinking affects the involvement of progenitor cells in the remodeling of wounded mouse skin and yields a histologically different result than an ECM scaffold subjected to normal degradation and remodeling. Remodeling induced by the two ECM treatment groups was also compared to the remodeling of untreated wounds and wounds repaired with autologous tissue.

4.2 MATERIALS AND METHODS

4.2.1 Preparation of UBM-ECM and UBM-ECM-X Scaffolds

Urinary bladder matrix (UBM-ECM) was prepared from the urinary bladders of market weight pigs (~110 –130 kg) as previously described [74]. In brief, urothelial cells were removed by soaking the urinary bladders in 1.0 N saline. Connective and adipose tissue were removed from the serosal surface of the urinary bladder, and the tunica serosa, tunica muscularis externa, tunica submucosa, and most of the tunica muscularis mucosa were mechanically removed, leaving a biomaterial composed of only the basement membrane and the subjacent tunica propria of the tunica mucosa. Decellularization was completed by treatment with 0.1% peracetic acid/4% ethanol for two hours followed by repeated rinsing with phosphate buffered saline (PBS) and deionized water. Complete decellularization was confirmed by both 4 -6-diamidino-2-phenylindole (DAPI) nuclear staining and hematoxylin and eosin (H&E) staining of 5 μm thick sections of the UBM-ECM. Crosslinked UBM-ECM (UBM-ECM-X) was prepared by soaking UBM in 10 mM carbodiimide overnight. UBM-ECM and UBM-ECM-X sheets were frozen, lyophilized and sterilized by exposure to ethylene oxide for 16 hours.

Retardation of UBM-ECM degradation after crosslinking was verified by incubating 1 mg pieces of UBM-ECM and UBM-ECM-X in 5 mL of 5% acetic acid for 4 days at 37ºC and quantifying protein released from each material into the acetic acid using the BCA Protein Assay (Pierce). Reported results are expressed as the mean ± standard error of the mean (SEM) from one representative assay (n=2 samples tested) of three assays performed. The statistical significance between samples was determined by Student's *t*-test with $\alpha = 0.05$.

4.2.2 Chimeric mice preparation

Forty-eight C57/BL6 mice were lethally irradiated and transplanted via tail injection with mononuclear cells from mice of the congenic strain C57BL-6-Tg(ACTB-EGFP)1Osb-J, in which all cells express green fluorescent protein (GFP). The effect of this transplant was the universal expression of GFP by all hematopoietic stem cells. All native tissue was negative for GFP, allowing the detection of any bone marrow-derived cells in the remodeled tissue. To verify GFP bone marrow chimerism, blood samples were collected and analyzed with a BD FACSVantage^{SE} Cell Sorter. Flow cytometric analysis showed that 83% ± 8% of cells from tail blood expressed GFP.

4.2.3 Surgical technique

Chimeric mice were anesthetized with inhalant isoflurane via nose cone. A 0.8 cm x 0.8 cm full-thickness segment of the dorsal skin, consisting of the epidermis, dermis, subcutaneous adipose tissue, and panniculus carnosus muscle, was surgically excised (Figure 17). The excised skin was replaced with either UBM-ECM, UBM-ECM-X or the excised autologous tissue, and then secured in place with non-absorbable sutures. Control mice were left untreated after the wound

was created. At 4, 7, 14, and 28 days post-surgery, a subgroup from each treatment group was sacrificed (n=3 mice for each treatment and timepoint). The entire wound and surrounding area was harvested from each mouse and fixed in 4% paraformaldehyde, then embedded in paraffin, sectioned and mounted to glass slides.

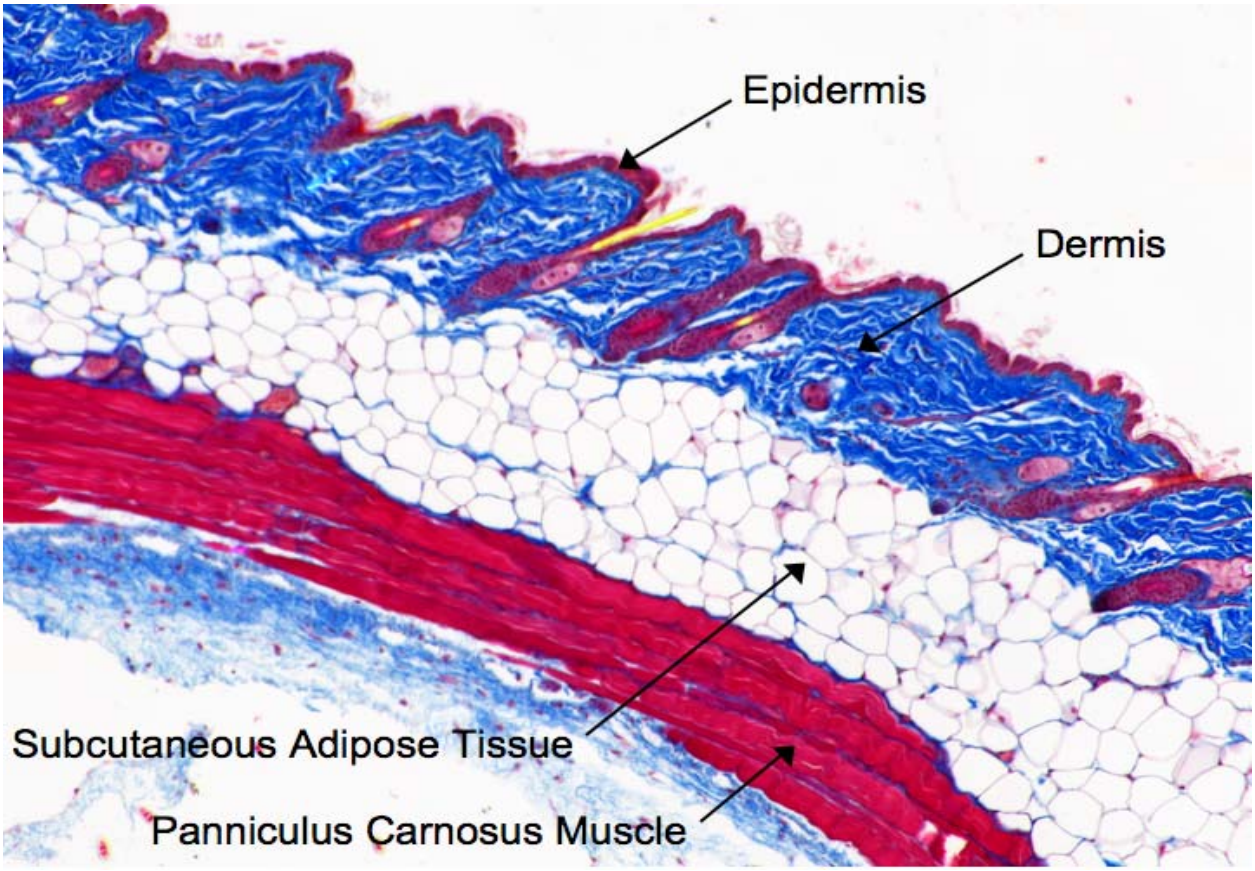

Figure 17. Representative image of Masson's trichrome stained excised mouse skin (100X magnification)

4.2.4 Wound size analysis

The size of the wound area was measured from digital photographs of the dorsum of the mice after sacrifice, using ImageJ software. Reported results are expressed as the mean ± SEM of measurements from three mice for each treatment and timepoint (n=3). The statistical significance between treatment groups was determined by one-way ANOVA with $\alpha = 0.05$.

4.2.5 Histological appearance of remodeling skin

Masson's trichrome staining was performed for evaluation of the morphology of the remodeling skin. The thickness of the remodeling skin of each sample at 14 and 28 days post-surgery was measured from Masson's trichrome stained slides in three locations across the remodeling area for each sample at 40X magnification, using ImageJ software. The mean thickness was then calculated for each sample. Reported results are expressed as the mean ± SEM of wound thickness for three mice for each treatment and timepoint (n=3). The statistical significance between treatment groups was determined by one-way ANOVA with $\alpha = 0.05$.

4.2.6 Collagen analysis of remodeling skin

Herovici staining was performed to analyze quantities of mature and immature collagen (collagen type I and collagen type III, respectively) in the remodeling skin at 28 days post-surgery. Four images of the remodeling area were taken from each slide and image analysis was performed using ImageJ software. To normalize for differences between different batches of Herovici stain, the pixels of area stained in the collagen type I red color range, collagen type III

blue color range, and the ratio of collagen type I:collagen type III were normalized to the same parameters measured in normal skin that was stained on the same slide. The mean results were then calculated for each sample. Reported results are expressed as the mean ± SEM of area representing collagen type I staining, area representing collagen type III staining, and the ratio of collagen type I:collagen type III for three mice for each treatment (n=3). The statistical significance between treatment groups was determined by one-way ANOVA with $\alpha = 0.05$ followed by post-hoc Tukey's test with $\alpha = 0.05$.

4.2.7 Bone marrow-derived cells in remodeling skin

4.2.7.1 GFP expression For analysis of GFP-expressing cells, slides were deparaffinized with xylene and rehydrated through a graded ethanol series and then counterstained with DAPI and photographed at 200X magnification using the Olympus Fluoview 1000 confocal microscope with lasers scanning at wavelengths of 488 nm (GFP) and 405 nm (DAPI). Four images of the remodeling area were taken from each slide and quantification of the number of cells expressing GFP and total number of cells was performed for each image using ImageJ software. The percentage of cells in the remodeling skin expressing GFP was calculated from these measurements. The mean number of GFP-positive cells and percentage of GFP-positive cells was then calculated for each sample. Reported results are expressed as the mean ± SEM of number of GFP-positive cells and percentage of GFP-positive cells for three mice for each treatment and timepoint (n=3). The statistical significance between treatment groups was determined by one-way ANOVA with a = 0.05 followed by post-hoc Tukey's test with $\alpha = 0.05$.

To confirm that cells with fluorescent signal at the 488 nm wavelength were GFP-positive cells, immunohistochemistry with an anti-GFP antibody was performed. Unstained

slides were deparaffinized with xylene and rehydrated through a graded ethanol series. Heat mediated antigen retrieval was performed using 10 mM citrate buffer, pH 6.0, for 15 minutes at 95-100ºC. After cooling, slides were washed three times with tris-buffered saline (TBS)/Tween 20 and then washed twice with PBS. Slides were then incubated in 2% bovine serum albumin (BSA) in PBS for 45 minutes at room temperature to prevent nonspecific antibody binding. Slides were washed three times with PBS and then incubated in primary antibody, rabbit polyclonal to GFP (Abcam ab6556) diluted to 1:1000 in 2% BSA in PBS, overnight at 4ºC. Slides were then washed 3 times with PBS, followed by incubation in 3% hydrogen peroxide in PBS for 30 minutes. Slides were washed three times with PBS, followed by incubation in secondary antibody, polyclonal goat anti-rabbit Ig-HRP (Dako P0448) diluted to 1:200 in 2% BSA in PBS, for one hour at room temperature. Slides were then washed twice with PBS, then once with tap water. ImmPACT DAB (Vector Laboratories SK-4105) was prepared according to product instructions and applied to slides at room temperature until staining developed. Slides were then washed in water for 5 minutes, counterstained with hematoxylin for 15 seconds, and washed with running water for 5 minutes. Finally, slides were dehydrated through a graded ethanol series and xylene, then coverslipped.

4.2.7.2. Fluorescent immunolabeling for F4/80, CD45, von Willebrand factor and CD34

Remodeling tissue at 28 days post-surgery was fluorescently immunolabeled for macrophage marker F4/80, hematopoietic cell marker CD45, endothelial cell marker von Willebrand factor, and CD34, which is expressed by several cell populations including hematopoietic stem cells, hair follicle bulge cells, endothelial cells, and mast cells. For fluorescent immunolabeling, unstained slides were deparaffinized with xylene and rehydrated through a graded ethanol series. For F4/80 and CD45 immunolabeling, heat mediated antigen retrieval was performed using 10

mM citrate buffer, pH 6.0, for 15 minutes at 95-100ºC. After cooling, slides were washed three times with TBS/Tween 20 and then washed twice with PBS. Slides were then incubated in 2% BSA in PBS for 45 minutes at room temperature to prevent nonspecific antibody binding. Slides were washed three times with PBS and then incubated in primary antibody, rat monoclonal to F4/80 (Abcam ab6640) diluted to 1:100 in 2% BSA in PBS or rat monoclonal to CD45 (BD Pharmingen 550539) diluted to 1:50 in 2% BSA in PBS, overnight at 4ºC. Slides were then washed 3 times with PBS, followed by incubation in secondary antibody, mouse adsorbed goat anti-rat IgG-Cy3 (Jackson ImmunoResearch Laboratories 112-165-167) diluted to 1:1000 or 1:500 in 2% BSA in PBS, for one hour at room temperature. Slides were washed three times with PBS and coverslipped with an aqueous mounting medium containing DAPI (Vector Laboratories) and imaged using the Olympus Fluoview 1000 confocal microscope.

For CD34 fluorescent immunolabeling, heat mediated antigen retrieval was performed using 10 mM citrate buffer, pH 6.0, for 15 minutes at 95-100ºC. After cooling, slides were washed three times with TBS/Tween 20 and then washed twice with PBS. Slides were then incubated in 2% BSA in PBS for 45 minutes at room temperature to prevent nonspecific antibody binding. Slides were washed three times with PBS and then incubated in primary antibody, rat monoclonal to CD34 (MEC-14.7) (Santa Cruz Biotechnology sc-18917), diluted to 1:100 in 2% BSA in PBS, overnight at 4ºC. Slides were then washed three times in PBS, followed by incubation in secondary antibody, mouse adsorbed goat anti-rat IgG-Cy3 (Jackson ImmunoResearch Laboratories 112-165-167) diluted to 1:1000 in 2% BSA in PBS. Slides were then washed three times with PBS, three times with deionized water, and coverslipped with an aqueous mounting medium containing DAPI and imaged using the Olympus Fluoview 1000 confocal microscope.

For von Willebrand factor fluorescent immunolabeling, proteinase K antigen retrieval was performed for 20 minutes at 37ºC, followed by three washes with PBS. Slides were then incubated in 2% BSA in PBS for 45 minutes at room temperature to prevent nonspecific antibody binding. Slides were washed once with PBS and then incubated in primary antibody, rabbit polyclonal to von Willebrand factor (Abcam ab6994) diluted to 1:100 in 2% BSA in PBS, overnight at 4ºC. Slides were then washed three times with PBS, followed by incubation in secondary antibody, human adsorbed goat anti-rabbit Ig-TRITC (Southern Biotech 4010-03) diluted to 1:500 in 2% BSA in PBS, for one hour at room temperature. Slides were then washed three times with PBS, three times with deionized water, and coverslipped with an aqueous mounting medium containing DAPI and imaged using the Olympus Fluoview 1000 confocal microscope.

To quantify fluorescently immunolabeled cells, three images of the remodeling area were taken from each slide and quantification of the number of cells staining positive for F4/80, CD45, and CD34 was performed for each image using ImageJ software. The area staining positive for von Willebrand factor was measured for each of three images of the remodeling area from each slide using ImageJ software. The mean number of positive staining cells or area was then calculated for each sample. Reported results are expressed as the mean ± SEM of number of positive staining cells for F4/80, CD45, and CD34 and area staining positive for von Willebrand factor for three mice for each treatment (n=3). The statistical significance between treatment groups was determined by one-way ANOVA with $\alpha = 0.05$ followed by post-hoc Tukey's test with $\alpha = 0.05$.

4.3 RESULTS

Quantitative analysis of protein released by *in vitro* degradation of UBM-ECM and UBM-ECM-X showed that UBM-ECM released a greater quantity of protein than UBM-ECM-X ($p<0.05$, Figure 18). This result confirmed that UBM-ECM-X was more resistant to degradation than UBM-ECM.

All wounds increased in size by 4 days post-surgery due to wound retraction (Figure 19). There were no significant differences in the sizes of the wounds between the different treatment groups. By 28 days post-surgery all wounds were closed and appeared normal upon gross inspection.

Images of Masson's trichrome stained remodeling tissue showed the progression of the healing wounds and morphological differences between the different treatment groups at all four timepoints examined (Figure 20). At 4 days post-surgery, the untreated group had formed a fibrin clot covering the wound area. The autologous repair and UBM-ECM treated wounds showed cells infiltrating both scaffolds and granulation tissue forming beneath the scaffolds. The UBM-ECM-X scaffolds were not adherent to the underlying host tissue and showed little host cell interaction.

At 7 days post-surgery, the untreated wounds began to form granulation tissue with a thick epithelial layer beneath the fibrin clot. The autologous repair wounds showed new tissue formation with many inflammatory cells present and the grafted autologous tissue being pushed up and removed from the wound. The UBM-ECM treated wounds had begun to form a highly cellular new tissue with a dense collagenous dermal layer and a thick epidermal layer. The UBM-ECM scaffolds were no longer visibly distinct in the Masson's trichrome stained tissue sections and had likely degraded by 7 days post-surgery. The UBM-ECM-X treated wounds still

showed little scaffold degradation but some granulation tissue had begun to form beneath the scaffold.

At 14 days post-surgery, all four treatment groups had the appearance of epithelialized new tissue. The untreated and UBM-ECM-X groups were highly cellular and had very thick epithelial layers. The autologous repair group still had the appearance of inflammation and some of the autograft was still present at the external surface of the wound area. For the UBM-ECM treated wounds, the inflammatory phase appeared to have subsided, epithelial thickness had decreased, hair follicles were beginning to form, and dermal matrix was reorganizing and less dense.

By 28 days post-surgery the untreated and autologous repair groups consisted of a dense and highly cellular dermis with little hair follicle formation and a thinner epithelium than at the previous timepoint. The UBM-ECM and UBM-ECM-X groups showed nearly normal hair follicle morphology and a thinner epithelium than at the previous timepoint as well as reorganization of the dermis and formation of the adipose tissue layer.

Measurements of the thickness of the remodeling skin showed no significant differences in thickness between the different treatment groups, or for any of the treatment groups compared to normal uninjured mouse skin (Figure 21).

Herovici stained images of the remodeling mouse skin at 28 days post-surgery showed a mixture of immature type III collagen (stained blue) and mature type I collagen (stained red) fibers (Figure 22). Quantification of the areas stained for collagen type I and collagen type III showed no significant differences between the different treatment groups (Figure 23). The collagen type I:collagen type III ratio of the UBM-ECM treated group was higher than the autologous repair group ($p<0.05$, Figure 24). These results suggest that the UBM-ECM treated

group, with remodeled skin composed of more mature collagen and less immature collagen, had completed more of the remodeling process in 28 days than the autologous repair group.

GFP-positive bone marrow-derived cells were visible throughout the remodeling skin in all treatment groups and timepoints (Figure 25). Immunostaining of the remodeling skin with anti-GFP antibody (Figure 26) confirmed the GFP fluorescence results. Quantification of the number of GFP-positive cells in the remodeling skin showed that at 4 days post-surgery the no treatment and autologous repair groups had more GFP-positive cells than normal uninjured skin ($p<0.05$, Figure 27). The autologous repair group had more GFP-positive cells than the UBM-ECM-X treatment group at 4 days post-surgery ($p<0.05$, Figure 27). At 7 and 14 days post-surgery, only the autologous repair group had more GFP-positive cells than normal uninjured skin ($p<0.05$, Figure 27). The autologous repair group had more GFP-positive cells than the UBM-ECM treatment group at 14 days post-surgery ($p<0.05$, Figure 27). At 28 days post-surgery, none of the treatment groups had more GFP-positive cells than normal uninjured skin (Figure 27). The percentage of GFP-positive cells in the remodeling skin showed similar trends to the number of GFP-positive cells at 4 days post-surgery, with the no treatment and autologous repair groups having a higher percentage of GFP-positive cells than normal uninjured skin (Figure 28). At 7 days post-surgery, the autologous repair and UBM-ECM treatment groups had a higher percentage of GFP-positive cells than in normal uninjured skin ($p<0.05$, Figure 28). At 14 days post-surgery, the percentage of GFP-positive cells in the UBM-ECM treatment group had decreased to normal levels, while the percentage of GFP-positive cells in the autologous repair group remained higher than in normal uninjured skin ($p<0.05$, Figure 28). At 28 days post-surgery, none of the treatment groups had a higher percentage of GFP-positive cells than normal uninjured skin (Figure 28). The UBM-ECM-X treatment group did not have significantly more

GFP-positive cells or a significantly higher percentage of GFP-positive cells than normal uninjured skin at any of the timepoints examined, while the UBM-ECM treatment group was higher than normal at 7 days post-surgery. These results suggest that the degrading scaffold recruited GFP-positive bone marrow-derived cells while the non-degrading scaffold did not. The UBM-ECM treated group decreased to a normal percentage of GFP-positive cells by 14 days post-surgery while the autologous repair group did not, suggesting that a strong inflammatory response was still occurring in the autologous repair group at this timepoint.

Images of fluorescently immunolabeled remodeling mouse skin at 28 days post-surgery (Figure 29) showed that cells staining positively for F4/80, CD45, CD34, and von Willebrand factor were present in all treatment groups. Quantification of F4/80-positive cells showed that only the autologous repair group had more F4/80-positive cells than normal uninjured mouse skin ($p<0.05$, Figure 30). Quantification of CD45-positive cells showed no significant differences in number of CD45-positive cells between the different treatment groups (Figure 31). Since not all GFP-positive cells were CD45-positive (i.e., of hematopoietic origin), these results suggest that mesenchymal bone marrow-derived cells also played a role in skin remodeling. Quantification of CD34-positive cells showed no significant differences in number of CD34-positive cells between the different treatment groups (Figure 32). Quantification of the area staining positive for von Willebrand factor also showed no significant differences between the different treatment groups (Figure 33).

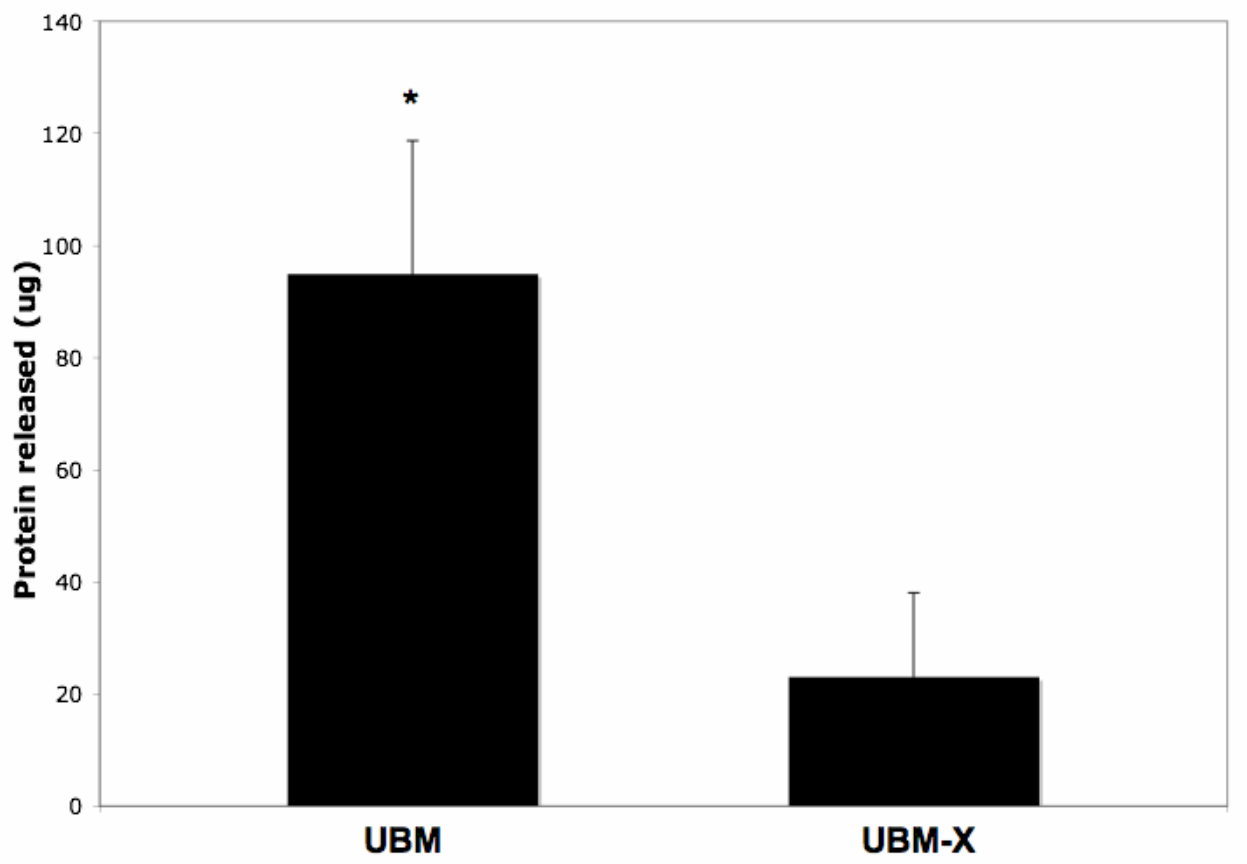

Figure 18. Quantification of protein released from UBM and UBM-X after *in vitro* degradation, verifying that carbodiimide crosslinking retards UBM degradation. Mean ± SEM (n=2); * = p<0.05 between UBM-ECM and UBM-ECM-X. Equivalent trends were observed on two further occasions.

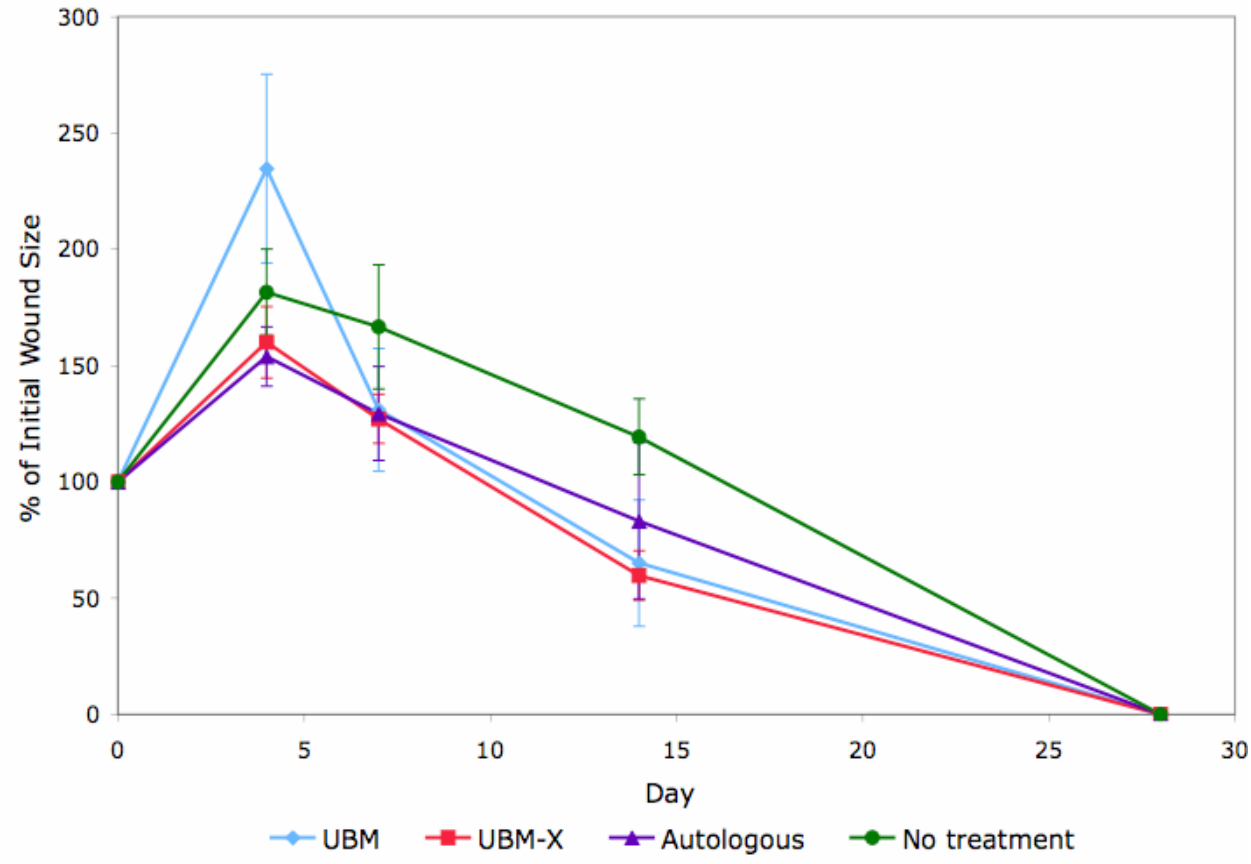

Figure 19. Wound size at 4, 7, 14, and 28 days post-surgery. Mean ± SEM (n=3). All wounds were closed by 28 days post-surgery.

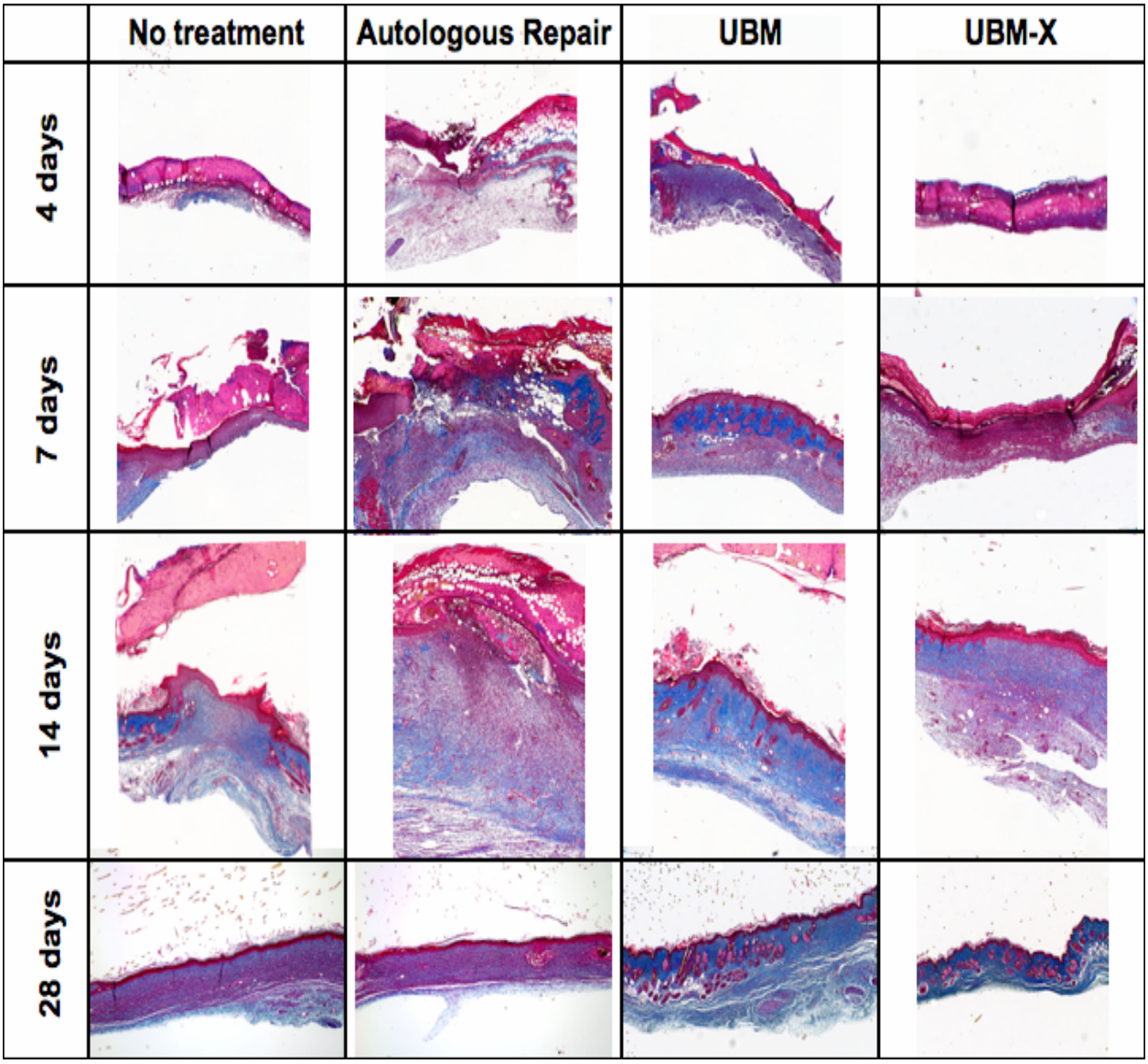

Figure 20. Representative images of Masson's trichrome stained remodeling mouse skin at 4, 7, 14, and 28 days post-surgery (40X magnification)

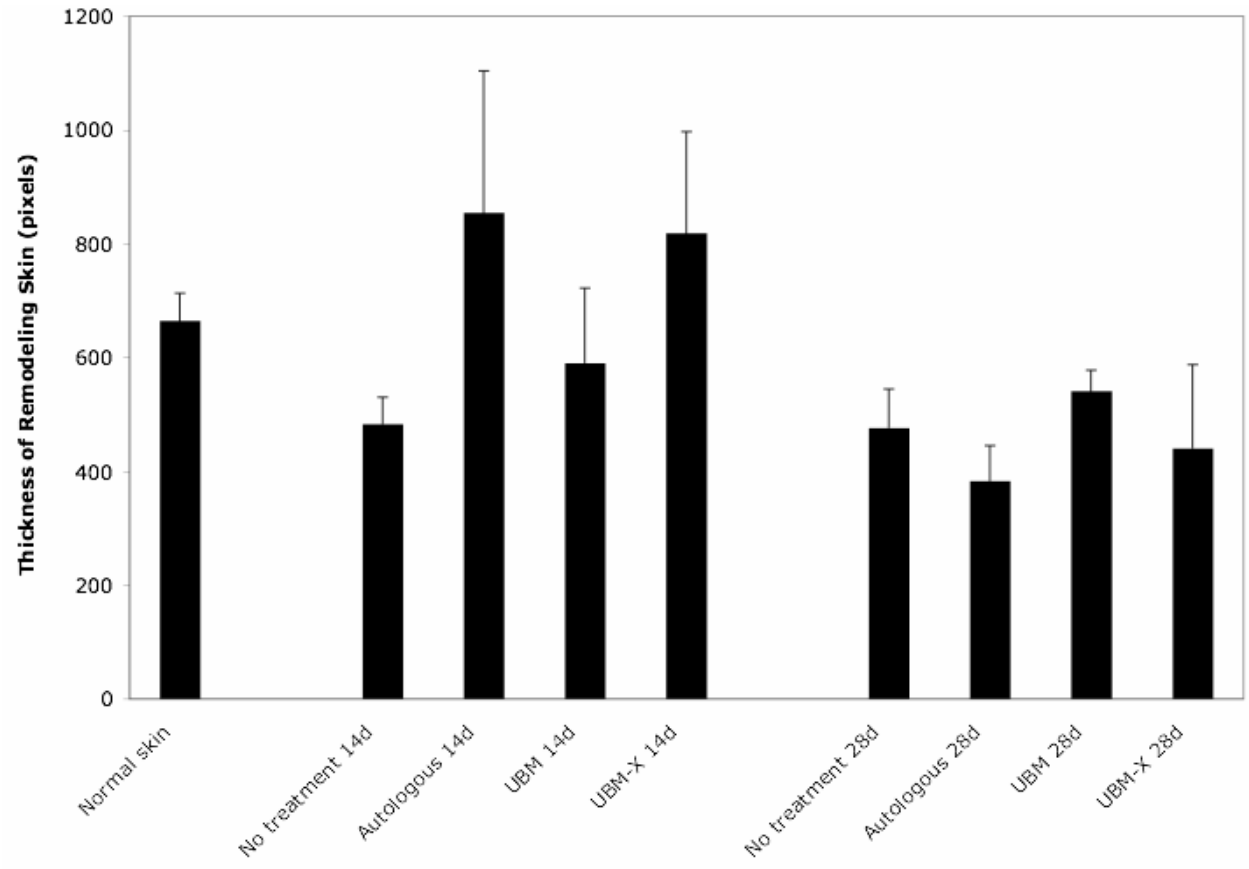

Figure 21. Thickness of remodeling mouse skin after 14 and 28 days. Mean ± SEM (n=3)

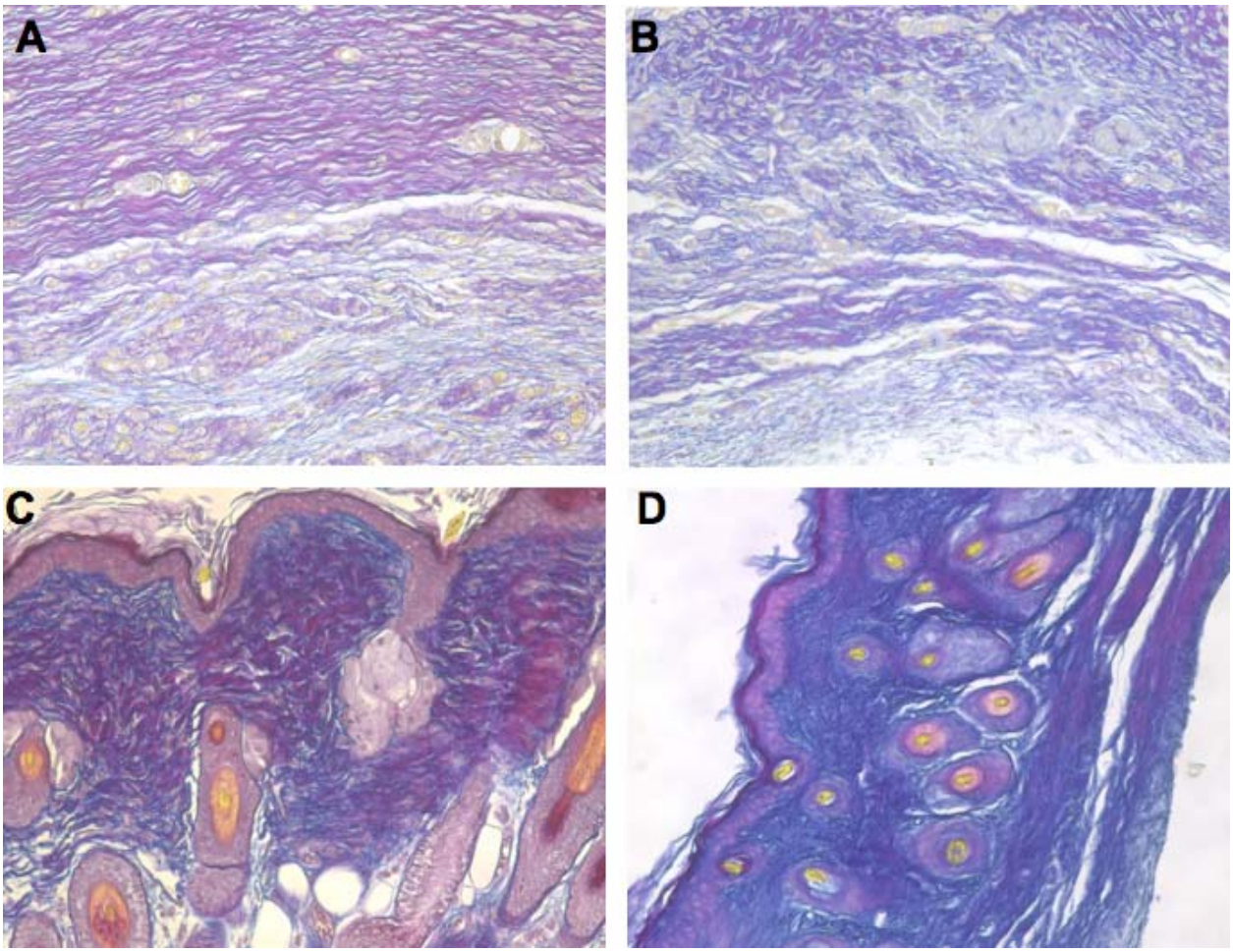

Figure 22. Herovici stained remodeling mouse skin at 28 days post-surgery (200X magnification). (A) No treatment; (B) Autologous repair; (C) UBM-ECM; (D) UBM-ECM-X

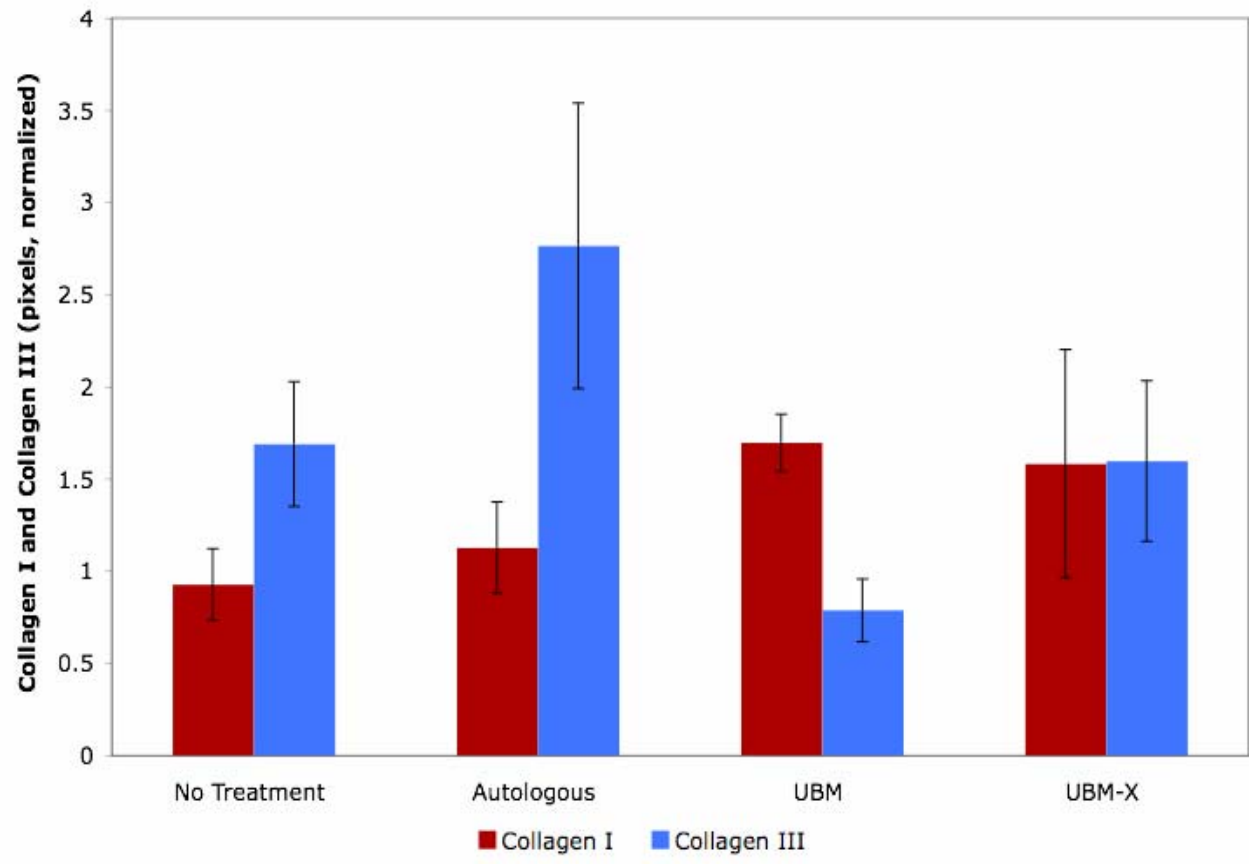

Figure 23. Herovici staining analysis of collagen type I and collagen type III in remodeling mouse skin at 28 days post-surgery. Mean ± SEM (n=3)

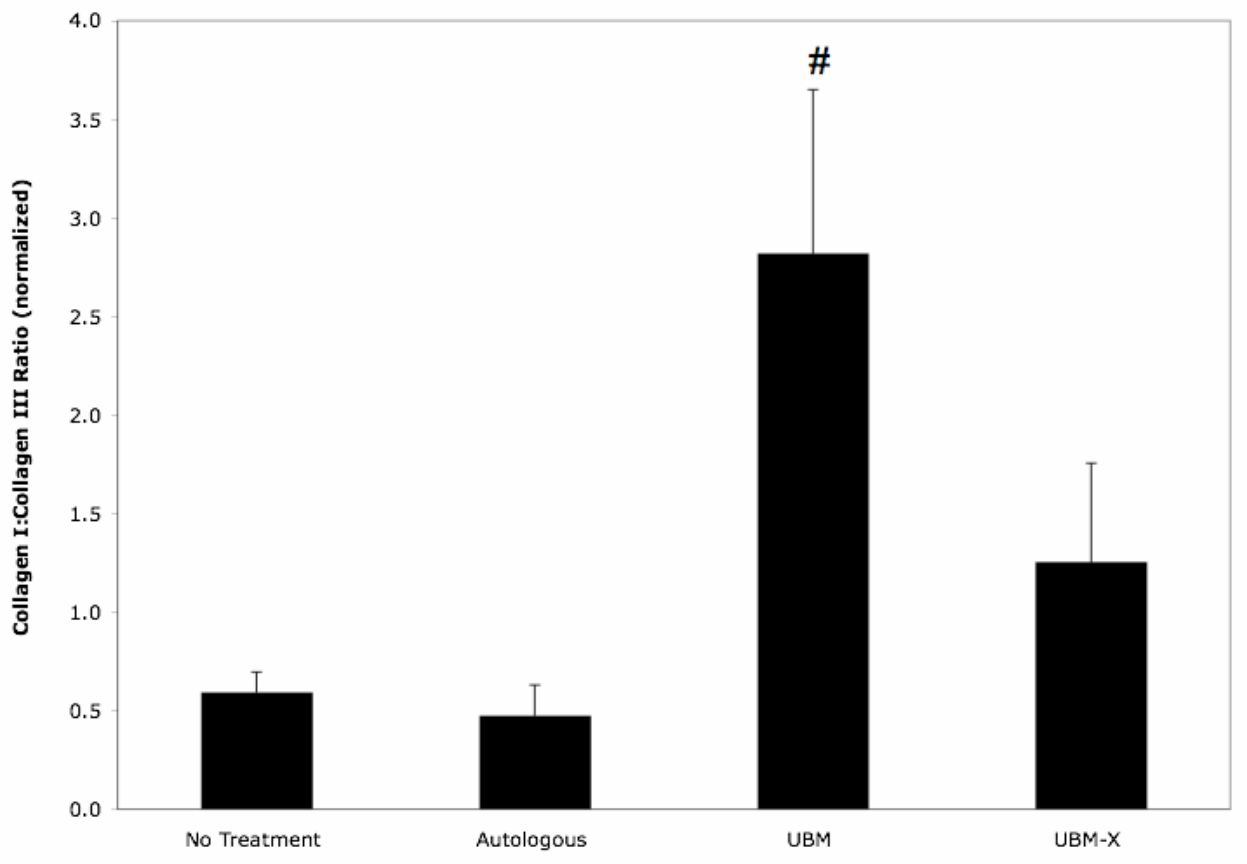

Figure 24. Herovici staining analysis of collagen type I:collagen type III ratio in remodeling mouse skin at 28 days post-surgery. Mean ± SEM (n=3); # = $p<0.05$ versus autologous repaired skin

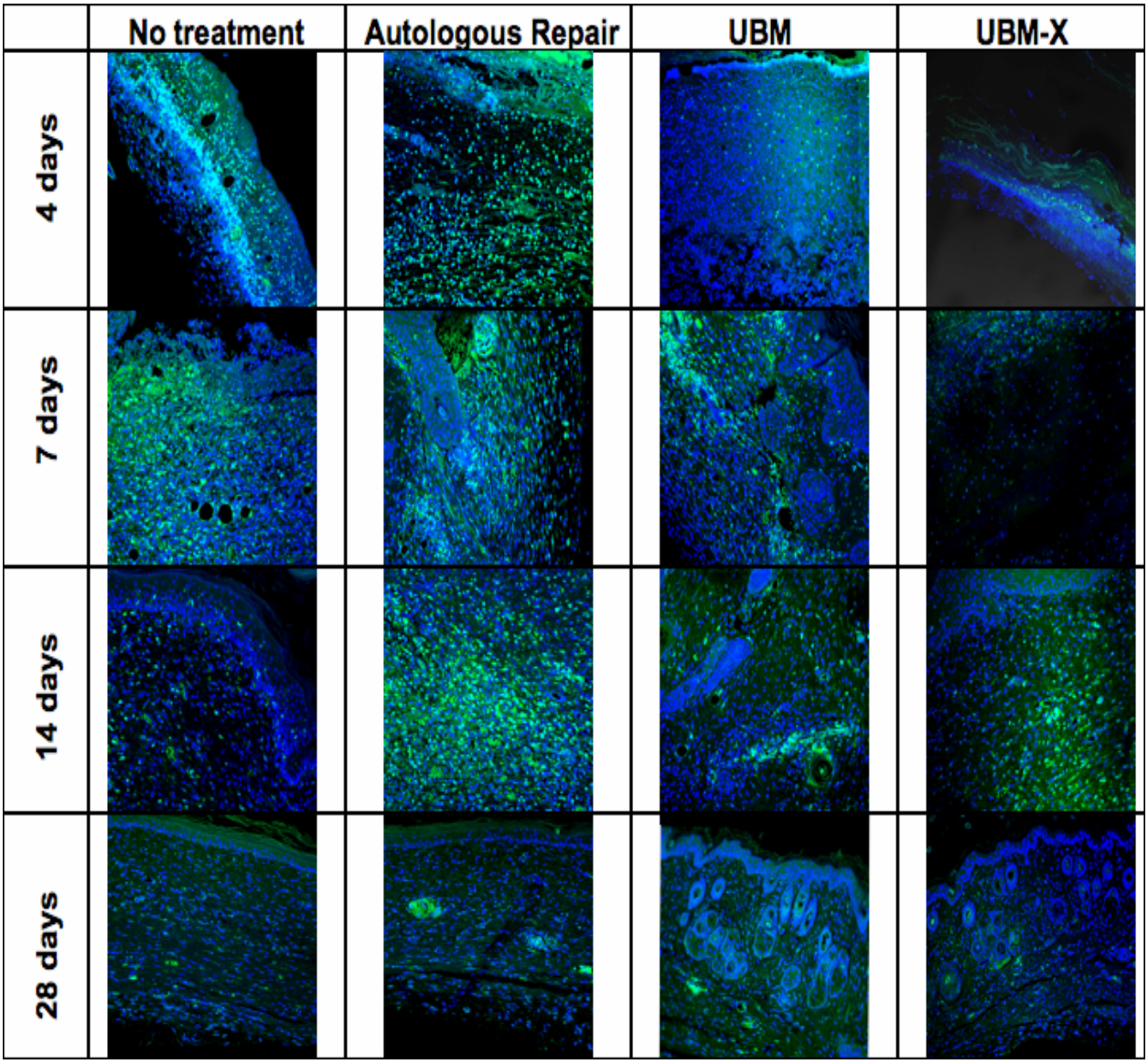

Figure 25. Representative images of GFP bone marrow-derived cells (green) counterstained with DAPI (blue) in remodeling mouse skin at 4, 7, 14, and 28 days post-surgery (200X magnification)

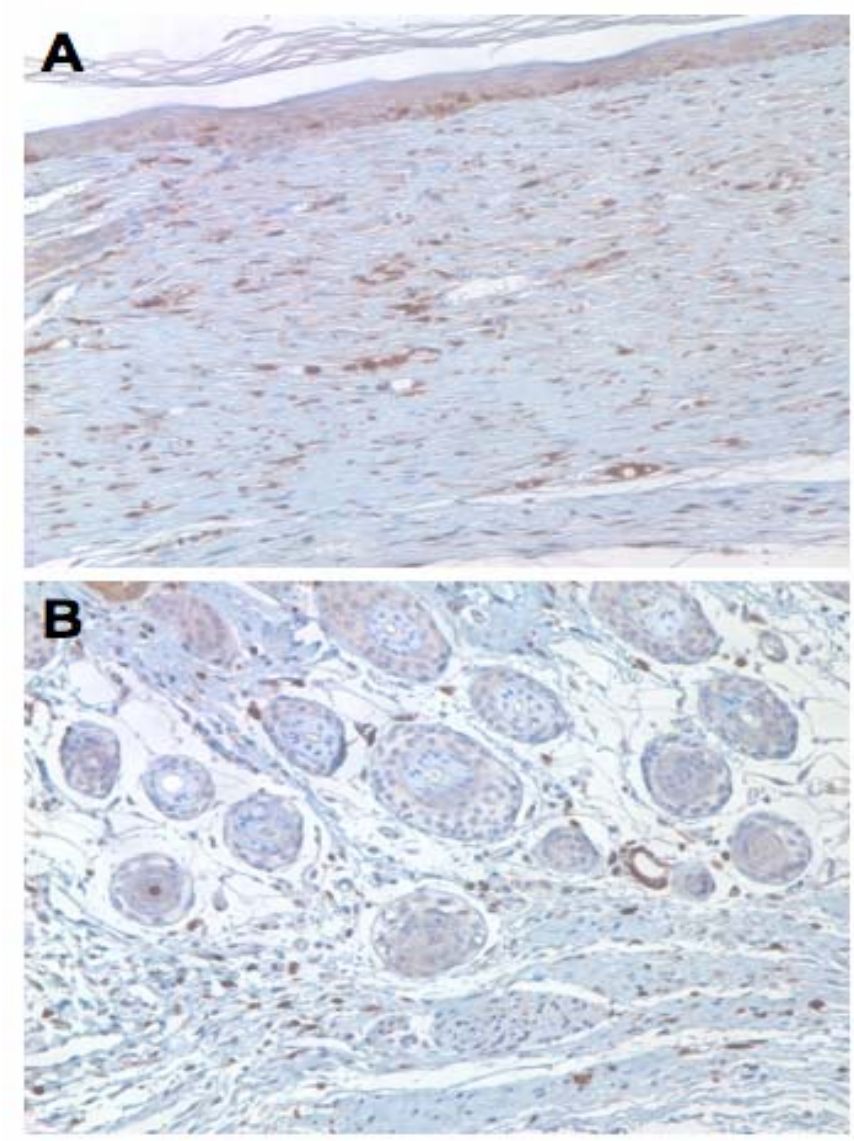

Figure 26. Representative images of remodeling mouse skin at 28 days post-surgery stained with anti-GFP antibody (brown) and counterstained with hematoxylin (blue) (200X magnification). (A) autologous repair; (B) UBM-ECM

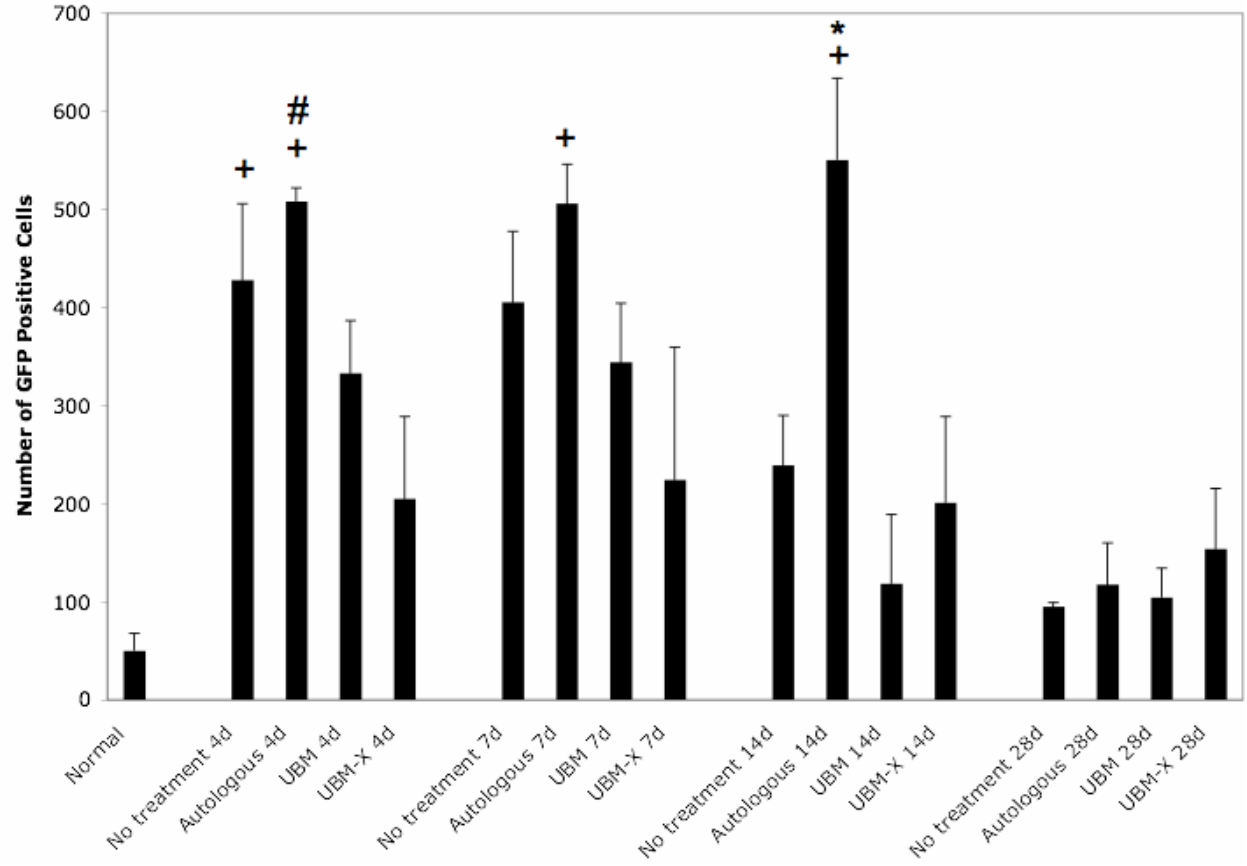

Figure 27. Quantification of number of bone marrow-derived GFP-positive cells in remodeling mouse skin at 4, 7, 14, and 28 days post-sugery. Mean ± SEM (n=3); + = $p<0.05$ versus normal uninjured skin, # = $p<0.05$ versus UBM-ECM-X at 4 days, * = $p<0.05$ versus UBM-ECM at 14 days

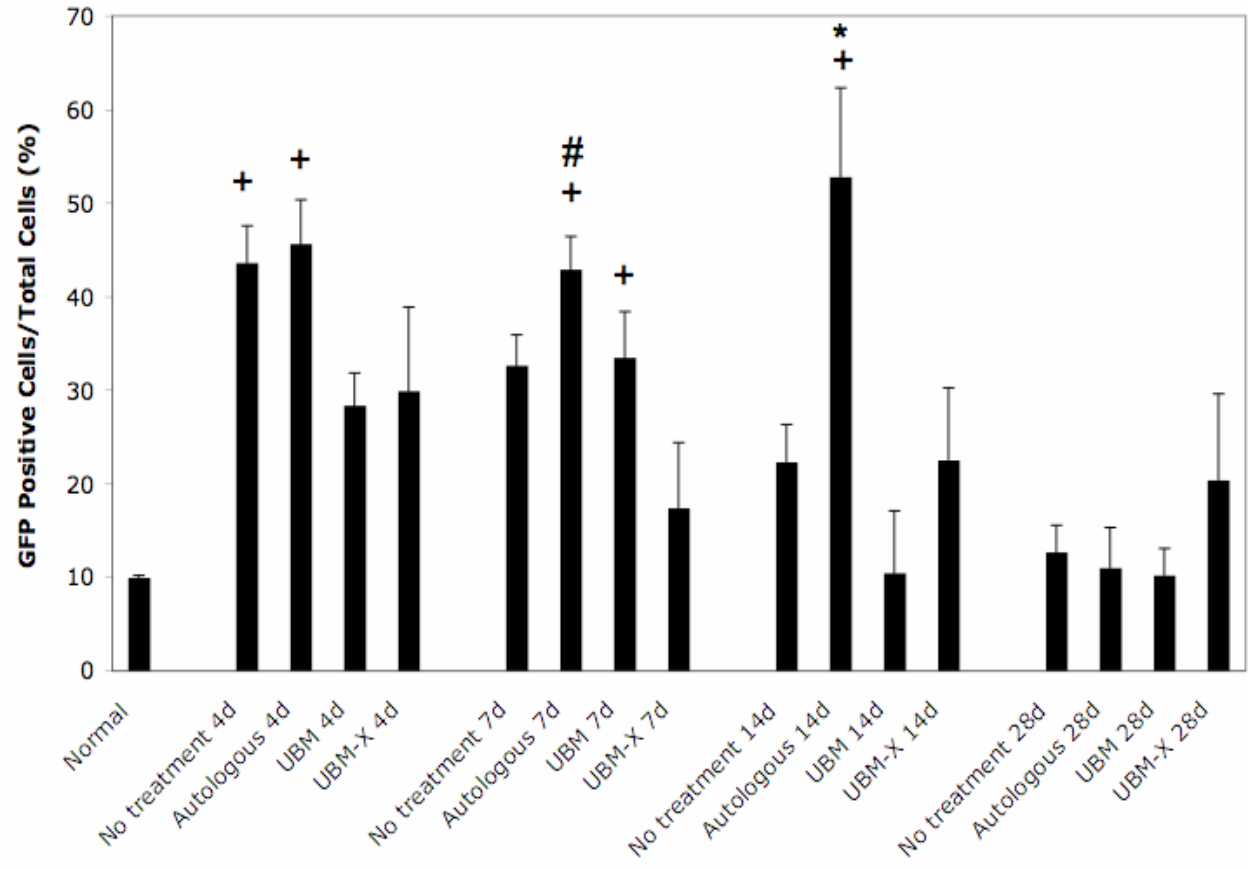

Figure 28. Quantification of percentage of bone marrow-derived GFP-positive cells in remodeling mouse skin at 4, 7, 14, and 28 days post-sugery. Mean ± SEM (n=3); + = p<0.05 versus normal uninjured skin, # = p<0.05 versus UBM-ECM-X at 7 days, * = p<0.05 versus UBM-ECM at 14 days

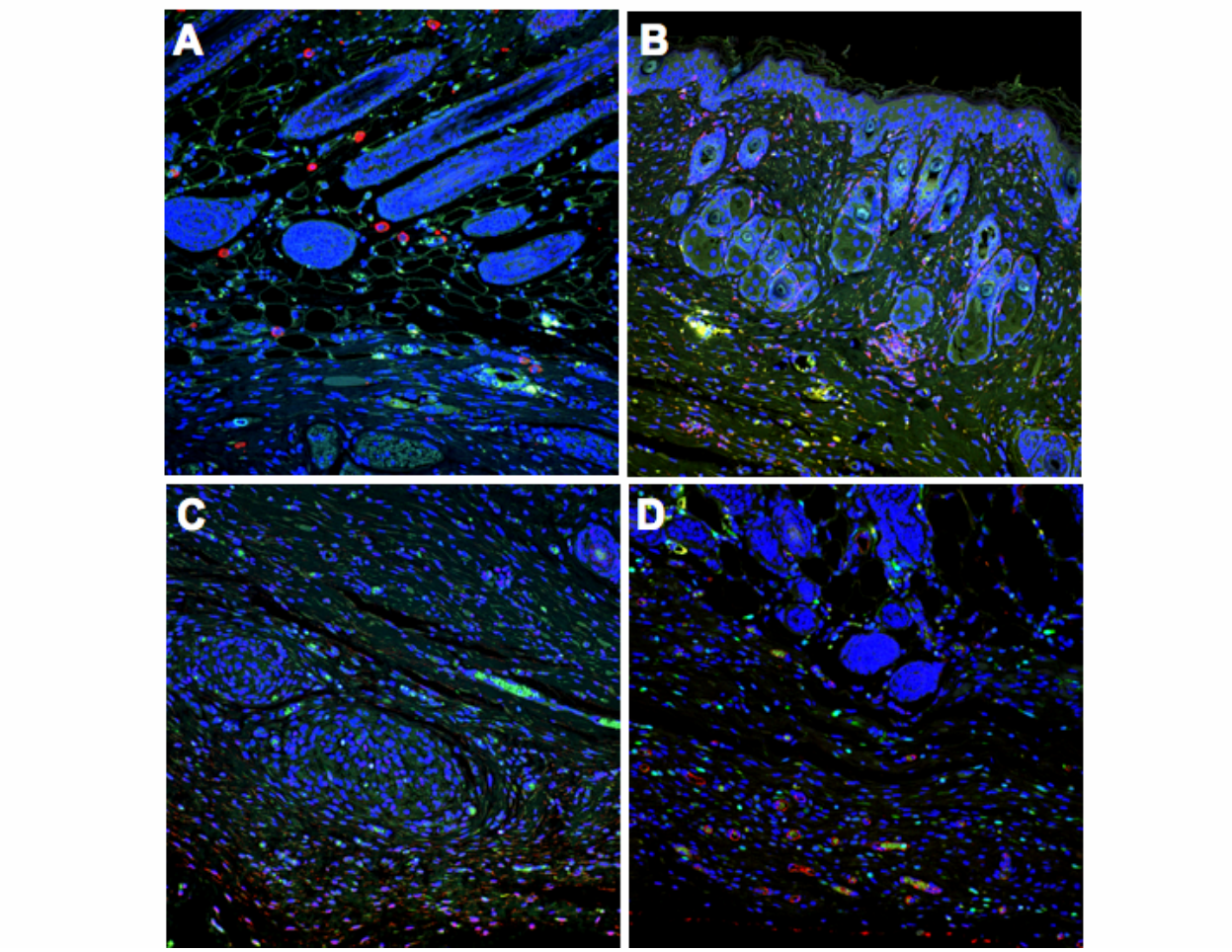

Figure 29. Representative images of fluorescently immunolabeled UBM-ECM treated remodeling mouse skin at 28 days post-surgery (200X magnification). Blue: nuclei, green: GFP, red:(A) F4/80; (B) CD45; (C) CD34; (D) von Willebrand factor

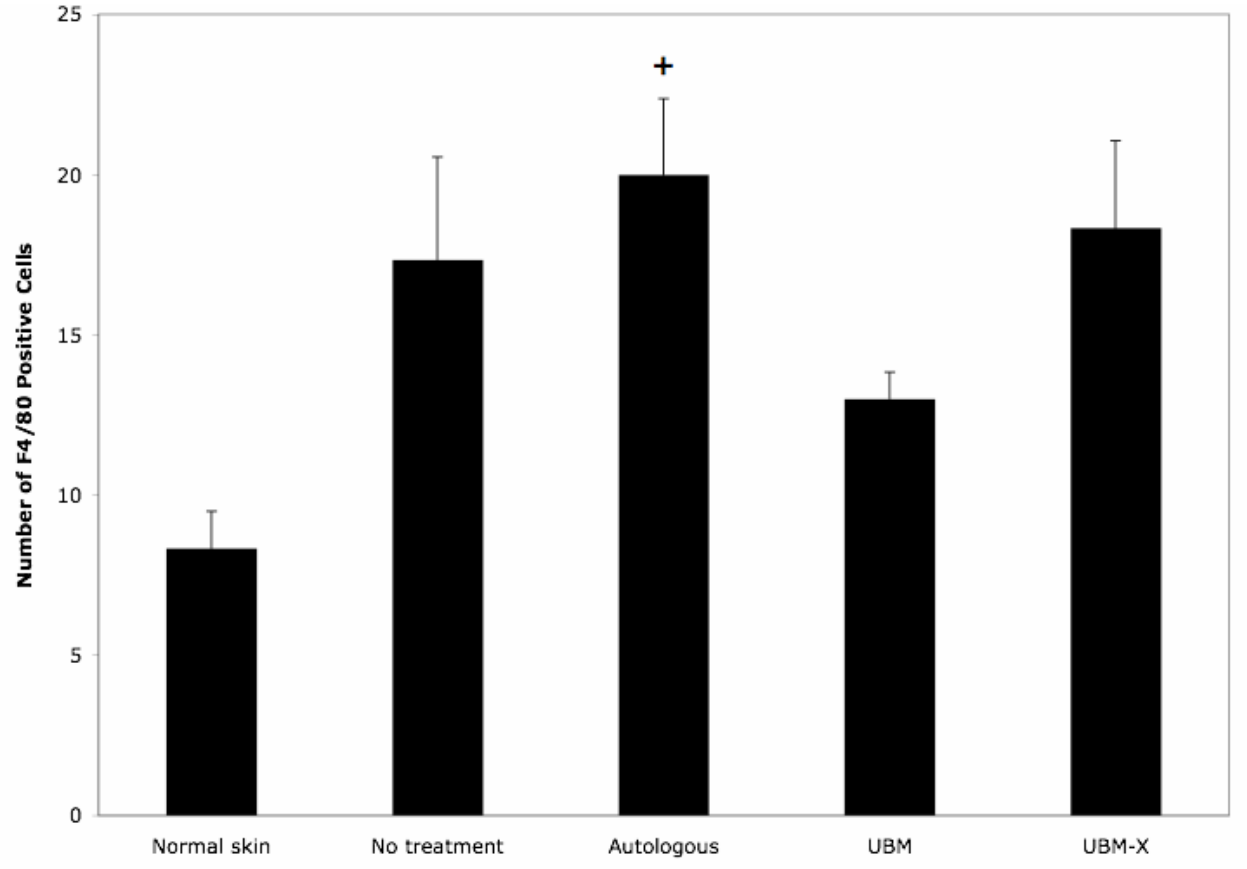

Figure 30. Quantification of F4/80-positive cells in remodeling mouse skin at 28 days post-surgery. Mean ± SEM (n=3); + = p<0.05 versus normal uninjured skin

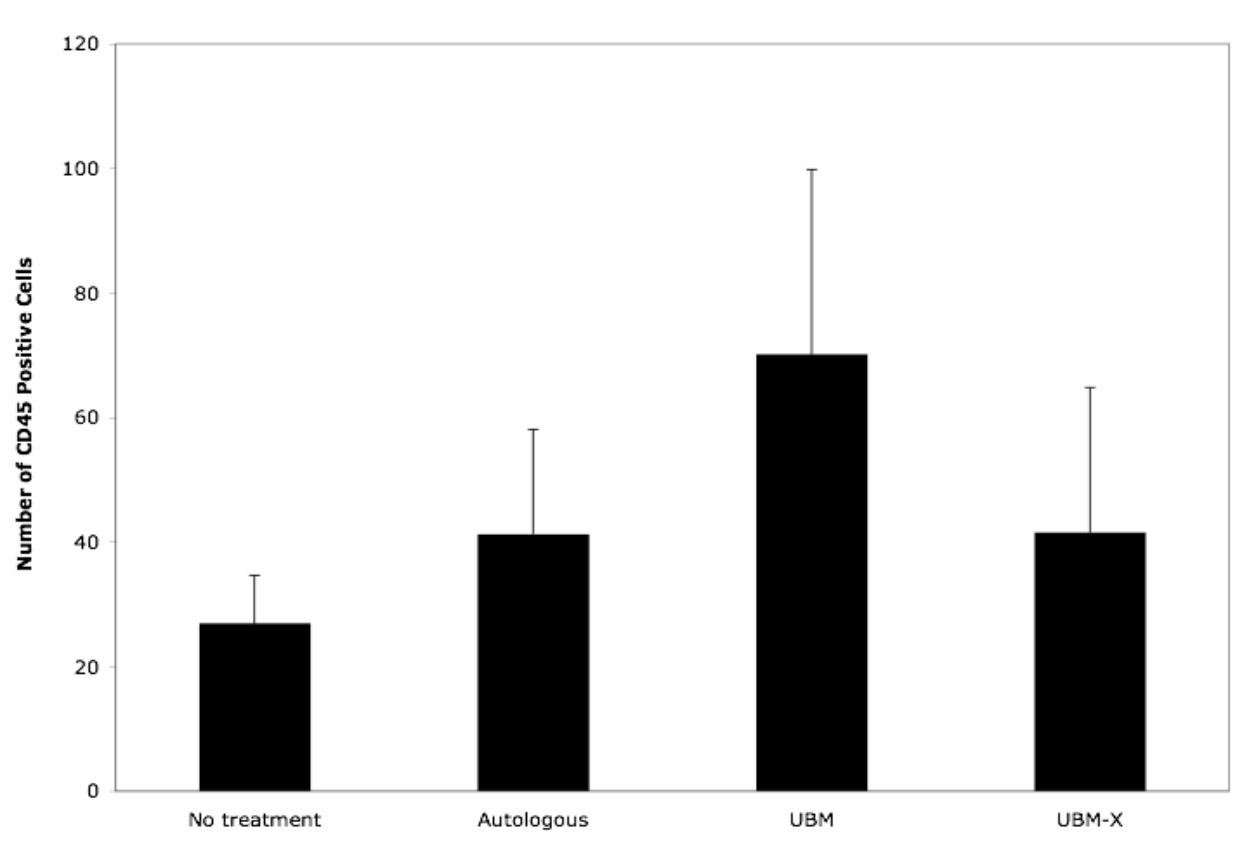

Figure 31. Quantification of CD45-positive cells in remodeling mouse skin at 28 days post-surgery. Mean ± SEM (n=3)

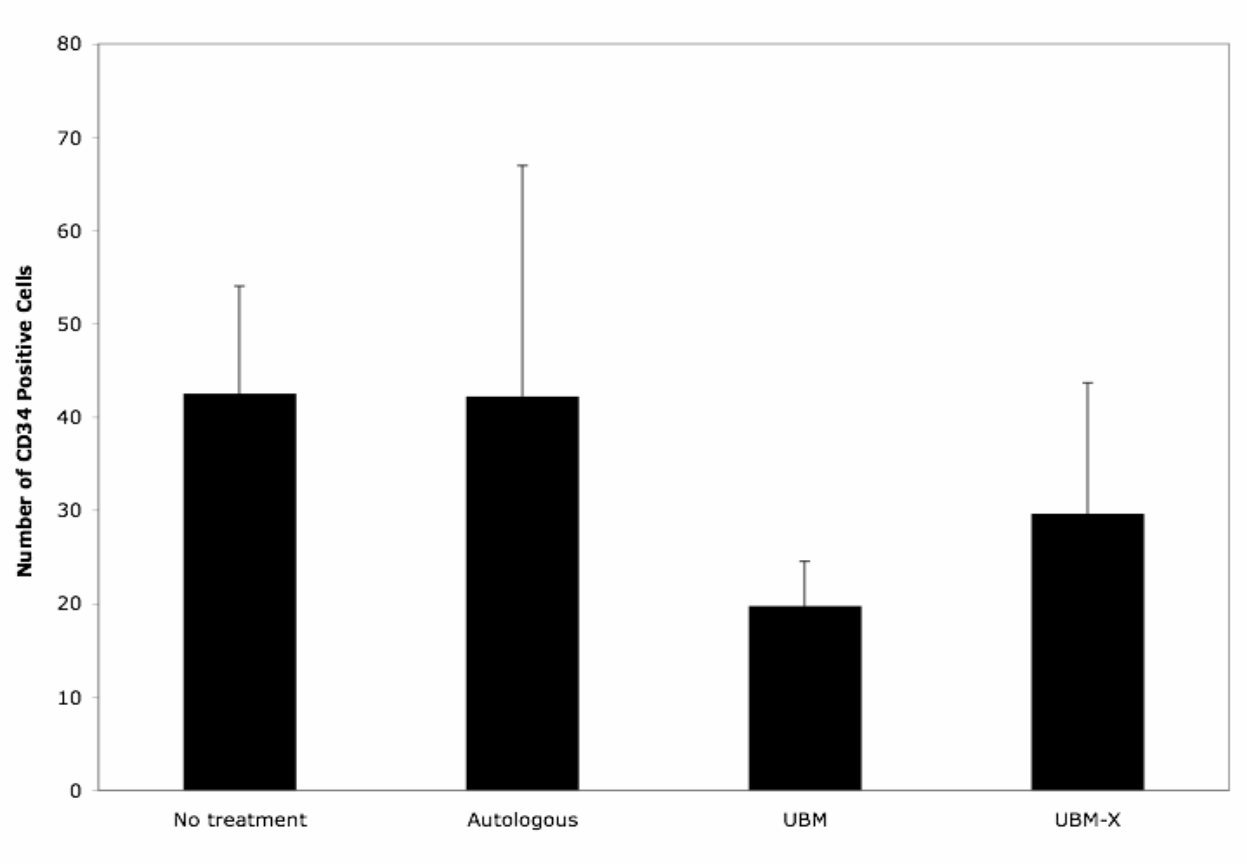

Figure 32. Quantification of CD34-positive cells in remodeling mouse skin at 28 days post-surgery. Mean ± SEM (n=3)

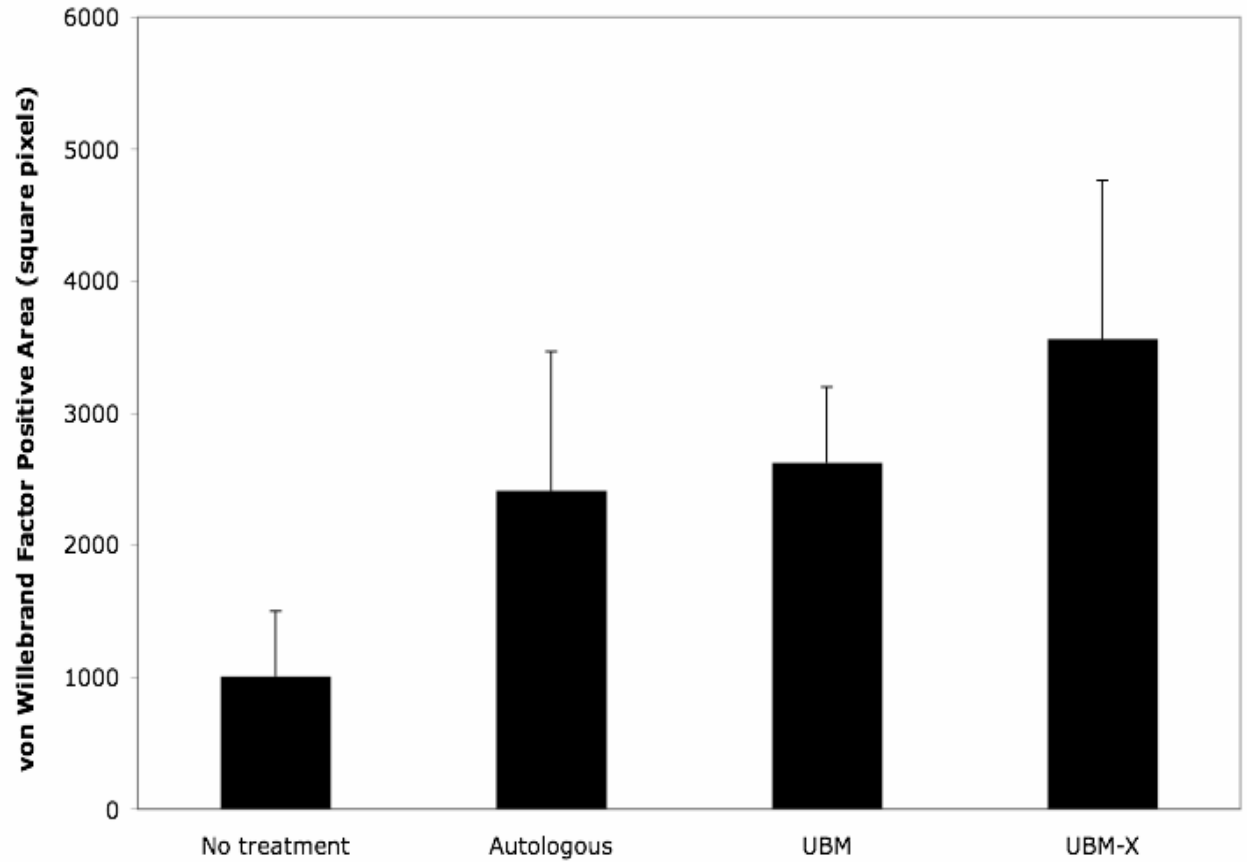

Figure 33. Quantification of von Willebrand factor stained area in remodeling mouse skin at 28 days post-surgery. Mean ± SEM (n=3)

4.4 DISCUSSION

The present study demonstrates that scaffold type affects the temporal remodeling response of a full thickness skin injury in mice. Wound treatment with a non-chemically crosslinked rapidly degrading ECM scaffold resulted in better early remodeling and an earlier end of the inflammatory stage than other treatments, as shown by Masson's trichrome stained images. At 28 days post-surgery, the wounds treated with the non-chemically crosslinked ECM scaffold showed a more mature collagen profile than wounds repaired with autologous tissue. The

chemically crosslinked ECM scaffolds degraded more slowly and appeared to lag behind the remodeling of the rapidly degrading ECM scaffolds, as did the autologous repaired and untreated wounds.

Bone marrow-derived cells participated in the early remodeling of wounded mouse skin but did not appear to participate in the long-term remodeling (beyond the levels found in normal uninjured mouse skin) for any of the treatment groups investigated. The rapidly degrading ECM scaffold, autologous repair, and untreated groups all recruited bone marrow-derived cells during early wound remodeling, but by 14 days post-surgery only the autologous tissue repaired group had more bone marrow-derived cells than normal uninjured mouse skin and by 28 days post-surgery all treatment groups showed a normal number and percentage of bone marrow-derived cells in the remodeling tissue. The chemically crosslinked ECM scaffold group did not show a significantly higher than normal number or percentage of bone marrow-derived cells at any of the timepoints investigated, suggesting that the prevention/retardation of degradation may reduce the participation of bone marrow-derived cells in the early stages of tissue remodeling.

Since untreated, autologous repair, and rapidly degrading ECM all recruited bone marrow-derived cells during early remodeling yet showed different remodeling outcomes over the timepoints examined, the phenotype of the bone marrow-derived cells at 28 days post-surgery was examined. No significant differences in the phenotype of the bone marrow-derived cells were observed between the different treatment groups at this timepoint, but the phenotype of the bone marrow-derived cells that participated in early remodeling of the mouse skin may indicate differences in the cell populations recruited to the different treatment groups. Additionally, based on the presence of more macrophages than in normal skin at 28 days post-surgery, a greater and more prolonged bone marrow-derived cell population response, and the

histological appearance of the remodeling tissue, the autologous repair group appeared to have a stronger and more prolonged inflammatory response than the other treatment groups.

The role of macrophages, one type of bone marrow-derived cell, in ECM and autologous repaired tissues has been an area of interest. A recent study showed that circulating macrophages are at least partially responsible for early degradation of SIS-ECM scaffolds and autografts in a rat body wall repair model [44]. Carbodiimide crosslinked SIS-ECM scaffolds in this body wall repair study inhibited macrophage-mediated scaffold degradation for up to two weeks [44], while the carbodiimide crosslinked UBM-ECM scaffolds in the present study inhibited scaffold degradation for just one week. This difference suggests that anatomic location of the ECM-induced repair affects the scaffold degradation rate. In addition, in contrast to the present study, a previous study showed that SIS-ECM repaired Achilles tendon in GFP bone marrow chimera mice recruited bone marrow-derived cells that participated in the long-term constructive remodeling of the tendon while autologous repair did not. These findings suggest that at least some of the mechanisms of ECM remodeling, such as the populations of cells recruited, may vary between different anatomic locations.

Local cells also play an important role in remodeling mouse skin. In particular, local dermal fibroblasts and epidermal keratinocytes migrate into the wound site, along with bone marrow-derived cells [145]. Previous studies have shown that degradation products of ECM scaffolds have chemoattractant activity for multipotential cells [68], endothelial cells [21], and epidermal keratinocytes [131] *in vitro*. If the same chemoattractant activity is present in degrading ECM scaffolds *in vivo*, as was suggested by a recent study investigating the chemoattractant activity of remodeling ECM-repaired tendons for multipotent cells *in vitro* [70],

the recruitment of local cells may partially explain the more rapid remodeling induced by the rapidly degrading ECM scaffold in the present study.

4.5 LIMITATIONS AND FUTURE WORK

One limitation to the present study is that there were only three mice per treatment group and timepoint. With a typical degree of variability between results for different animals, it is difficult to draw firm conclusions from data with n=3. If additional animals had been available for the present study, increasing the sample size to eight mice per treatment group and timepoint would have given this study greater statistical power. Also if additional animals had been available, excised remodeling skin from additional mice could have been dispersed into single cell suspension, stained with antibodies, and analyzed by flow cytometry for additional quantitative analysis of cell phenotype using a wide panel of antigens and combinations of antigens.

An additional limitation to the present study is that scaffold degradation was not completely prevented in this model by carbodiimide crosslinking. A future study could investigate differences in cell recruitment of naturally occurring ECM and chemically crosslinked ECM in GFP bone marrow chimera mice that have been injected with clodronate liposomes to deplete circulating monocytes/macrophages. Investigating these issues in a different organ model within the GFP bone marrow chimera mice, in which scaffolds degrade more slowly than in skin wounds, or in an anatomic location in which bone marrow-derived cells do not play a role in normal tissue homeostasis or long-term remodeling (such as the Achilles

tendon) may also address the hypothesis more completely. Despite the complicating factors inherent in *in vivo* studies, *in vitro* studies to show that prevention of ECM degradation prevents cell recruitment would be experimentally difficult/impossible to do.

5.0 DISSERTATION SYNOPSIS

ECM scaffolds have been shown to induce site-specific constructive remodeling of injured tissue, and the results of several previous studies suggest that the degradation products of these scaffolds recruit cells that participate in the constructive remodeling process. ECM contains intact signaling molecules (i.e., growth factors) and matricryptic molecules that are activated by ECM degradation. Additionally, ECM scaffolds have been shown to generate degradation products with bioactivities that are not present within intact ECM scaffolds. This dissertation investigated the hypothesis that degradation products of ECM scaffolds possess chemoattractant properties for progenitor cell populations that participate in constructive remodeling.

The first specific aim investigated different methods of *in vitro* degradation of ECM, to determine if *in vitro* methods that were more physiologically relevant than methods used in preliminary studies yielded degradation products with chemoattractant activity. Both pepsin and collagenase digestion of UBM-ECM resulted in degradation products with chemoattractant activity for two distinct progenitor cell populations.

The second specific aim investigated the hypothesis that ECM degradation products from a given tissue have more potent chemoattractant properties for progenitor cells derived from the same tissue type than for progenitor cells derived from other tissues. Although ECM derived from skin, liver, small intestine, and urinary bladder all showed chemoattractant activity for at least one progenitor cell population, a tissue-specific chemotactic effect was not observed in

studies using skin, liver, and intestinal progenitor cells *in vitro*. However, results showed that the age and species from which ECM is harvested has an effect on the chemoattractant potential of the ECM for some progenitor cell populations.

The third specific aim investigated the hypothesis that prevention or retardation of ECM degradation *in vivo* would reduce bone marrow-derived progenitor cell involvement in constructive remodeling, yielding a different histomorphologic outcome than if ECM degradation had occurred normally. Bone marrow-derived cells participated in the early remodeling of wounded mouse skin treated with rapidly degrading UBM-ECM, as well as untreated and autologous repaired skin wounds. By 28 days post-surgery, the number of bone marrow-derived cells returned to similar numbers as found in normal uninjured mouse skin, suggesting that the marrow-derived cells do not participate in the long-term constructive remodeling of mouse skin. Chemically crosslinked UBM-ECM, which degraded more slowly than naturally occurring UBM-ECM, did not recruit more bone marrow-derived cells than are found in normal uninjured mouse skin at any time investigated in this study. Wounds treated with rapidly degrading UBM-ECM also appeared to remodel more rapidly than any of the other treatment groups and showed a more mature collagen profile at 28 days post-surgery than wounds repaired with autologous tissue. These results suggest that scaffold type affects the temporal remodeling of injured mouse skin and that while bone marrow-derived cells participate in remodeling of skin wounds in mice, local tissue cells may also play an important role.

Suggested future work has been described at the end of each chapter. Overall, the work presented in this dissertation is a step toward understanding the cell recruitment involved in constructive remodeling induced by ECM scaffolds. Additional studies investigating other *in vitro* methods of ECM degradation, particularly matrix metalloproteinase and human white blood

cell mediated-degradation of ECM, would be of interest. Based on the finding that the age of the tissue from which the ECM is harvested has an effect on the chemoattractant potential of the ECM degradation products, the chemoattractant activity of ECM digests from other human fetal tissues should be evaluated. In addition, porcine ECM could be isolated from pigs over a variety of ages and evaluated for chemoattractant activity. Identification of the specific molecules responsible for the chemoattractant activity of the ECM digests is an important next step that is currently in progress. Finally, additional studies examining the recruitment of bone marrow-derived cells by degrading and non-degrading ECM scaffolds *in vivo* could be performed in anatomical locations in which ECM degrades more slowly (such as the abdominal wall) or in which bone marrow-derived cells do not play a role in normal tissue homeostasis or long-term remodeling (such as the Achilles tendon), with the assistance of flow cytometry for additional quantitative analysis of cell phenotype using a wide panel of antigens and combinations of antigens.

APPENDIX A

ANTIBACTERIAL ACTIVITY WITHIN DEGRADATION PRODUCTS OF BIOLOGIC SCAFFOLDS COMPOSED OF EXTRACELLLAR MATRIX

A.1 INTRODUCTION

Biological scaffolds composed of extracellular matrix (ECM) have been successfully used as templates for the constructive remodeling of numerous tissues in preclinical studies and human clinical applications [1-12]. Such biological scaffolds have been surprisingly resistant to bacterial infection [64, 65, 129, 146], even in clinical applications that are at high risk for bacterial contamination [33, 147-149]. Generally, naturally occurring biomaterials such as those composed of purified collagen or intact ECM are more resistant to bacterial infection than synthetic biomaterials [64, 65, 129, 146, 150].

Porcine-derived ECM composed of small intestinal submucosa (SIS-ECM) has been successfully used as a resorbable biological scaffold for tissue engineering applications in over 500,000 human patients to date, and has shown resistance to deliberate bacterial infection in preclinical studies [64, 65, 129, 146]. Interestingly, the antibacterial activity associated with the SIS-ECM is not a property of the intact ECM itself [69], but rather of the degradation products of the ECM [22]. *In vitro* studies have shown that acid/heat digested SIS-ECM and acid/heat digested urinary bladder submucosa (UBS)-ECM both possess antibacterial activity against gram positive *Staphylococcus aureus* and gram negative *Escherichia coli*. The greatest antibacterial activity appears to be present in degradation peptides between 5-16 kDa [22].

The objective of the present study was to determine if antimicrobial activity similar to that found in SIS-ECM and UBS-ECM is detectable in the degradation products of ECM

scaffolds derived from the liver (L-ECM) and superficial layers (tunica propria and basement membrane) of the porcine urinary bladder (UBM-ECM). These ECM materials have been studied as biologic scaffolds for tissue engineering/regenerative medicine applications and the presence of such activity within these materials could have significant clinical applications.

A.2 MATERIALS AND METHODS

A.2.1 PREPARATION OF ECM POWDERS

Porcine urinary bladders and livers were harvested from market weight pigs (~110 -130 kg) immediately following euthanasia. UBM-ECM was prepared as previously described [74, 75, 151]. In brief, connective and adipose tissue were removed from the serosal surface of the bladder, and the tunica serosa, tunica muscularis externa, tunica submucosa, and most of the tunica muscularis mucosa were mechanically removed. The luminal urothelial cells of the tunica mucosa were dissociated by soaking in a 1.0 N saline solution, leaving a biomaterial composed of only the basement membrane and the subjacent tunica propria of the tunica mucosa, and the resident cell population of those two layers.

L-ECM was prepared by slicing lobes of porcine liver to 5 mm sections, then rinsing the slices in deionized water with agitation on an orbital shaker for a total of three 30-minute rinses. Slices were then placed on a polypropylene mesh and subjected to uniform pressure to burst the hepatocytes. The tissue slices were returned to a flask and submerged in 0.02% trypsin/0.05% EDTA for 1 hour at 37°C, agitated at room temperature in 3% (v/v) Triton X-100 for 1 hour, then in 4% (w/v) deoxycholic acid for 1 hour. Tissue slices were rinsed with deionized water and massaged between each treatment step [74].

Both types of ECM were decellularized by treatment with 0.1% peracetic acid/4% ethanol for two hours and rinsed with phosphate buffered saline (PBS) and deionized water.

Complete decellularization was confirmed by both 4'-6-Diamidino-2-phenylindole (DAPI) nuclear staining and hematoxylin and eosin staining. The ECMs were then lyophilized in sheet form, and frozen. The frozen sheets were comminuted into a particulate form using a Waring commercial blender and Wiley Mill with a #60 mesh screen [75].

A.2.2 DEGRADATION OF ECM

ECM was digested using mild acid and heat. Adapting a previously described procedure [22], lyophilized, particulate ECM was hydrated by placing 10 mg dry weight of ECM in 140 mL of 1X PBS with protease inhibitors (5 mM Benzoamide, 1 mM Phenylmethanesulfonyl fluoride (PMSF), and 10 mM N-ethylmaleimide (NEM)) and stirring for one to two hours, then filtering with vacuum through Whatman #42 filter paper in a Buchner Funnel. The retentate material, which remained hydrated, was collected and suspended in 110 mL of 0.5 N acetic acid. The suspension was transferred to a stirred, glass lined autoclave reactor (Autoclave Engineers, Erie, PA), heated to 120°C over 55 minutes, and held at 120°C for 30 minutes with constant stirring. The suspension was then cooled to 60°C in 2 to 4 minutes and then to room temperature in 15 to 20 minutes. The acid-digested suspension was then removed from the autoclave reactor and filtered in series, through cheesecloth, Fischer P8 filter paper, and Whatman #42 filter paper, with the use of vacuum for the last two filtration steps. The filtrate material was collected and snap-frozen on dry ice and ethanol at an angle to maximize surface area. Samples were lyophilized, yielding a dry ECM digest capable of long-term storage.

A.2.3 AMMONIUM SULFATE PRECIPITATION OF ECM DIGESTS

The lyophilized ECM digest was resuspended in [0.1 M sodium phosphate/0.15 M sodium chloride] pH 6.8, with 2 mM PMSF (Resuspension Buffer) at 200 mg dry sample mass per milliliter. The sample was rocked at room temperature for 45 minutes to resuspend, centrifuged at 12000 rpm for 1 hour, and finally filtered through a 0.45 mm syringe filter. A bicinchoninic acid (BCA) assay (Pierce Biotechnology, Rockford, IL) was performed to estimate protein concentration of the suspension. The suspension was then diluted with Resuspension Buffer to a concentration of 10 mg protein per milliliter. Ammonium sulfate was added to the suspension to saturation percentages of 10%, 20%, 30%, 40%, 50%, 60%, 70%, 80%, and 100%. The saturation percentage was slowly increased by 10% daily, with constant stirring at 4°C to avoid localized precipitation of proteins. At each percentage mark, the solution was centrifuged at 12000 rpm resulting in the formation of a firm pellet. The supernatant was removed from the tubes and stored at 4°C overnight. 2 mM fresh PMSF was added the following morning before adding additional salt. The precipitated pellets were resuspended in Resuspension Buffer, snap frozen, and stored at -80°C. Samples of the supernatants and resuspended pellets were desalted, concentrated, and pH neutralized with Microcon YM-3 centrifugal filter devices, with a 3 kD molecular weight cutoff (Millipore, Billerica, MA). Desalted samples were snap frozen and stored at -80°C for further analysis.

A.2.4 ANTIMICROBIAL ASSAY

Tryptic soy agar plates were streaked with *Staphylococcus aureus* (American Type Culture Collection 29213, wound isolate) and *Escherichia coli* (American Type Culture Collection

25922, clinical isolate), and an isolated colony from each was used to inoculate 10 mL of tryptic soy broth. The bacteria were grown in suspension overnight in a 37°C shaker. The bacteria were then diluted to 5 x 10^5 CFU/mL [22], and 150 mL of bacterial suspension were added to each well of a 96-well microplate. 16.5 mL of each sample to be tested for antibacterial activity was added to the bacterial suspension. Samples tested include desalted UBM-ECM or L-ECM digest ammonium sulfate fractions, a three-fold dilution of each fraction, a negative control of media alone, and positive controls of antibiotics (vancomycin for *S. aureus* and tetracycline for *E. coli*). Each sample was tested in duplicate. The bacterial growth in each well was monitored over the course of 24 hours by absorbance readings at 570 nm with a BioRad 680 microplate reader. Statistical significance of the absorbance values between samples was determined by the paired t-test. The absorbance reading of each UBM-ECM or L-ECM fraction was compared to the negative control of media alone for each time point.

A.3 RESULTS

Degradation products from both UBM-ECM and L-ECM demonstrated antibacterial activity against both *S. aureus* and *E. coli*. All UBM-ECM and L-ECM digest desalted ammonium sulfate pellets and supernatants were tested for antibacterial activity. Those fractions demonstrating statistically significant inhibition of bacterial growth are shown in Figures 34, 35, and 36. The most potent antibacterial activity was present in the UBM-ECM pellet precipitated at 60% ammonium sulfate saturation. This sample effectively inhibited *S. aureus* growth for 24 hours (Figure 34). This same sample also effectively inhibited *E. coli* growth for 9 hours (Figure 35). The L-ECM digest precipitated with 60% ammonium sulfate showed strong antibacterial activity against both *E. coli* and *S. aureus* (Figures 34 and 35). Furthermore, the L-ECM pellet that precipitated at 40% ammonium sulfate saturation showed the greatest activity of all samples tested against *S. aureus*, inhibiting growth for the full 24 hours of the assay (Figure 34). These results suggest that there are multiple antibacterial molecules present in ECM degradation products, and that differences exist between antimicrobial peptides present in L-ECM and UBM-ECM.

The ECM digest samples that were diluted three-fold showed antibacterial activity only against *S. aureus* (Figure 36). The diluted samples of the UBM-ECM digest 60% ammonium sulfate pellet and L-ECM 40% ammonium sulfate pellet were equally as effective at inhibiting bacterial growth as the undiluted samples at the same ammonium sulfate saturation. The diluted

L-ECM digest at 60% ammonium sulfate concentration pellet also demonstrated a small amount of antibacterial activity against *S. aureus*. Interestingly, the UBM-ECM digest pellet that precipitated at 20% ammonium sulfate saturation, which had no measurable antibacterial activity when undiluted, strongly inhibited *S. aureus* growth when diluted three-fold (Figure 36).

Absorbance readings at t=0 varied due to the opacity of some samples when added to the bacterial suspension. Some samples contained precipitates that dissolved after incubation with the bacterial suspension. Within a few hours of incubation these samples no longer appeared to be opaque by visual inspection; this observation was supported by absorbance readings. After 24 hours, the appearance of wells containing samples that demonstrated a strong antibacterial effect showed a striking difference from wells in which bacterial proliferation occurred (Figure 37).

A preliminary characterization of UBM-ECM and L-ECM fractions that showed antibacterial activity included determination of protein concentration by BCA assay. The UBM-ECM pellets that precipitated at 60% and 20% ammonium sulfate saturation had protein concentrations of approximately 80 mg protein/mL, and 90 mg protein/mL, respectively. The L-ECM pellets that precipitated at 40% and 60% ammonium sulfate saturation had protein concentrations of approximately 50 mg protein/mL and 10 mg protein/mL, respectively. SDS-PAGE was performed to estimate the molecular weight of the UBM-ECM fractions that demonstrated antibacterial activity, with an approximate molecular weight range of 7-15 kDa.

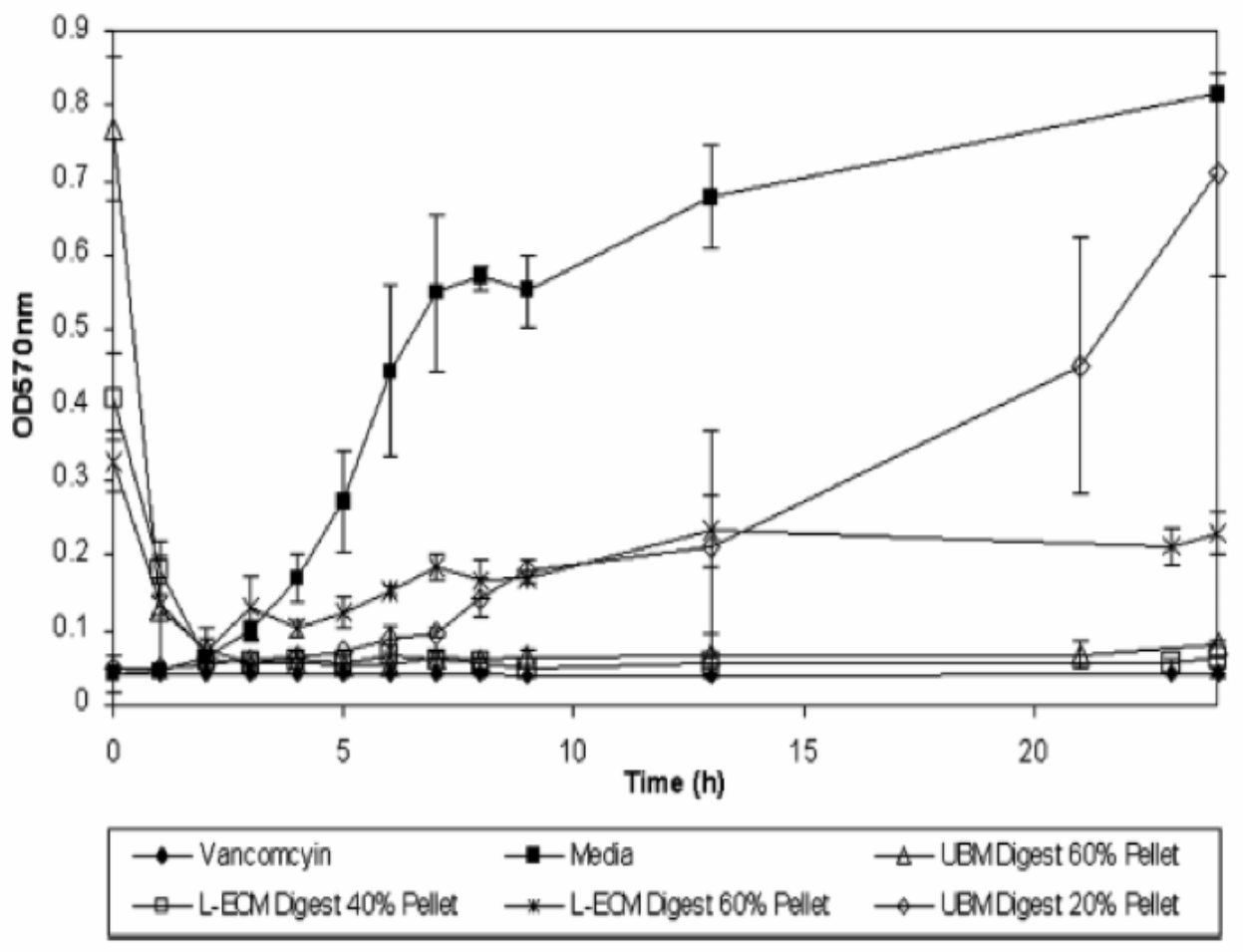

Figure 34. Effect of porcine urinary bladder (UBM-ECM) and liver (L-ECM) extracellular matrix digest ammonium sulfate fractions on *Staphylococcus aureus* growth. All absorbance values were statistically significant compared with the negative control of media with $p < 0.05$ except L-ECM digest 40% pellet at 2 h; L-ECM digest 60% pellet at 2 and 3 h; UBM-ECM digest 20% pellet at 4, 5, 21, and 24 h; and UBM-ECM digest 60% pellet at 1 and 2h.

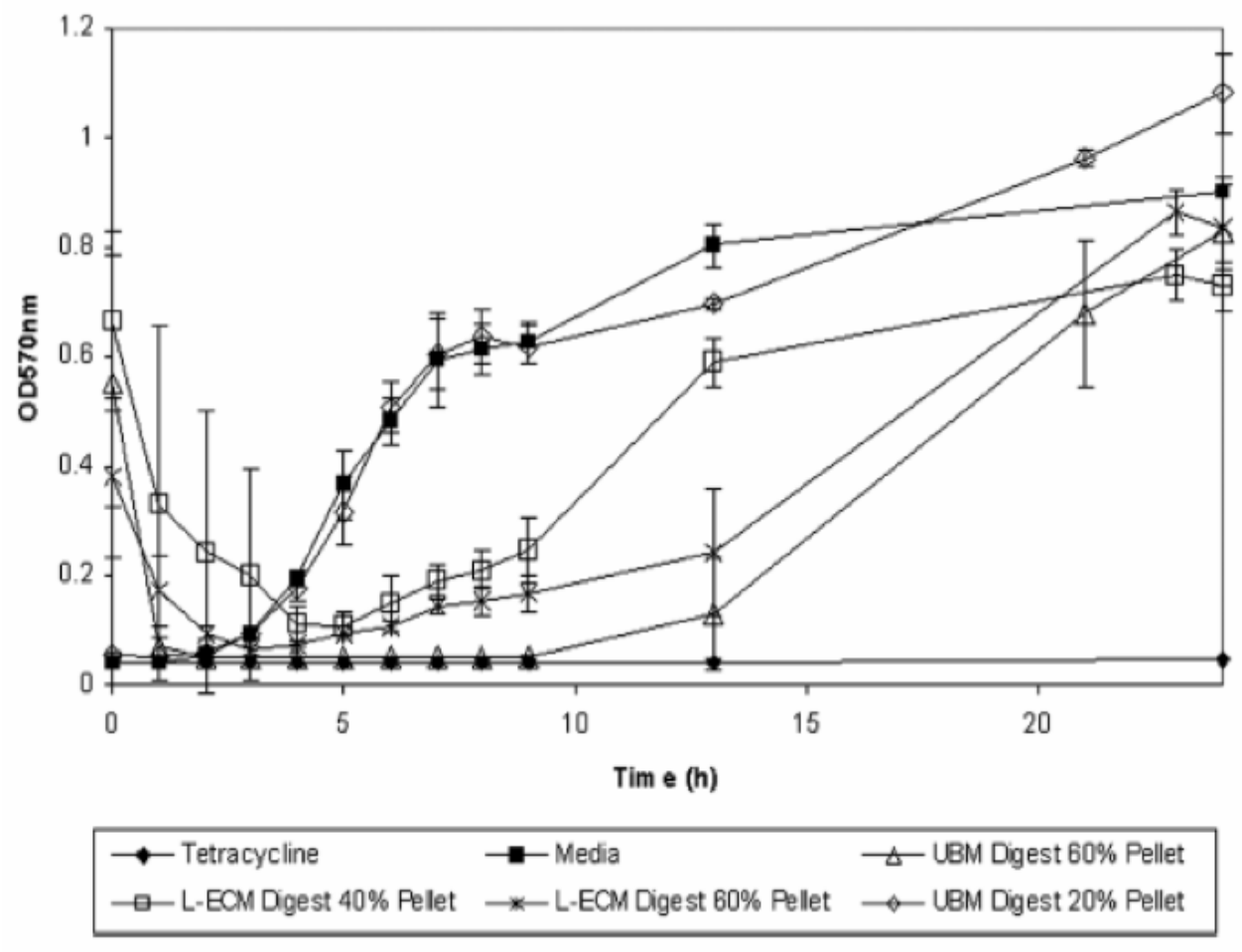

Figure 35. Effect of porcine urinary bladder (UBM-ECM) and liver (L-ECM) extracellular matrix digest ammonium sulfate fractions on *Escherichia coli* growth. All absorbance values were statistically significant compared with the negative control of media with $p < 0.05$ except L-ECM digest 40% pellet at 0–4, 13, 23, and 24 h; L-ECM digest 60% pellet at 0–2, 23, and 24 h; UBM-ECM digest 20% pellet at all time points; and UBM-ECM digest 60% pellet at 0, 1, 5, 21, and 24 h.

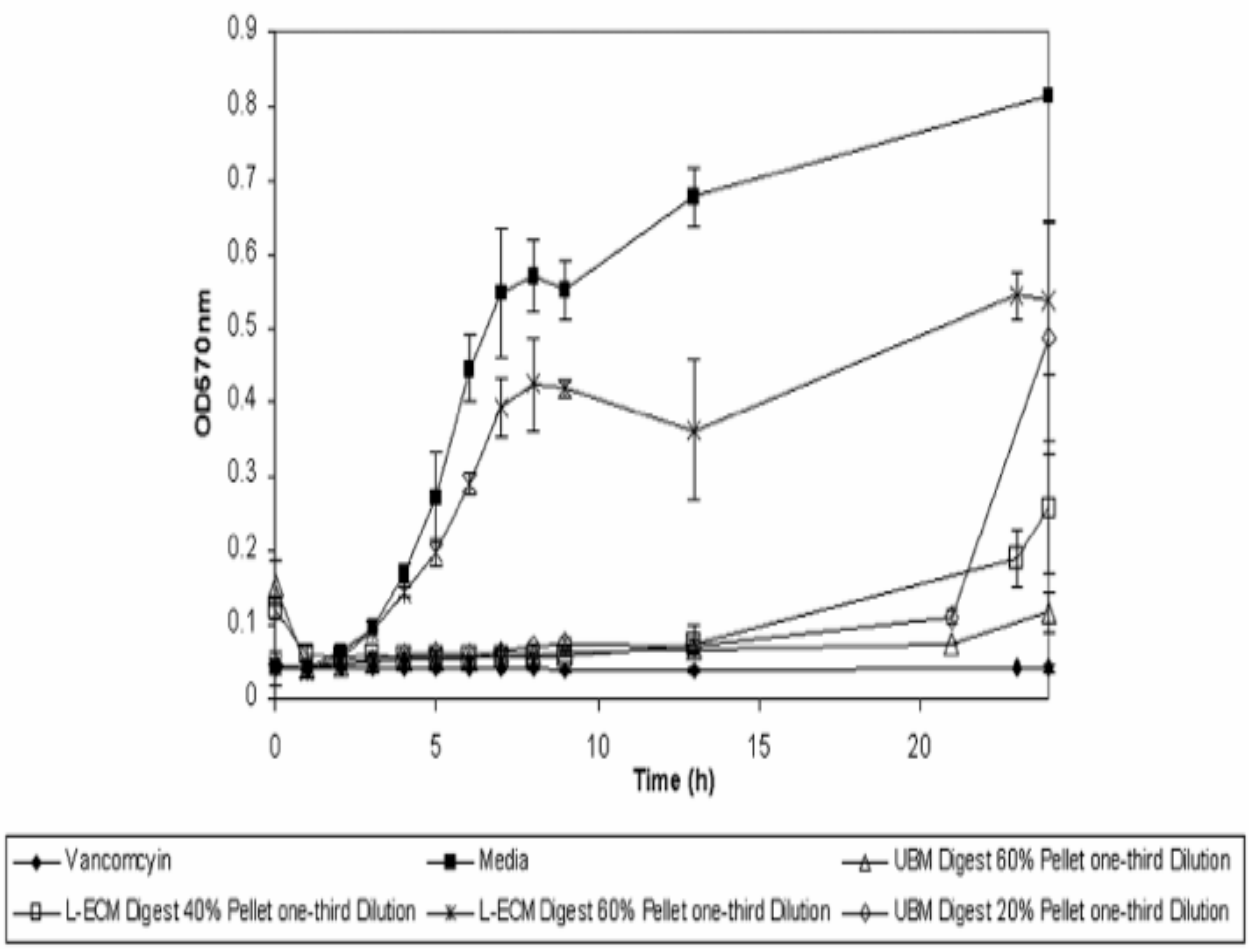

Figure 36. Effect of diluted porcine urinary bladder (UBM-ECM) and liver (L-ECM) extracellular matrix digest ammonium sulfate fractions on *Staphylococcus aureus* growth. All absorbance values were statistically significant compared with the negative control of media with $p < 0.05$ except L-ECM digest 40% pellet at 1, 2, and 23 h; L-ECM digest 60% pellet at 0–3, and 8–24 h; UBM-ECM digest 20% pellet at 0–2, 4, and 24 h; and UBM-ECM digest 60% pellet at 0, 1, and 4 h.

Figure 37. Appearance of microplate containing *Staphylococcus aureus* after 24 hour incubation at 37°C. The clear well, E8, contains liver extracellular matrix (L-ECM) digest 40% ammonium sulfate pellet. The surrounding samples did not exhibit strong antibacterial activity

A4. DISCUSSION

The present study demonstrates that the degradation products of UBM-ECM and L-ECM scaffold materials possess antibacterial activity against both *S. aureus* and *E. coli*. Urinary bladder-derived ECM has been used in numerous regenerative medicine applications, including bladder regeneration, urethral repair, and esophageal repair [12, 152, 153]. Liver-derived ECM has also been evaluated as a biologic scaffold for use in regenerative medicine [154].

The antimicrobial peptides present in the degradation products of UBM-ECM and L-ECM were released by acid/heat digestion and fractionated by ammonium sulfate precipitation. Ammonium sulfate precipitation of the degraded ECM resulted in fractions that showed variable degrees of antibacterial activity against *S. aureus* and *E. coli*. Certain fractions showed greater antibacterial activity at lower concentrations of total protein. These observations suggest that each ammonium sulfate fraction contains a complex mixture of proteins. This mixture may include both antimicrobial peptides as well as inhibitors of those peptides, the combination of which cause a net effect of antibacterial activity when present in specific concentrations. The full spectrum of antimicrobial activity of these low molecular weight peptides has not been determined, including their efficacy against anaerobic bacteria.

Certain ammonium sulfate precipitated fractions from both ECMs maintained strong antibacterial activity against gram positive *S. aureus* for a longer period of time than against gram negative *E. coli*. While the antibacterial activity against *S. aureus* persisted for the full 24

hours of the assay, the antibacterial activity against *E. coli* declined as the antibacterial peptides present in the digest fractions either lost activity or were stoichiometrically overwhelmed by the bacteria. The short-term antibacterial effects of ECM degradation products may be particularly beneficial in preventing an implant infection by providing immediate protection while the host inflammatory cell response and humoral immune response become activated. In addition, as the ECM bioscaffold is subjected to progressive degradation *in vivo* and is remodeled by host tissues, antimicrobial peptides may continue to be released, providing a sustained antibacterial effect.

Degradation of the ECM is one of the earliest events following tissue injury. ECM degrades rapidly and is completely resorbed within 90 days [14, 16, 155]. Degradation products of ECM derived from several tissues have previously shown biologic properties such as antimicrobial, chemotactic, and angiogenic activity [21, 22, 156]. The methods used in the present study to digest the ECM cause cleavage of inactive parent molecules and the production of bioactive fragment molecules. The degradation products of several types of collagen, fibronectin, and laminin are known to produce fragment molecules with angiogenic, anti-angiogenic, and chemotactic properties [46-48, 61, 156, 157]. The present study suggests that antimicrobial activity can be added to the list of bioactive properties that result from ECM degradation. The harsh *in vitro* methods used in the present study may or may not relate to the degradation of ECM bioscaffolds that occurs *in vivo*. It seems improbable that the acid/heat digestion of different types of ECM would by chance produce bioactive peptides that are not created by physiological degradation processes. It remains to be shown however that *in vivo* degradation mechanisms generate the same types of bioactive peptides.

Naturally occurring antimicrobial peptides (AMPs) that play key roles in innate immunity have been isolated from plants (thionins), several insect orders (cecropins), amphibians (magainins), and mammals (defensins). Most AMPs have certain common features, including small size (12-100 amino acid residues), polycationic charge, amphipathic structure, and a common mechanism for killing bacteria, which involves direct electrostatic interaction with microbial cell membranes, followed by physical disruption of the membrane [158]. Most AMPs are produced as part of the innate immune defense system and stored in the granules of cells involved in immune response. AMPs are synthesized as propeptides that are activated by proteolytic cleavage, releasing the active antimicrobial peptide, which may have microbicidal effects against gram negative bacteria, gram positive bacteria, yeast, or enveloped viruses [158, 159].

At least eighteen AMPs, with a broad range of antimicrobial activity, have been identified from various porcine cells and tissues [158, 160-162]. The upper portion of porcine small intestine, when immersed in boiling water, frozen, and extracted with cold 0.5 M acetic acid [163] has been shown to possess several AMPs [160-162]. Using this method, a cecropin-like AMP with activity against *E. coli* and other gram negative bacteria was the first porcine AMP to be purified and identified, in 1989 [162]. Since then, additional porcine AMPs have been isolated from the small intestine [160, 161], as well as from polymorphonuclear leukocytes and lymphocytes [158]. It may not be surprising then that both *in vitro* and *in vivo* antimicrobial activity was found in the SIS-ECM biologic scaffold [22, 64, 65, 129, 146]. One porcine defensin, pBD-1, was cloned and found to be expressed by the epithelia of both the gastrointestinal and respiratory tracts as well as in urinary bladder, liver, skin, kidney, lymph node, and others [164].

Naturally occurring AMPs that have been identified from porcine sources generally have molecular weights of less than 10kD [158], which coincides with the 5-16 kD molecular weight range of the fraction of SIS-ECM and UBS-ECM extracts that possess antimicrobial activity [22]. The present study shows that the UBM-ECM and L-ECM antibacterial peptides also exist within this molecular weight range based on SDS-PAGE analysis (not shown). However it is currently unknown if the ECM-derived antibacterial peptides are the same as any of the already identified porcine AMPs or represent novel AMPs. Further purification, isolation, and identification of these antimicrobial peptides from ECM degradation products will better elucidate the mechanism by which they are produced and their *in vivo* functionality.

Antibacterial activity has now been shown in four different types of non-chemically cross-linked ECM, suggesting that this biological activity may be a common feature of all ECM. The findings of the present study lend support to the use of ECM biologic scaffolds for regenerative medicine applications, particularly for use in sites with high potential for bacterial contamination.

BIBLIOGRAPHY

1. Badylak, S.F., et al., *Small intestinal submucosa as a large diameter vascular graft in the dog.* J Surg Res, 1989. **47**(1): p. 74-80.

2. Badylak, S.F., et al., *The use of xenogeneic small intestinal submucosa as a biomaterial for Achilles tendon repair in a dog model.* J Biomed Mater Res, 1995. **29**(8): p. 977-85.

3. Badylak, S., et al., *Resorbable bioscaffold for esophageal repair in a dog model.* J Pediatr Surg, 2000. **35**(7): p. 1097-103.

4. Badylak, S., et al., *Extracellular matrix for myocardial repair.* Heart Surg Forum, 2003. **6**(2): p. E20-6.

5. Vaught, J.D., et al., *Detrusor regeneration in the rat using porcine small intestinal submucosal grafts: functional innervation and receptor expression.* J Urol, 1996. **155**(1): p. 374-8.

6. Kropp, B.P., et al., *Regenerative urinary bladder augmentation using small intestinal submucosa: urodynamic and histopathologic assessment in long-term canine bladder augmentations.* J Urol, 1996. **155**(6): p. 2098-104.

7. Kropp, B.P., et al., *Experimental assessment of small intestinal submucosa as a bladder wall substitute.* Urology, 1995. **46**(3): p. 396-400.

8. Dahms, S.E., et al., *Free ureteral replacement in rats: regeneration of ureteral wall components in the acellular matrix graft.* Urology, 1997. **50**(5): p. 818-25.

9. Atala, A., *Experimental and clinical experience with tissue engineering techniques for urethral reconstruction.* Urol Clin North Am, 2002. **29**(2): p. 485-92, ix.

10. Dejardin, L.M., S.P. Arnoczky, and R.B. Clarke, *Use of small intestinal submucosal implants for regeneration of large fascial defects: an experimental study in dogs.* J Biomed Mater Res, 1999. **46**(2): p. 203-11.

11. Badylak, S.F., *Xenogeneic extracellular matrix as a scaffold for tissue reconstruction.* Transpl Immunol, 2004. **12**(3-4): p. 367-77.

12. Badylak, S.F., et al., *Esophageal reconstruction with ECM and muscle tissue in a dog model.* J Surg Res, 2005. **128**(1): p. 87-97.

13. Gilbert, T.W., et al., *Repair of the thoracic wall with an extracellular matrix scaffold in a canine model.* J Surg Res, 2008. **147**(1): p. 61-7.

14. Badylak, S.F., et al., *Small intestional submucosa: a rapidly resorbed bioscaffold for augmentation cystoplasty in a dog model.* Tissue Eng, 1998. **4**(4): p. 379-87.

15. Nieponice, A., et al., *An extracellular matrix scaffold for esophageal stricture prevention after circumferential EMR.* Gastrointest Endosc, 2009. **69**(2): p. 289-96.

16. Record, R.D., et al., *In vivo degradation of 14C-labeled small intestinal submucosa (SIS) when used for urinary bladder repair.* Biomaterials, 2001. **22**(19): p. 2653-9.

17. Gilbert, T.W., A.M. Stewart-Akers, and S.F. Badylak, *A quantitative method for evaluating the degradation of biologic scaffold materials.* Biomaterials, 2007. **28**(2): p. 147-50.

18. Badylak, S.F., et al., *Marrow-derived cells populate scaffolds composed of xenogeneic extracellular matrix.* Exp Hematol, 2001. **29**(11): p. 1310-8.

19. Zantop, T., et al., *Extracellular matrix scaffolds are repopulated by bone marrow-derived cells in a mouse model of achilles tendon reconstruction.* J Orthop Res, 2006. **24**(6): p. 1299-309.

20. Brennan, E.P., et al., *Antibacterial Activity within Degradation Products of Biological Scaffolds Composed of Extracellular Matrix.* Tissue Eng, 2006. **12**(10): p. 2949-55.

21. Li, F., et al., *Low-molecular-weight peptides derived from extracellular matrix as chemoattractants for primary endothelial cells.* Endothelium, 2004. **11**(3-4): p. 199-206.

22. Sarikaya, A., et al., *Antimicrobial activity associated with extracellular matrices.* Tissue Eng, 2002. **8**(1): p. 63-71.

23. Valentin, J.E., et al., *Extracellular matrix bioscaffolds for orthopaedic applications. A comparative histologic study.* J Bone Joint Surg Am, 2006. **88**(12): p. 2673-86.

24. Badylak, S.F., *The extracellular matrix as a scaffold for tissue reconstruction.* Semin Cell Dev Biol, 2002. **13**(5): p. 377-83.

25. Badylak, S.F., et al., *The use of extracellular matrix as an inductive scaffold for the partial replacement of functional myocardium.* Cell Transplant, 2006. **15 Suppl 1**: p. S29-40.

26. Chen, M.K. and S.F. Badylak, *Small bowel tissue engineering using small intestinal submucosa as a scaffold.* J Surg Res, 2001. **99**(2): p. 352-8.

27. Clarke, K.M., et al., *Intestine submucosa and polypropylene mesh for abdominal wall repair in dogs.* J Surg Res, 1996. **60**(1): p. 107-14.

28. Cobb, M.A., et al., *Histology after dural grafting with small intestinal submucosa.* Surg Neurol, 1996. **46**(4): p. 389-93; discussion 393-4.

29. Cobb, M.A., et al., *Porcine small intestinal submucosa as a dural substitute.* Surg Neurol, 1999. **51**(1): p. 99-104.

30. Kropp, B.P., et al., *Rabbit urethral regeneration using small intestinal submucosa onlay grafts.* Urology, 1998. **52**(1): p. 138-42.

31. Kropp, B.P., et al., *Characterization of small intestinal submucosa regenerated canine detrusor: assessment of reinnervation, in vitro compliance and contractility.* J Urol, 1996. **156**(2 Pt 2): p. 599-607.

32. Lantz, G.C., et al., *Small intestinal submucosa as a small-diameter arterial graft in the dog.* J Invest Surg, 1990. **3**(3): p. 217-27.

33. Mantovani, F., et al., *Reconstructive urethroplasty using porcine acellular matrix.* Eur Urol, 2003. **44**(5): p. 600-2.

34. Musahl, V., et al., *The use of porcine small intestinal submucosa to enhance the healing of the medial collateral ligament--a functional tissue engineering study in rabbits.* J Orthop Res, 2004. **22**(1): p. 214-20.

35. Robinson, K.A., et al., *Extracellular matrix scaffold for cardiac repair.* Circulation, 2005. **112**(9 Suppl): p. I135-43.

36. Suckow, M.A., et al., *Enhanced bone regeneration using porcine small intestinal submucosa.* J Invest Surg, 1999. **12**(5): p. 277-87.

37. Anderson, J.M., *Inflammation, Wound Healing, and the Foreign-Body Response*. 2 ed. Biomaterials Science: An Introduction to Materials in Medicine, ed. B.D. Ratner, Hoffman, A.S., Schoen, F.J., Lemons, J.E. 2004: Elsevier. 296-304.

38. Coury, A.J., *Chemical and Biochemical Degradation of Polymers*. 2 ed. Biomaterials Science: An Introduction to Materials in Medicine, ed. B.D. Ratner, Hoffman, A.S., Schoen, F.J., Lemons, J.E. 2004: Elsevier. 411-430.

39. *Acute and Chronic Inflammation*, in *Robbins and Cotran Pathologic Basis of Disease*, V. Kumar, Abbas, A.K., Fausto, N., Editor. 2005, Elsevier. p. 47-86.

40. Woessner, J.F., Nagase, H., *Matrix Metalloproteinases and TIMPs*. 2000, New York: Oxford.

41. Gilbert, T.W., A.M. Stewart-Akers, and S.F. Badylak, *A quantitative method for evaluating the degradation of biologic scaffold materials.* Biomaterials, 2006.

42. van Amerongen, M.J., et al., *The enzymatic degradation of scaffolds and their replacement by vascularized extracellular matrix in the murine myocardium.* Biomaterials, 2006. **27**(10): p. 2247-57.

43. Yannas, I.V., *Natural Materials*. 2 ed. Biomaterials Science: An Introduction to Materials in Medicine, ed. B.D. Ratner, Hoffman, A.S., Schoen, F.J., Lemons, J.E. 2004: Elsevier. 127-136.

44. Valentin, J.E., et al., *Macrophage Participation in the Degradation and Remodeling of ECM Scaffolds.* Tissue Eng Part A, 2009.

45. Davis, G.E., et al., *Regulation of tissue injury responses by the exposure of matricryptic sites within extracellular matrix molecules.* Am J Pathol, 2000. **156**(5): p. 1489-98.

46. Schenk, S. and V. Quaranta, *Tales from the crypt[ic] sites of the extracellular matrix.* Trends Cell Biol, 2003. **13**(7): p. 366-75.

47. Ortega, N. and Z. Werb, *New functional roles for non-collagenous domains of basement membrane collagens.* J Cell Sci, 2002. **115**(Pt 22): p. 4201-14.

48. Mott, J.D. and Z. Werb, *Regulation of matrix biology by matrix metalloproteinases.* Curr Opin Cell Biol, 2004. **16**(5): p. 558-64.

49. Xu, J., et al., *Proteolytic exposure of a cryptic site within collagen type IV is required for angiogenesis and tumor growth in vivo.* J Cell Biol, 2001. **154**(5): p. 1069-79.

50. Xu, R., et al., *NC1 domain of human type VIII collagen (alpha 1) inhibits bovine aortic endothelial cell proliferation and causes cell apoptosis.* Biochem Biophys Res Commun, 2001. **289**(1): p. 264-8.

51. Ramchandran, R., et al., *Antiangiogenic activity of restin, NC10 domain of human collagen XV: comparison to endostatin.* Biochem Biophys Res Commun, 1999. **255**(3): p. 735-9.

52. Ambesi, A., et al., *Anastellin, a fragment of the first type III repeat of fibronectin, inhibits extracellular signal-regulated kinase and causes G(1) arrest in human microvessel endothelial cells.* Cancer Res, 2005. **65**(1): p. 148-56.

53. Senior, R.M., G.L. Griffin, and R.P. Mecham, *Chemotactic activity of elastin-derived peptides.* J Clin Invest, 1980. **66**(4): p. 859-62.

54. Senior, R.M., G.L. Griffin, and R.P. Mecham, *Chemotactic responses of fibroblasts to tropoelastin and elastin-derived peptides.* J Clin Invest, 1982. **70**(3): p. 614-8.

55. Ponce, M.L., et al., *Identification of a potent peptide antagonist to an active laminin-1 sequence that blocks angiogenesis and tumor growth.* Cancer Res, 2003. **63**(16): p. 5060-4.

56. Slevin, M., S. Kumar, and J. Gaffney, *Angiogenic oligosaccharides of hyaluronan induce multiple signaling pathways affecting vascular endothelial cell mitogenic and wound healing responses.* J Biol Chem, 2002. **277**(43): p. 41046-59.

57. Chen, W.Y. and G. Abatangelo, *Functions of hyaluronan in wound repair.* Wound Repair Regen, 1999. **7**(2): p. 79-89.

58. Deed, R., et al., *Early-response gene signalling is induced by angiogenic oligosaccharides of hyaluronan in endothelial cells. Inhibition by non-angiogenic, high-molecular-weight hyaluronan.* Int J Cancer, 1997. **71**(2): p. 251-6.

59. Mongiat, M., et al., *Endorepellin, a novel inhibitor of angiogenesis derived from the C terminus of perlecan.* J Biol Chem, 2003. **278**(6): p. 4238-49.

60. Senger, D.R. and C.A. Perruzzi, *Cell migration promoted by a potent GRGDS-containing thrombin-cleavage fragment of osteopontin.* Biochim Biophys Acta, 1996. **1314**(1-2): p. 13-24.

61. Cornelius, L.A., et al., *Matrix metalloproteinases generate angiostatin: effects on neovascularization.* J Immunol, 1998. **161**(12): p. 6845-52.

62. Pike, S.E., et al., *Vasostatin, a calreticulin fragment, inhibits angiogenesis and suppresses tumor growth.* J Exp Med, 1998. **188**(12): p. 2349-56.

63. Senior, R.M., et al., *Val-Gly-Val-Ala-Pro-Gly, a repeating peptide in elastin, is chemotactic for fibroblasts and monocytes.* J Cell Biol, 1984. **99**(3): p. 870-4.

64. Badylak, S.F., et al., *Host protection against deliberate bacterial contamination of an extracellular matrix bioscaffold versus Dacron mesh in a dog model of orthopedic soft tissue repair.* J Biomed Mater Res B Appl Biomater, 2003. **67**(1): p. 648-54.

65. Badylak, S.F., et al., *Comparison of the resistance to infection of intestinal submucosa arterial autografts versus polytetrafluoroethylene arterial prostheses in a dog model.* J Vasc Surg, 1994. **19**(3): p. 465-72.

66. El-Kassaby, A.W., et al., *Urethral stricture repair with an off-the-shelf collagen matrix.* J Urol, 2003. **169**(1): p. 170-3; discussion 173.

67. Nieponice, A., T.W. Gilbert, and S.F. Badylak, *Reinforcement of esophageal anastomoses with an extracellular matrix scaffold in a canine model.* Ann Thorac Surg, 2006. **82**(6): p. 2050-8.

68. Reing, J.E., et al., *Degradation products of extracellular matrix affect cell migration and proliferation.* Tissue Eng Part A, 2009. **15**(3): p. 605-14.

69. Holtom, P.D., et al., *Porcine small intestine submucosa does not show antimicrobial properties.* Clin Orthop Relat Res, 2004(427): p. 18-21.

70. Beattie, A.J., et al., *Chemoattraction of progenitor cells by remodeling extracellular matrix scaffolds.* Tissue Eng Part A, 2009. **15**(5): p. 1119-25.

71. Bagorda, A. and C.A. Parent, *Eukaryotic chemotaxis at a glance.* J Cell Sci, 2008. **121**(Pt 16): p. 2621-4.

72. Stephens, L., L. Milne, and P. Hawkins, *Moving towards a better understanding of chemotaxis.* Curr Biol, 2008. **18**(11): p. R485-94.

73. Badylak, S.F., *The extracellular matrix as a biologic scaffold material.* Biomaterials, 2007. **28**(25): p. 3587-93.

74. Brown, B., et al., *The basement membrane component of biologic scaffolds derived from extracellular matrix.* Tissue Eng, 2006. **12**(3): p. 519-26.

75. Gilbert, T.W., et al., *Production and characterization of ECM powder: implications for tissue engineering applications.* Biomaterials, 2005. **26**(12): p. 1431-5.

76. Sweeney, P.J.a.W., J.M, *Enzymes of Molecular Biology*, ed. M.M. Burrell. 1993, Totowa, NJ: Humana Press. 290-291.

77. Bond, M.D. and H.E. Van Wart, *Purification and separation of individual collagenases of Clostridium histolyticum using red dye ligand chromatography.* Biochemistry, 1984. **23**(13): p. 3077-85.

78. Freytes, D.O., et al., *Preparation and rheological characterization of a gel form of the porcine urinary bladder matrix.* Biomaterials, 2008. **29**(11): p. 1630-7.

79. Clark, L.D., R.K. Clark, and E. Heber-Katz, *A new murine model for mammalian wound repair and regeneration.* Clin Immunol Immunopathol, 1998. **88**(1): p. 35-45.

80. Gourevitch, D., et al., *Matrix metalloproteinase activity correlates with blastema formation in the regenerating MRL mouse ear hole model.* Dev Dyn, 2003. **226**(2): p. 377-87.

81. Leferovich, J.M., et al., *Heart regeneration in adult MRL mice.* Proc Natl Acad Sci U S A, 2001. **98**(17): p. 9830-5.

82. Naviaux, R.K., et al., *Retained features of embryonic metabolism in the adult MRL mouse.* Mol Genet Metab, 2009. **96**(3): p. 133-44.

83. Mongan, N.P., K.M. Martin, and L.J. Gudas, *The putative human stem cell marker, Rex-1 (Zfp42): structural classification and expression in normal human epithelial and carcinoma cell cultures.* Mol Carcinog, 2006. **45**(12): p. 887-900.

84. Csete, M., *Oxygen in the cultivation of stem cells.* Ann N Y Acad Sci, 2005. **1049**: p. 1-8.

85. Ivanovic, Z., et al., *Primitive human HPCs are better maintained and expanded in vitro at 1 percent oxygen than at 20 percent.* Transfusion, 2000. **40**(12): p. 1482-8.

86. Ma, T., et al., *Hypoxia and stem cell-based engineering of mesenchymal tissues.* Biotechnol Prog, 2009. **25**(1): p. 32-42.

87. Badylak, S.F., et al., *Macrophage phenotype as a determinant of biologic scaffold remodeling.* Tissue Eng Part A, 2008. **14**(11): p. 1835-42.

88. Brown, B.N., et al., *Macrophage phenotype and remodeling outcomes in response to biologic scaffolds with and without a cellular component.* Biomaterials, 2009. **30**(8): p. 1482-91.

89. Badylak, S.F., *Regenerative medicine approach to heart valve replacement.* Circulation, 2005. **111**(21): p. 2715-6.

90. Brittan, M. and N.A. Wright, *Gastrointestinal stem cells.* J Pathol, 2002. **197**(4): p. 492-509.

91. Kim, C.F., et al., *Identification of bronchioalveolar stem cells in normal lung and lung cancer.* Cell, 2005. **121**(6): p. 823-35.

92. Vaananen, H.K., *Mesenchymal stem cells.* Ann Med, 2005. **37**(7): p. 469-79.

93. Herrera, M.B., et al., *Isolation and characterization of a stem cell population from adult human liver.* Stem Cells, 2006. **24**(12): p. 2840-50.

94. Moore, K.A. and I.R. Lemischka, *Stem cells and their niches.* Science, 2006. **311**(5769): p. 1880-5.

95. Gimble, J.M., A.J. Katz, and B.A. Bunnell, *Adipose-derived stem cells for regenerative medicine.* Circ Res, 2007. **100**(9): p. 1249-60.

96. Wilson, A. and A. Trumpp, *Bone-marrow haematopoietic-stem-cell niches.* Nat Rev Immunol, 2006. **6**(2): p. 93-106.

97. Levy, V., et al., *Epidermal stem cells arise from the hair follicle after wounding.* Faseb J, 2007. **21**(7): p. 1358-66.

98. Mimeault, M., R. Hauke, and S.K. Batra, *Stem cells: a revolution in therapeutics-recent advances in stem cell biology and their therapeutic applications in regenerative medicine and cancer therapies.* Clin Pharmacol Ther, 2007. **82**(3): p. 252-64.

99. Peault, B., et al., *Stem and progenitor cells in skeletal muscle development, maintenance, and therapy.* Mol Ther, 2007. **15**(5): p. 867-77.

100. Crisan, M., et al., *A perivascular origin for mesenchymal stem cells in multiple human organs.* Cell Stem Cell, 2008. **3**(3): p. 301-13.

101. Janes, S.M., S. Lowell, and C. Hutter, *Epidermal stem cells.* J Pathol, 2002. **197**(4): p. 479-91.

102. Jensen, U.B., S. Lowell, and F.M. Watt, *The spatial relationship between stem cells and their progeny in the basal layer of human epidermis: a new view based on whole-mount labelling and lineage analysis.* Development, 1999. **126**(11): p. 2409-18.

103. Jones, P.H., S. Harper, and F.M. Watt, *Stem cell patterning and fate in human epidermis.* Cell, 1995. **80**(1): p. 83-93.

104. Roh, C. and S. Lyle, *Cutaneous stem cells and wound healing.* Pediatr Res, 2006. **59**(4 Pt 2): p. 100R-3R.

105. Cotsarelis, G., *Epithelial stem cells: a folliculocentric view.* J Invest Dermatol, 2006. **126**(7): p. 1459-68.

106. Lyle, S., et al., *Human hair follicle bulge cells are biochemically distinct and possess an epithelial stem cell phenotype.* J Investig Dermatol Symp Proc, 1999. **4**(3): p. 296-301.

107. Larouche, D., et al., *Keratin 19 as a stem cell marker in vivo and in vitro.* Methods Mol Biol, 2005. **289**: p. 103-10.

108. Brivanlou, A.H., et al., *Stem cells. Setting standards for human embryonic stem cells.* Science, 2003. **300**(5621): p. 913-6.

109. Richards, M., et al., *The transcriptome profile of human embryonic stem cells as defined by SAGE.* Stem Cells, 2004. **22**(1): p. 51-64.

110. Dan, Y.Y., et al., *Isolation of multipotent progenitor cells from human fetal liver capable of differentiating into liver and mesenchymal lineages.* Proc Natl Acad Sci U S A, 2006. **103**(26): p. 9912-7.

111. Schmelzer, E., et al., *Human hepatic stem cells from fetal and postnatal donors.* J Exp Med, 2007. **204**(8): p. 1973-87.

112. Malhi, H., et al., *Isolation of human progenitor liver epithelial cells with extensive replication capacity and differentiation into mature hepatocytes.* J Cell Sci, 2002. **115**(Pt 13): p. 2679-88.

113. Nowak, G., et al., *Identification of expandable human hepatic progenitors which differentiate into mature hepatic cells in vivo.* Gut, 2005. **54**(7): p. 972-9.

114. Dan, Y.Y. and G.C. Yeoh, *Liver stem cells: a scientific and clinical perspective.* J Gastroenterol Hepatol, 2008. **23**(5): p. 687-98.

115. Cheng, H. and C.P. Leblond, *Origin, differentiation and renewal of the four main epithelial cell types in the mouse small intestine. V. Unitarian Theory of the origin of the four epithelial cell types.* Am J Anat, 1974. **141**(4): p. 537-61.

116. Montgomery, R.K. and D.T. Breault, *Small intestinal stem cell markers.* J Anat, 2008. **213**(1): p. 52-8.

117. Quaroni, A., et al., *Epithelioid cell cultures from rat small intestine. Characterization by morphologic and immunologic criteria.* J Cell Biol, 1979. **80**(2): p. 248-65.

118. Tai, C.C., et al., *Induction of fibroblast growth factor 10 (FGF10) in the ileal crypt epithelium after massive small bowel resection suggests a role for FGF10 in gut adaptation.* Dev Dyn, 2009. **238**(2): p. 294-301.

119. Hashimoto, T., et al., *Regulation of ATP-sensitive potassium channel subunit Kir6.2 expression in rat intestinal insulin-producing progenitor cells.* J Biol Chem, 2005. **280**(3): p. 1893-900.

120. Kojima, H., et al., *Combined expression of pancreatic duodenal homeobox 1 and islet factor 1 induces immature enterocytes to produce insulin.* Diabetes, 2002. **51**(5): p. 1398-408.

121. Sellaro, T.L., et al., *Maintenance of Hepatic Sinusoidal Endothelial Cell Phenotype In Vitro Using Organ-Specific Extracellular Matrix Scaffolds.* Tissue Eng, 2007. **13**(9): p. 2301-10.

122. Werb, Z. and J.R. Chin, *Extracellular matrix remodeling during morphogenesis.* Ann N Y Acad Sci, 1998. **857**: p. 110-8.

123. Bullard, K.M., M.T. Longaker, and H.P. Lorenz, *Fetal wound healing: current biology.* World J Surg, 2003. **27**(1): p. 54-61.

124. Lagasse, E., personal communication, 2009.

125. Manohar, R., personal communication, 2009.

126. Freytes, D.O., et al., *Biaxial strength of multilaminated extracellular matrix scaffolds.* Biomaterials, 2004. **25**(12): p. 2353-61.

127. Jones, P.H. and F.M. Watt, *Separation of human epidermal stem cells from transit amplifying cells on the basis of differences in integrin function and expression.* Cell, 1993. **73**(4): p. 713-24.

128. Adzick, N., Longaker, MT (Eds), *Fetal Wound Healing*. 1992, New York, NY: Elsevier Scientific Press.

129. Shell, D.H.t., et al., *Comparison of small-intestinal submucosa and expanded polytetrafluoroethylene as a vascular conduit in the presence of gram-positive contamination.* Ann Surg, 2005. **241**(6): p. 995-1001; discussion 1001-4.

130. Illingworth, C.M., *Trapped fingers and amputated finger tips in children.* J Pediatr Surg, 1974. **9**(6): p. 853-58.

131. Brennan, E.P., et al., *Chemoattractant activity of degradation products of fetal and adult skin extracellular matrix for keratinocyte progenitor cells.* J Tissue Eng Regen Med, 2008. **2**(8): p. 491-8.

132. Metcalf, D., *Concise review: hematopoietic stem cells and tissue stem cells: current concepts and unanswered questions.* Stem Cells, 2007. **25**(10): p. 2390-5.

133. Caplan, A.I., *Why are MSCs therapeutic? New data: new insight.* J Pathol, 2009. **217**(2): p. 318-24.

134. Krause, D.S., et al., *Multi-organ, multi-lineage engraftment by a single bone marrow-derived stem cell.* Cell, 2001. **105**(3): p. 369-77.

135. Van Arnam, J.S., et al., *Engraftment of bone marrow-derived epithelial cells.* Stem Cell Rev, 2005. **1**(1): p. 21-7.

136. Asahara, T., et al., *Isolation of putative progenitor endothelial cells for angiogenesis.* Science, 1997. **275**(5302): p. 964-7.

137. Shi, Q., et al., *Evidence for circulating bone marrow-derived endothelial cells.* Blood, 1998. **92**(2): p. 362-7.

138. Timmermans, F., et al., *Endothelial progenitor cells: Identity defined?* J Cell Mol Med, 2008.

139. Fathke, C., et al., *Contribution of bone marrow-derived cells to skin: collagen deposition and wound repair.* Stem Cells, 2004. **22**(5): p. 812-22.

140. Bellini, A. and S. Mattoli, *The role of the fibrocyte, a bone marrow-derived mesenchymal progenitor, in reactive and reparative fibroses.* Lab Invest, 2007. **87**(9): p. 858-70.

141. Badiavas, E.V., et al., *Participation of bone marrow derived cells in cutaneous wound healing.* J Cell Physiol, 2003. **196**(2): p. 245-50.

142. Li, J., Kirsner, R.S., *Extracellular matrix and wound healing*. 2 ed. Wound Healing, ed. A.F. Falabella, Kirsner, R.S. 2005: Taylor and Francis. 40.

143. Rawlins, J.M., et al., *Quantifying collagen type in mature burn scars: a novel approach using histology and digital image analysis.* J Burn Care Res, 2006. **27**(1): p. 60-5.

144. Fitzgerald, A.M., et al., *Human skin histology as demonstrated by Herovici's stain: a guide for the improvement of dermal substitutes for use with cultured keratinocytes?* Burns, 1996. **22**(3): p. 200-2.

145. Singer, A.J. and R.A. Clark, *Cutaneous wound healing.* N Engl J Med, 1999. **341**(10): p. 738-46.

146. Jernigan, T.W., et al., *Small intestinal submucosa for vascular reconstruction in the presence of gastrointestinal contamination.* Ann Surg, 2004. **239**(5): p. 733-8; discussion 738-40.

147. Kim, B.S., C.E. Baez, and A. Atala, *Biomaterials for tissue engineering.* World J Urol, 2000. **18**(1): p. 2-9.

148. Kim, M.S., et al., *Preparation of porcine small intestinal submucosa sponge and their application as a wound dressing in full-thickness skin defect of rat.* Int J Biol Macromol, 2005. **36**(1-2): p. 54-60.

149. Ruiz, C.E., et al., *Transcatheter placement of a low-profile biodegradable pulmonary valve made of small intestinal submucosa: a long-term study in a swine model.* J Thorac Cardiovasc Surg, 2005. **130**(2): p. 477-84.

150. Carlson, G.A., et al., *Bacteriostatic properties of biomatrices against common orthopaedic pathogens.* Biochem Biophys Res Commun, 2004. **321**(2): p. 472-8.

151. Freytes, D.O., R.S. Tullius, and S.F. Badylak, *Effect of storage upon material properties of lyophilized porcine extracellular matrix derived from the urinary bladder.* J Biomed Mater Res B Appl Biomater, 2006. **78**(2): p. 327-33.

152. Piechota, H.J., et al., *Functional rat bladder regeneration through xenotransplantation of the bladder acellular matrix graft.* Br J Urol, 1998. **81**(4): p. 548-59.

153. Sievert, K.D., et al., *Homologous acellular matrix graft for urethral reconstruction in the rabbit: histological and functional evaluation.* J Urol, 2000. **163**(6): p. 1958-65.

154. Lin, P., et al., *Assessing porcine liver-derived biomatrix for hepatic tissue engineering.* Tissue Eng, 2004. **10**(7-8): p. 1046-53.

155. Gilbert, T.W., et al., *Degradation and remodeling of small intestinal submucosa in canine Achilles tendon repair.* J Bone Joint Surg Am, 2007. **89**(3): p. 621-30.

156. Haviv, F., et al., *Thrombospondin-1 mimetic peptide inhibitors of angiogenesis and tumor growth: design, synthesis, and optimization of pharmacokinetics and biological activities.* J Med Chem, 2005. **48**(8): p. 2838-46.

157. O'Reilly, M.S., et al., *Endostatin: an endogenous inhibitor of angiogenesis and tumor growth.* Cell, 1997. **88**(2): p. 277-85.

158. Zhang, G., C.R. Ross, and F. Blecha, *Porcine antimicrobial peptides: new prospects for ancient molecules of host defense.* Vet Res, 2000. **31**(3): p. 277-96.

159. Carretero, M., et al., *A cutaneous gene therapy approach to treat infection through keratinocyte-targeted overexpression of antimicrobial peptides.* Faseb J, 2004. **18**(15): p. 1931-3.

160. Agerberth, B., et al., *Isolation of three antibacterial peptides from pig intestine: gastric inhibitory polypeptide (7-42), diazepam-binding inhibitor (32-86) and a novel factor, peptide 3910.* Eur J Biochem, 1993. **216**(2): p. 623-9.

161. Agerberth, B., et al., *Amino acid sequence of PR-39. Isolation from pig intestine of a new member of the family of proline-arginine-rich antibacterial peptides.* Eur J Biochem, 1991. **202**(3): p. 849-54.

162. Lee, J.Y., et al., *Antibacterial peptides from pig intestine: isolation of a mammalian cecropin.* Proc Natl Acad Sci U S A, 1989. **86**(23): p. 9159-62.

163. Chen, Z.W., et al., *Isolation and characterization of porcine diazepam-binding inhibitor, a polypeptide not only of cerebral occurrence but also common in intestinal tissues and with effects on regulation of insulin release.* Eur J Biochem, 1988. **174**(2): p. 239-45.

164. Zhang, G., et al., *Molecular cloning and tissue expression of porcine beta-defensin-1.* FEBS Lett, 1998. **424**(1-2): p. 37-40.